OCULAR DRUG DELIVERY USING MICRONEEDLES

A Thesis
Presented to
The Academic Faculty

By

Ninghao (Jason) Jiang

In Partial Fulfillment
of the Requirements for the Degree
Doctor of Philosophy in Chemical and Biomolecular Engineering

Georgia Institute of Technology
December, 2006

OCULAR DRUG DELIVERY USING MICRONEEDLES

Approved by:

Dr. Mark R. Prausnitz, Chairman
School of Chemical & Biomolecular Engineering
Georgia Institute of Technology

Dr. Athanassios Sambanis
School of Chemical & Biomolecular Engineering
Georgia Institute of Technology

Dr. Mark G. Allen
School of Chemical & Biomolecular Engineering
Georgia Institute of Technology

Dr. Henry F. Edelhauser
Department of Ophthalmology
Emory University

Dr. Dayle H. Geroski
Department of Ophthalmology
Emory University

Dr. John Nickerson
Department of Ophthalmology
Emory University

Date Approved:
November 7, 2006

To my dearest parents

For their love, trust and supports

ACKNOWLEGMENT

I would like to thank my advisor, my thesis committee members, my research colleagues, my family and my friends who made this thesis possible. I would like to thank my thesis advisor, Mark Prausnitz for his support during my thesis work. Without his guidance, it would be difficult for me to complete my study. I would like to thank Henry Edelhauser for his expertise in ocular drug delivery. I would like to thank Mark Allen for letting me using laser room in MEMS facility. I would also like to thank the rest of my thesis committee members: Athanassios Sambanis, Dayle Geroski and John Nickerson, for their willingness to server on my committee and their guidance on my road to complete my study. In addition, I would like to thank Bernard McCarey and Glenn Holly at Emory University for help with the *in vivo* animal study.

I would like to thank all my research colleagues for their supports and helps during my staying in the lab. Especially, I would like to thank Harvinder Gill and Wijaya Martanto for their thoughtful suggestions in experimental designs and analysis. I would like to thank Daniel Hallow for constantly putting up with my love taps; Deepta Ghate and Samir Patel for help me to conduct the animal study; Junghwan Park for teaching me the polymer microneedle fabrication procedure; Charlene Rincon for making the polymer films; Robyn Schlicher for her help and guidance regarding life in graduate school; Jyoti Gupta and Josh Hutcheson for always offering me free food. I would like to thank my undergraduate research assistant, Jason Moore, for helping me finishing the hollow microneedle study. I would also like to thank Tracey Couse for her help with histology. In addition, I would give special thanks to Donna Bondy and Trudy Walker for always

looking after me. I will definitely miss the cookies Donna makes and the candies Trudy gives me.

I would like to thank Kerry Taft at Georgia Eye Bank for providing me the human sclera tissue; Dr. Uday Kompella and Swita Raghava for supplying nanoparticles for my experiment; Dr. Aurelie Edwards for her helps in diffusion modeling. My thanks also go to all my fellow lab members: Samantha Andrews, Prerona Chakravarty, Leonard Chu, Youngbin Choy, Harvinder Gill, Jyoti Gupta, Daniel Hallow, Yeuchun Kim, Jeong-Woo Lee, James Norman, JungHwan Park, Samir Patel and Sean Sullivan. I would also like to thank my research funding agency, NIH.

I would like to thank my parents for their constant encouragement and supports over the past fiver years. Without them, I would not have the willing to pursue my Ph.D. degree. I would like to thank all my friends in my life who helped me to grow as a better human being. Last but not least, I would like to thank my dear lord for always giving me strength and wisdom when I needed them the most.

TABLE OF CONTENTS

LIST OF TABLES

LIST OF FIGURES

LIST OF SYMBOLS and ABBREVIATIONS

A	surface area
ANOVA	analysis of variance
ARMD	age-related macular degeneration
BSA	bovine serum albumin
BSS	balanced salt solution
C_{bath}	original concentration in the donor solution
$C_{cuvette}$	concentration in the cuvette
C_{donor}	concentration in the donor solution measured over time
C_{exp}	experimentally measured concentration
C_{sclera}	concentration in the sclera
C_{theor}	theoretically predicted concentration
CAD	Computer Aided Design
d	scleral thickness
D_{trans}	effective transverse diffusivity
Δt	sampling time
D.E.	drug encapsulated efficiency
DNA	deoxyribonucleic acid
EPO	erythropoietin
FITC	fluorescein isothiocyanate
GAG	glycosaminoglycan
GnRH	gonadotropin-releasing hormone

i	number of measurements
K_D	sclera-to-saline distribution coefficient
K_{eq}	free-to-bond sulforhodamine ratio at equilibrium
M	mass flow rate
MAPE	mean absolute percent error
MEMS	Micro-Electro-Mechanical Systems
MW	molecular weight
n	number of measurements
NaFl	sodium fluorescein
PBS	phosphate buffered saline
pDNA	plasmid DNA
PEG	polyethylene glycol
PLA	poly lactic acid
PLGA	poly lactic co-glycolic acid
PVP	poly vinyl pyrrolidone
RIE	reactive iron etching
SS	stainless steel
UV	ultraviolet
V	volume
v_s	aqueous humor production rate

SUMMARY

Traditional methods of drug delivery to the eye include topical application, intraocular injection and systemic administration; however, each method has its limitation to efficiently deliver drugs to the back of the eye. Therefore, developing more effective ocular drug delivery methods with fewer vision threatening complications is essential to improve the treatments of posterior segment ocular diseases. Microneedles, which were developed for transdermal delivery, have the potential to deliver drug across the ocular tissues in a minimally invasive way because of their small size. To test this hypothesis, the goals of this study were (1) to provide experimental measurements coupled with a theoretical modeling to quantify the distribution of a model compound during lateral diffusion within the sclera *in vitro*, (2) to assess the capability of using coated solid metal microneedles to deliver drugs into the ocular tissue in both *in vitro* and *in vivo* scenarios and (3) to infuse solutions into the sclera tissue *in vitro* using hollow glass microneedles and examine the physiological barriers for flow.

To familiarize with the drug diffusion properties within the sclera, we first measured the lateral diffusion of a model compound, sulforhodamine, through human cadaver sclera. Experimentally, we determined that lateral diffusion of sulforhodamine depended strongly on both time and position along the tissue. The measured sclera-to-saline distribution coefficient of 13.6 indicated significant binding between molecules and tissue. These data were fitted to a theoretical model, which yielded an effective lateral diffusion coefficient for sulforhodamine of 3.82e-6 cm^2/s. This finding suggested that a point source of sulforhodamine would take up to 6 weeks to diffuse throughout the sclera in a human eye. Comparison with transscleral diffusion indicated similar diffusion

coefficients, although lateral diffusion was approximately three times faster. This study presented the first experimental data on lateral diffusion within the sclera. Using the developed theoretical model, drug distribution in the sclera can be estimated for various drug delivery scenarios, for example, from an implant.

This work also studied the use of solid metal microneedles, having lengths of 500-750 μm, to deliver drugs into the eye. Using a specially formulated coating solution, these needles were coated with compounds of various sizes (fluorescein, DNA and proteins). *In vitro* insertion tests showed that the microneedles were mechanically strong enough to penetrate into human cadaver sclera, and the coating solution rapidly dissolved off the needles after insertion and had been deposited within the tissue. We then assessed this system in an *in vivo* animal model, in which single, fluorescein-coated microneedles were inserted into the rabbit cornea for delivery. Fluorescein concentration in the anterior segment of the eye was immediately increased after needle insertion, reached to a peak value after 3 h, and decreased to background level with 24 h. Compared to topical administration of equivalent fluorescein dose as the needle coating, microneedles showed a bioavailability of 60 times greater. The administration of pilocarpine using coated microneedles yielded similar results, which caused rapid and extended pupil contraction. Safety studies reported no inflammation responses caused by the microneedle insertion. This the first study demonstrating the capability of using microneedles for ocular drug delivery to treat diseases in both anterior and posterior regions of the eye.

Hollow glass microneedles, fabricated using a micropipette puller, were also studied for delivery within human cadaver sclera. Microneedles were inserted 720-1080 μm into different regions of the sclera, and delivered up to 18 μl fluid on average into the

tissue after needle retractions of 200-300 μm. Infusion pressure showed an insignificant impact on the delivery. The main barrier in scleral delivery appeared to be the complex alignment of tightly packed GAG and collagen fibers, which micron-sized particles were unable to flow through. The presence of either hyaluronidase or collagenase enhanced microsphere delivery by breaking down the fibers.

Altogether, this work provides the first studies of using microneedles as a novel tool to deliver drugs either within or across the ocular tissue for disease treatments in a minimally invasive way. With further optimization, the ultimate aim of the study is to provide a targeted, controlled drug delivery to treat diseases, such as diabetic retinopathy and macular degeneration, in the posterior segment of the eye.

1 INTRODUCTION

Drug delivery to the eye using current methods is an extremely inefficient process by topical or systemic administration. Intraocular injection is more efficient, but introduces safety concerns. There is a demand for improved methods of drug delivery to the eye that increase efficiency and safety. The principal route for local ophthalmic drug delivery system remains the topical application of solutions to the surface of the eye as eye drops. Conventional eye drops typically act transiently, which enter the eye by either diffusion across the cornea or across the sclera (Robinson and Lee 1988; Lang 1995; Tasman 1995). Drug delivery to intraocular tissues toward the back of the eye, such as retina and choroid, by this approach, however, is limited by: (i) the significant barrier to solute flux provided by the corneal epithelium and conjunctiva; and (ii) precorneal drug losses that are due to tear drainage and tear fluid turnover (Geroski and Edelhauser 2000). Other drug delivery methods, such as intraocular injections or ocular implants demonstrated improved delivery efficiencies; however, we need to consider additional factors including safety issues and patient compliance. The ideal route for drug delivery to the back tissues of the eye will be transscleral, due to large surface area of the sclera. The average 16.3-cm^2 surface area of the human sclera (Olsen, Aaberg et al. 1998) accounts for 95% of the total surface area of the globe and provides a significantly larger avenue for drug diffusion to the inside of the eye than the 1-cm^2 surface area of the cornea.

Over the past decade, the concept of microneedles for transdermal drug delivery has found acceptance, and studies have shown the potential of using microneedles to enhance drug delivery across the skin (McAllister, Allen et al. 2000; Davis 2003;

Martanto 2005). This thesis addresses, for the first time, the possibility that microneedles could be used for drug delivery to the eye. While guided by the advantages of microneedles and their successes in transdermal studies, we are hoping to apply the same technique in drug delivery to the posterior segments of the eye. Using microneedles as the new tool in ocular drug delivery can offer the following advantages: (1) they may minimize pain and tissue damage relative to hypodermic injections because they are small enough to avoid simulating nerves or significant tissue trauma; (2) they should be well tolerated and thereby increase patient compliance since a single application might be suitable for long-term use; and (3) they will provide a localized and target drug delivery to the back of the eye.

Depending on the type of microneedles we use, we can improve the drug delivery efficiency in various fashions. This study is mainly focused on using two different types of microneedles: solid metal and hollow glass microneedles. For solid microneedles, drug formulations are coated onto the shafts of the needles. The insertion of coated microneedles into the sclera or cornea should deposit drug directly into the ocular tissue area bypassing the epithelial barriers of corneal epithelium and conjunctiva. The coated drug that dissolves off the needle shaft is stored in the sclera or corneal tissue, and is delivered into the eye by diffusion. Using hollow glass microneedles, we can pre-load drug solutions into the hollow lumen region of the needle. After insertion into the sclera, the drug is injected into the ocular tissue using pressure-driven flow. Coupling with an insertion device, we can precisely control the insertion depth of the needle into the tissue. Both methods should achieve the following goals in drug delivery to the back of the eye: (1) increasing the amount of drug delivered relative to topical administration; (2) more

localized drug delivery relative to systemic administration; (3) safer delivery approach relative to intraocular injection; and (4) prolonged drug release periods.

2 BACKGROUND

2.1 Ocular drug delivery

A big challenge that ophthalmologists face today is effectively delivering drugs to the back (retinal, choroid and vitreous body) of the eye. The most conventional way of ocular delivery is using eye drops, but only a small amount of the drug can actually reach the targeted area. Most of them are washed away by the tear fluid on the surface of the eye. Alternative methods, such as intraocular injections and implantation, offer better delivery efficiency; however, complications associated with safety and patient compliance must be considered. The development of microneedles showed excellent potential as a novel drug delivery tool for transdermal drug delivery (Trimmer, Ling et al. 1995; McAllister, Wang et al. 2003; Martanto, Davis et al. 2004). They could minimize tissue damage with their small size and provide targeted delivery. Using the same concept, microneedles might be used in ocular drug delivery to treat diseases such as macular degeneration and diabetic retinopathy. The thesis addresses this concept for the first time.

2.1.1 Anatomy of the eye

The human eye can be viewed as a deformed spherical shell of tissues with a diameter of 23-24 mm (Fatt and Wissman 1992). Its interior is filled largely with water in the form of aqueous humor and the vitreous body, as well as additional structures such as the lens and iris. The exterior shell of the eye consists of three layers: the outer sclera, the middle choroid and the inner retina (Figure 2.1.1.1).

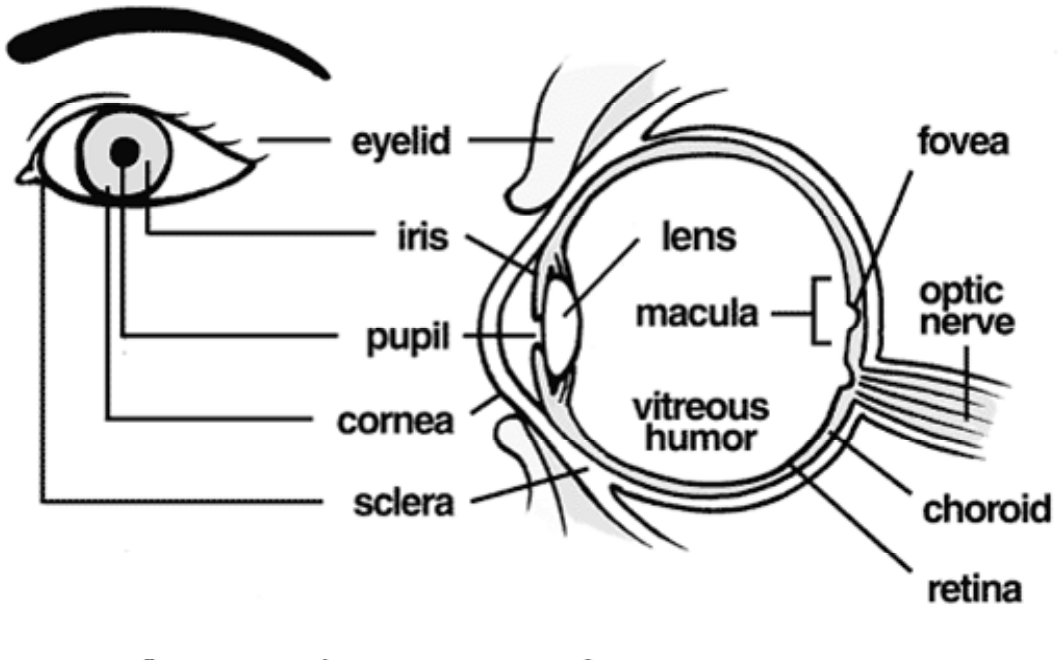

Figure 2.1.1. Anatomy of the human eye (copied from www.mvrf.org).

The transparent portion of the eye is the cornea, which represents 7% of the total surface area on human eye. The thickness of the human cornea in the central region is about 0.52 mm, thickening to about 0.67 mm at the limbus (Hogan, Alvarado et al. 1971). It is a multilayered tissue containing a superficial layer of epithelial cells, followed deeper by Bowman's layer, stroma, Descemet's membrane and finally a monolayer of endothelial cell at the base. The cornea is considered to be the main pathway for the permeation of drugs into the eye (Robinson 1993), and it provides 2/3 of the optical focusing power for the eye.

The sclera is a thin spherically shaped connective tissue that gives the eye its shape. It is attached to the ocular muscles, which control the movement of the eye. The front portion of the sclera can be seen externally as the "white of the eye". On its anterior surface adjacent to the cornea, the sclera is covered by conjunctiva, a transparent layer of cells. The remainder of the sclera consists of a layer called Tenon's capsule, a thin

connective tissue layer overlying the episclera. The episclera can be distinguished from the sclera itself by being more loosely woven and rich in blood vessels. The sclera is lined internally by the choroid, which contains blood vessels, and the retina, which contains the nerves involved in sight. In the human eye, the sclera is about 0.6 to 0.89 mm at the limbus, thinning to 0.4 to 0.5 mm at the equator and thickening again to 1.0 mm at the posterior pole (Hogan, Alvarado et al. 1971).

Transport properties of the sclera are of interest relative to the transport of drugs applied topically to the eye, due to its large surface area. This includes diffusion of drugs across the conjunctiva and sclera to the anterior segment structures (Ahmed and Patton 1985; Edelhauser and Maren 1988) and of drugs applied directly to the scleral surface (Mietz, Addicks et al. 1994) to deliver drugs to the posterior pole in treatment of posterior segment diseases. In addition, regional differences in scleral thickness could be used to further optimize drug diffusion if sustained-release delivery devices or systems could be placed in regions where sclera permeability was the greatest (Geroski and Edelhauser 2000).

2.1.2 Common vision problems

Blindness and visual impairment extract a great price from individuals and society, and they are also an enormous cost to the federal government, estimated conservatively at $4 billion annually (Tielsch 2000). Among people 40 years and older (approximately 95.2 million people) in the U.S., more than 1 million are legally blind and more than 3.4 million people are considered visually impaired. The most common causes of vision loss

are age-related macular degeneration, glaucoma and diabetic retinopathy, and patients' lives are greatly affected by these diseases.

Age-related macular degeneration (ARMD) is the most common cause of severe loss of central vision in people aged over 50 in the Western world (Vingerling, Klaver et al. 1995). It is a disease caused by damage to tissues that provide physiological support to the light-sensitive cells in the retina (Figure 2.1.2). The disease is categorized into two stages: dry disease, which is the background disease, and wet disease, which occurs when abnormal blood vessels form as a complication of the dry disease and cause vision loss. The vision loss results from loss of function of the macula, the center of the retina, which is responsible for central visual tasks such as reading, driving and recognizing faces. Recently, therapeutic drugs, such as Macugen (Pegaptanib sodium injection) and Lucentis (Ranibizumab injection) have been shown to help preserving vision in patience with ARMD by slowing vision loss. The recommended dose of Macugen is 0.3 mg of intravitreal injection administered once every 6 weeks. Lucenis is injected intravitreally into the eye at a dose of 0.5 mg on a monthly basis; however, each dose costs close to $2000 (Jimenez 2006), which most ARMD patients could not afford if they had to take a monthly dose in perpetuity.

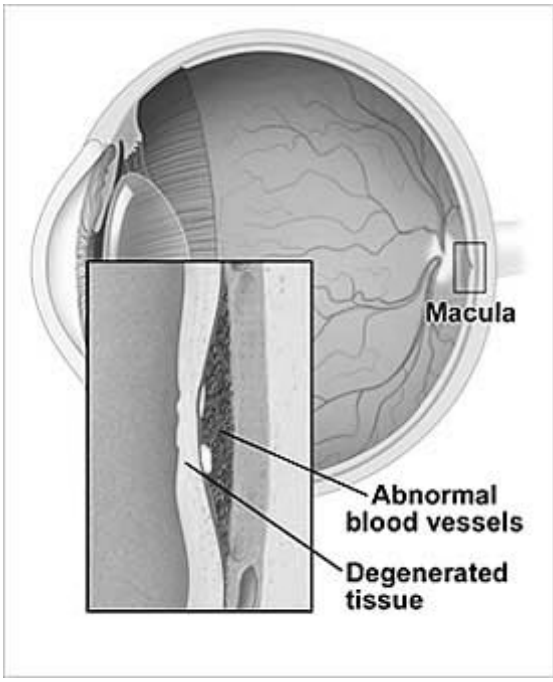

Figure 2.1.2. Age-related macular degeneration is a disease caused by formation of abnormal blood vessels leading to rapid vision loss (copied from www.mayoclinic.org).

Glaucoma, the second leading cause of adult blindness in the U.S., is a group of diseases usually associated with an increased pressure within the eye (Figure 2.1.3). This elevated pressure can cause damage to the cells that form the optic nerve, the structure responsible for transmitting visual information from the eye to the brain. The damage is progressive with loss of peripheral vision first, followed by loss in central vision and potentially blindness. About 2.2 million Americans age 40 and over have this disease. Because the condition does not cause symptoms in its early stages, half of patients do not know until it reaches the later phase (U.S.News 2006).

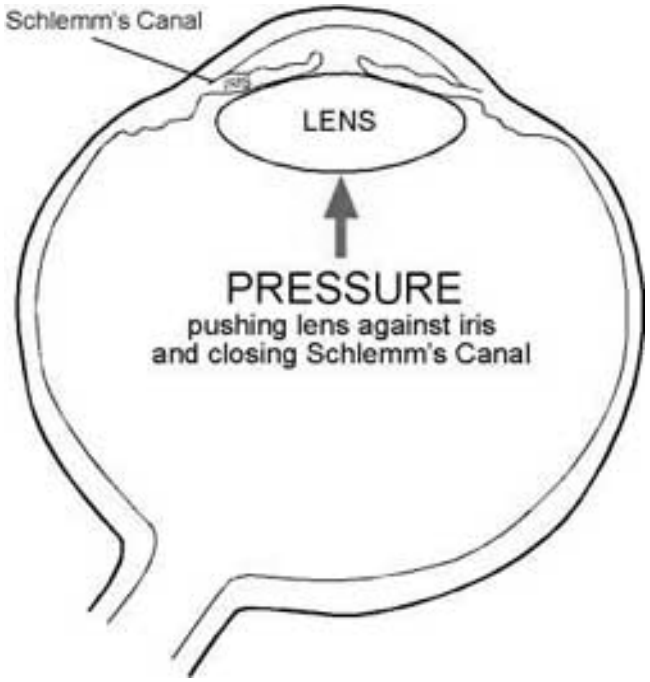

Figure 2.1.3. Glaucoma is a disease that caused by elevation of intraocular pressure within the eye (copied from www.uic.edu)

The treatment of glaucoma primarily entails the use of eye drop solutions containing drugs such as prostaglandin analogues (improving fluid drainage), beta-blockers (reducing the amount of aqueous humor that the eye makes), alpha-adrenergic agonists (lessen the amount of aqueous humor as well as increasing fluid drainage) and carbonic anhydrase inhibitors (reducing the amount of aqueous humor). Normally these drops need to be applied to the eye 3-5 times per day, which often leads to poor patient compliance, especially among elders.

Approximately 16 million people in the U.S. have diabetes, and nearly 49% of them are affected by diabetic retinopathy, which is an eye disease affecting the blood vessels in the retina. When blood vessels in the retina are damaged, they may leak fluid or blood and grow fragile, brush-like branches and scar tissue (Figure 2.1.4). This symptom of diabetic retinopathy can blur or distort the images that the retina sends to the

brain. Recent studies show that injection of steroids can reduce the progression of the disease (Jonas, Kreissig et al. 2003).

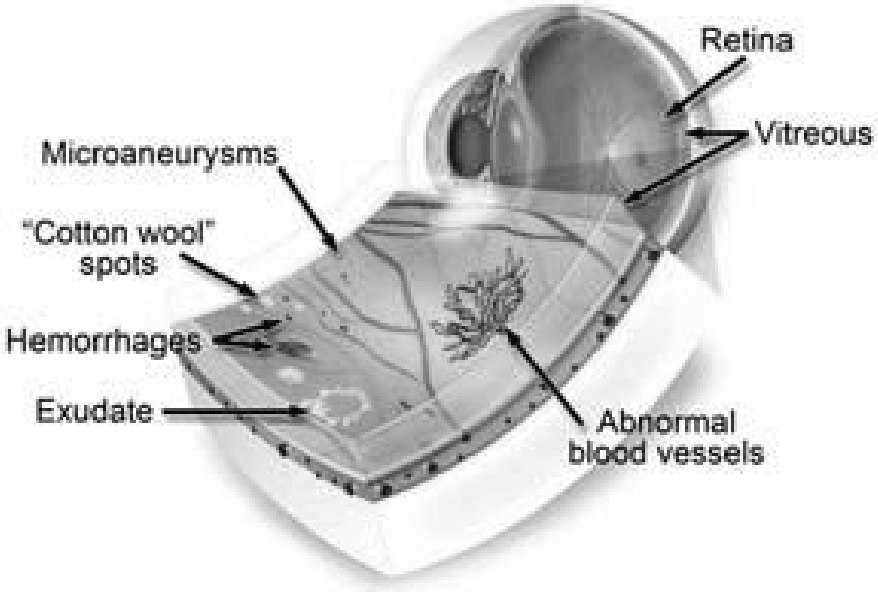

Figure 2.1.4. Diabetic retinopathy is a retinal disease caused by changes in the blood vessels of the eye as a complication of diabetes (copied from www.eyemdlink.com).

2.1.3 Conventional ocular drug delivery methods

The eye, like every nervous organ of the body, is naturally well protected from the systemic circulation. The local delivery of drugs into the posterior segment of the eye, particularly into the retina, at efficient concentration with reduced local or general side effects, is one of the main issues ophthalmologists face today. Currently the posterior segment disease treatments focus on four approaches to delivery drugs – topical, systemic, intraocular injection and periocular injection (Geroski and Edelhauser 2000). A comparison of using each delivery method is shown in Table 2.1:

Mode of delivery	Advantage	Disadvantages
Topical	Ease of access	Frequent applications
		Negligible levels in posterior segment
Systemic	Ease of access	Frequent applications
		Systemic adverse reactions
Intraocular	Targeted delivery	Frequent applications
	Higher efficiency	Complications of intraocular injections
Periocular	Targeted delivery	Low delivery efficiency
	Safer	

Table 2.1. The advantages and disadvantages of common approaches to deliver drugs to the posterior segment of the eye.

Traditional therapies include topical applications of drugs with eye drops. This mode of delivery can be easily accessed; however, it requires often-repeated applications (up to 5 times per day). In general, the treatment by drops is ineffective to treat the diseases in the back of the eye due to various barriers. The drug is rapidly washed away by tears and cannot reach the vitreous body, the retina and the choroid at sufficient levels. Additionally, the ineffectiveness is due to the long diffusion path length, counter-directional intraocular convection, and corneal impermeability to large molecules (Stjernschantz and Astin 1993; Maurice 2001).

Although a systemic delivery approach can deliver drugs to the eye, the administrated drugs have poor access to the tissues in the back of the eye due to two barriers: blood aqueous and blood-retinal barriers (Stjernschantz and Astin 1993). The blood-aqueous barrier, which is the anatomical mechanism that prevents exchange of materials between the chambers of the eye and the blood, prevents the substances from

entering the aqueous humor of the eye. The blood-retinal barrier, which is a transport barrier formed by tightly-joined endothelial cells, severely limits drug entry into the extravascular space of the retina and into the vitreous. The retinal pigmented epithelium also has tight junctions that form an effective barrier. Consequently, large systemic doses are required, and this can induce toxicity and unwanted side effects.

The traditional therapies of delivering drugs to the back of the eye that are more effective are intravitreal (into the eye) injections. The main problem with both methods is that after a drug is injected, its concentration in the system decreases exponentially with time as the body consumes it. This means that in order to maintain clinically helpful concentration of the drug in the eye, frequent injections of the drug are required. In addition, the injections can potentially induce complications, such as retinal detachments, cataracts, infections and pain (Herrero-Vanrell and Refojo 2001; Maurice 2001).

In recent years, there is a regenerated interest in the periocular (around the eye) delivery of drugs, which the drug is interfaced with the sclera. Drug delivered by periocular injection can reach the posterior segment by three main routes: transscleral, systemic circulation (through the choroid) and the anterior route through the tear film, cornea, aqueous humor and the vitreous body (Ghate and Edelhauser 2006). Systemic absorption is low via the subconjunctival route, which can lower systemic side effects while providing a localized drug effect (Gudauskas, Kumi et al. 1985).

2.1.4 Sclera permeability

The sclera is an elastic and microporous tissue composed of proteoglycans and closely packed collage fibrils (Foster and Sainz de la Maza 1994; Newell 1996)

containing 70% water. Its large surface area (16.3 cm^2) (Olsen, Aaberg et al. 1998) provides a significantly larger avenue for drugs to diffuse into the eye than the 1-cm^2 surface area of the cornea. Over the years, a series of studies have shown the sclera to be permeable to a range of drugs and solutes. Maurice and Polar (1977) have reported that the sclera generally offers less resistance to solute diffusion than does the cornea. While the cornea is relatively impermeable to solutes having a molecular size over 1 kDa, dextran (40 kDa) and serum albumin (69 kDa) can readily penetrate across the scleral tissue (Olsen, Edelhauser et al. 1995). More recently, Ambati et al. (2000) have shown the sclera to be permeable to higher molecular weight dextrans, as well as to the proteins IgG and bovine serum albumin, BSA). An inverse relationship was found between scleral permeability and solute molecule weight. The permeability of the sclera to carbonic anhydrase inhibitors is similar to the permeability of the corneal stroma (Edelhauser and Maren 1988). Hydrocortisone permeability is five times greater in sclera than in corneas with intact epithelia (Unlu and Robinson 1998). The scleral permeabilities of adrenergic blocking agents are also found to be significantly higher than their corneal permeability (Ahmed and Patton 1987). In addition, a theoretical model (Edwards and Prausnitz 1998) was developed to predict sclera permeability for a broad range of molecules. This model did not require any fitted parameters and was validated with steady-state transport data from 20 compounds including small drugs and macromolecules. Later on, a complementary model which predicts molecule transient transport behavior was developed (Prausnitz, Edwards et al. 1998) and was validated with experimental data on carboxyfluorescein flux.

Scleral permeability can be increased by scleral thinning, increasing tissue hydration and increasing temperature (Ghate and Edelhauser 2006). Age, cryotherapy and diode laser photocoagulation do not seem to have a significant impact on scleral permeability (Olsen, Edelhauser et al. 1995). Studies have shown that prostaglandins can improve scleral permeability by increasing expression of matrix metalloproteases and they can be used to enhance transscleral delivery of peptides into the back of the eye (Kim, Lindsey et al. 2001; Weinreb 2001; Weinreb, Lindsey et al. 2004). A recent study showed that 0.01 and 0.05% benzalkonium chloride, could be used to increase transscleral penetration of drugs with minimal toxicity (Okabe, Kimura et al. 2005)

2.1.5 Transscleral delivery

An ideal route to deliver drugs to the posterior segment of the eye would be transscleral, which takes advantages of the large surface area of the sclera. In addition, regional differences in scleral thickness could be used to further optimize transscleral drug delivery if sustain-release delivery devices or systems could be placed in regions where scleral permeability was the greatest (Geroski and Edelhauser 2000). A wide variety of drug delivery systems, including periocular injection, ocular implants of gel formulations or biodegradable polymers, and iontophoresis have shown potential for transscleral application.

A major method of drug delivery to the posterior segments is periocular injection, which includes subconjunctival, retrobulbar, peribulbar and posterior subtenon injections. This approach is safer and less invasive than intravitreal injection and also offers the potential for localized, sustained-release drug delivery. Weijtens et al. (1999) found that

periocular injection is more effective compared with oral administration for delivering dexamethasome into the back of the human eye. Lee et al. (2001) injected radiolabelled mannitol subconjunctivally in rabbits and concluded that, after subconjunctival injection, direct penetration through the sclera is the predominant pathway for drug delivery to the posterior segment with minimal contribution from the recirculation pathway and the transcorneal pathway.

A transscleral implant made out of either a gel formulation or biodegradable polymers can also be used as a minimally invasive method for drug delivery, since the human eye has a high tolerance of foreign bodies on the sclera (for example, the scleral buckle used in retinal-detachment surgery). *In situ* polymeric gels, such as pluronic F-127 and fibrin glue, are viscous liquids that on exposure to physiological conditions will shift to a gel phase. Preliminary studies showed that these gels can provide slow, uniform sustained release of dexamethasone across human sclera (Lee, Geroski et al. 2004) . Yasukawa et al. (2006) investigated using biodegradable implants, composed of hydrophilic or hydrophobic polymers, in the shape of rods, plugs, discs or sheets, and an implantable rod is presently being assessed in a Phase II trial to treat macular edema secondary to diabetic retinopathy or branch-retinal vein occlusion.

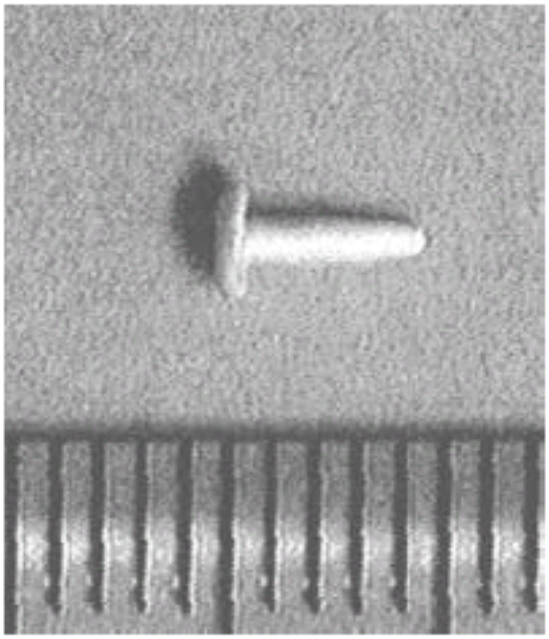

Figure 2.1.5. A scleral implant of biodegradable polymer, PLA. The device weights 8.5 mg and is 5.0 mm long (Yasukawa, Ogura et al. 2006).

Iontophoresis has been proven to increase transscleral delivery of various drug classes, including fluorescein, antibiotics and steroids (Sarraf and Lee 1994). However, this method may cause further complications in the eye, such as retinal edema, disruption of the normal retinal architecture and retinal pigment epithelial hyperplasia (Lam, Fu et al. 1991). Further improvements may be needed with this approach.

2.2 History of microneedles

The creation of microneedles for transdermal drug delivery seeks to combine the benefits of both conventional hypodermic needle injection and transdermal patches, while reducing the limitations associated with each technique. The overarching motivation for microneedles is that they can provide a minimally invasive means to transport drug molecules into the tissue. Over the past decade, numerous designs of microneedles have

been developed using tools from the microelectronic industry. Microneedles have been fabricated with a range of sizes, shapes and materials, from solid spike microneedles to biodegradable polymer microneedles to hollow microneedles. Depending on the microneedle type, it can have its unique functionality. Typically, these microneedles are hundreds of microns in length, on the order of one hundred microns at the base and having a sharp tip that is ones to tens of microns in diameter. When scaled up to mass production, microneedles are likely to be inexpensive enough to be used as disposable devices.

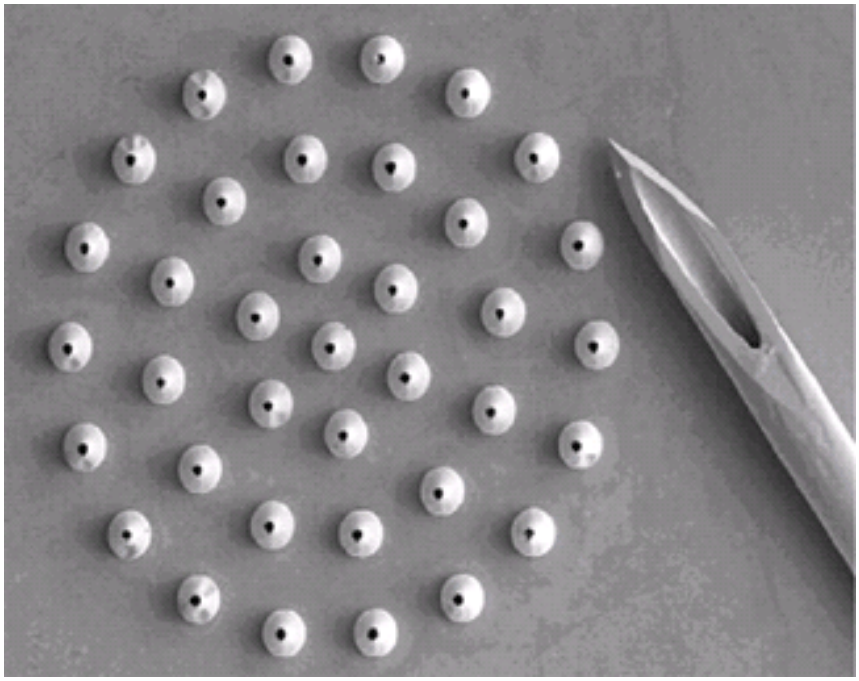

Figure 2.2.1. Microscopic image shows a hollow metallic microneedle array (500 μm tall) next to a conventional hypodermic syringe needle used for drug delivery.

2.2.1 Solid microneedles

Solid microneedles were designed to create micron-size pores in the tissue, which act as direct pathways allowing drug molecules or particles to transport into the tissue. These microneedles tend to have sharp tips and have good mechanical strength. They could be mass-produced at low cost.

2.2.1.1 Silicon microprobes

In the early phase of microneedle development, pyramidal silicon microprobes were found (Hashmi, Ling et al. 1995). Using a spin casting method, a photoresist is placed onto a silicon-dioxide coated wafer; the wafer is then brought in contact with a photomask and is exposed to UV light. The transferred pattern (from photomask to photoresist) is then etched into the silicon dioxide masking layer. The photoresist is then removed and the wafer is anisotropically wet-etched in potassium hydroxide solution to create arrays of pyramidal probes. With the goals of delivering genetic materials to cells, these microprobles are ten to hundreds of microns in height and have very sharp tips. These structures were used to transfect DNA into cells of plants (Trimmer, Ling et al. 1995) and mammals (Reed, Clarence et al. 1998).

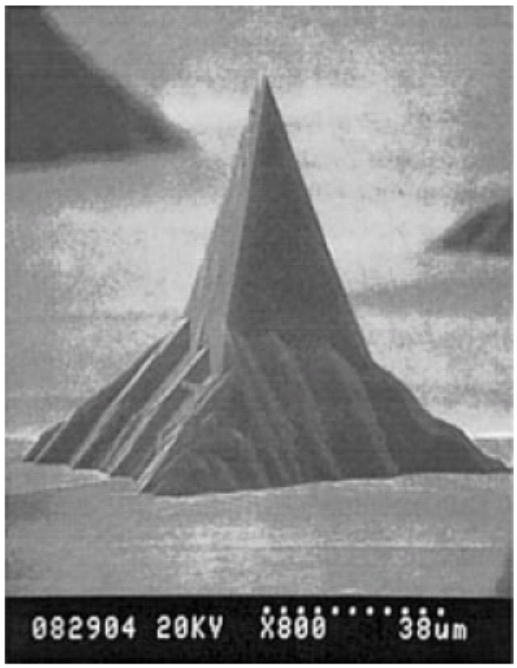

Figure 2.2.2. A single silicon microprobe fabricated by anisotropic silicon etching and used to deliver genes to plant and mammalian cells (Trimmer, Ling et al. 1995).

2.2.1.2 Silicon microneedles

The simplest forms of the microneedles are solid spikes. Besides being solid, their unifying characteristics include being very sharp and usually have fairly simple fabrication schemes. Using a deep-reactive ion etching method, silicon microneedles were fabricated. The fabrication steps include depositing a chromium masking layer onto a silicon wafer, patterning it using photolithography into dots with the size of the desired needle base. The wafer is etched with an oxygen/fluorine plasma mixture to create the high aspect ratio silicon microneedles. These needles were used to create micron-scale holes in the skin through which molecules can be more easily transported.

Henry et al. (1998) conducted the first study to determine if silicon microneedles could be used to increase transdermal drug delivery. The penetration of microneedles through the upper layer of skin (stratum corneum) created direct pathways for molecules

that would not normally be able to diffuse through skin barrier due to size or water solubility. These microneedles as shown in Figure 2.2.3 were demonstrated to increase the permeability of *in vitro* human epidermis by 3-4 orders of magnitude.

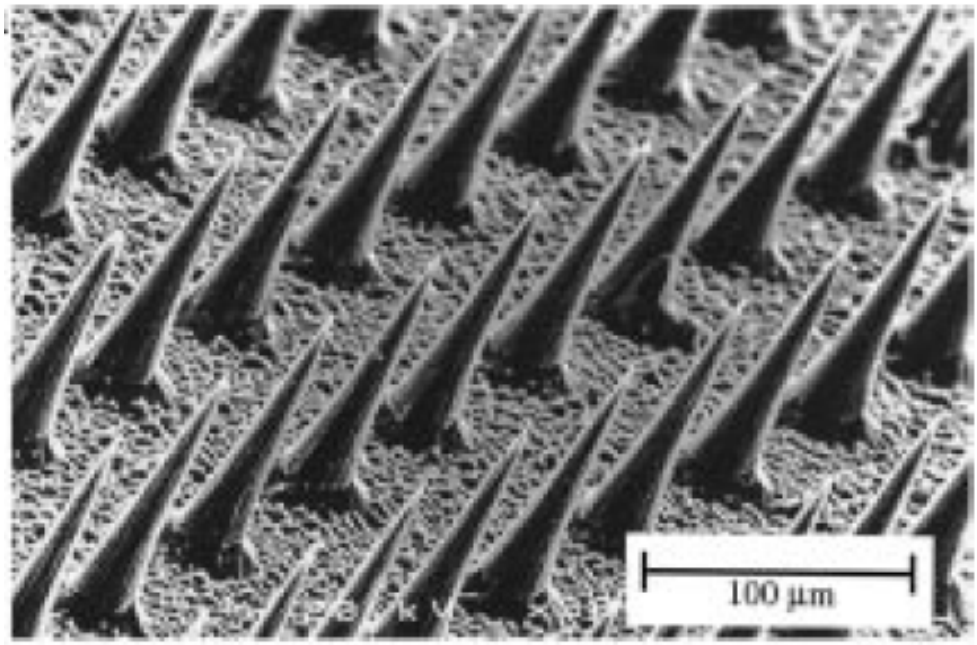

Figure 2.2.3. Arrays of solid silicon microneedles used in transdermal drug delivery study and demonstrated enhancement of dermal permeability (Henry, McAllister et al. 1998)

In a follow-up study, McAllister et al (2000) showed that epidermis permeability to calcein, fluorescently-tagged bovine serum albumin (BSA) and nanospheres can be increased up to 10,000 fold after treatment with silicon microneedles. In addition, Kaushik et al. (2001) tested the pain level associating with the insertion of silicon microneedle arrays into human skin *in vivo*. The study showed that the microneedles caused an insignificant amount of pain compared to conventional hypodermic needle insertion, and no subjects reported any adverse reactions. In a separate study, Chabri et al.

(2004) inserted silicon microneedles into human epidermal sheets *in vitro* and delivered pDNA (LPD), a nonviral gene therapy vector, into the tissue.

2.2.1.3 Metal microneedles

Metal is considered a better alternative material for microneedles since it has good mechanical strength, is relatively inexpensive and can be fabricated with ease. Solid, stainless steel microneedles can be made by a laser-cutting technique. The resulting needle structures are bent out of the sheet, and electropolished. The needles can be in either single microneedles or multi-needle array form. Martanto et al (2004) used stainless steel solid microneedles to deliver insulin to diabetic hairless rats *in vivo*. Needle arrays were inserted into the rat skin using a high-velocity injector. A solution of insulin was placed on top of the microneedle arrays and left in place for 4 h. Over this time period, blood glucose level steadily decreased by as much as 80% compared to the control subject.

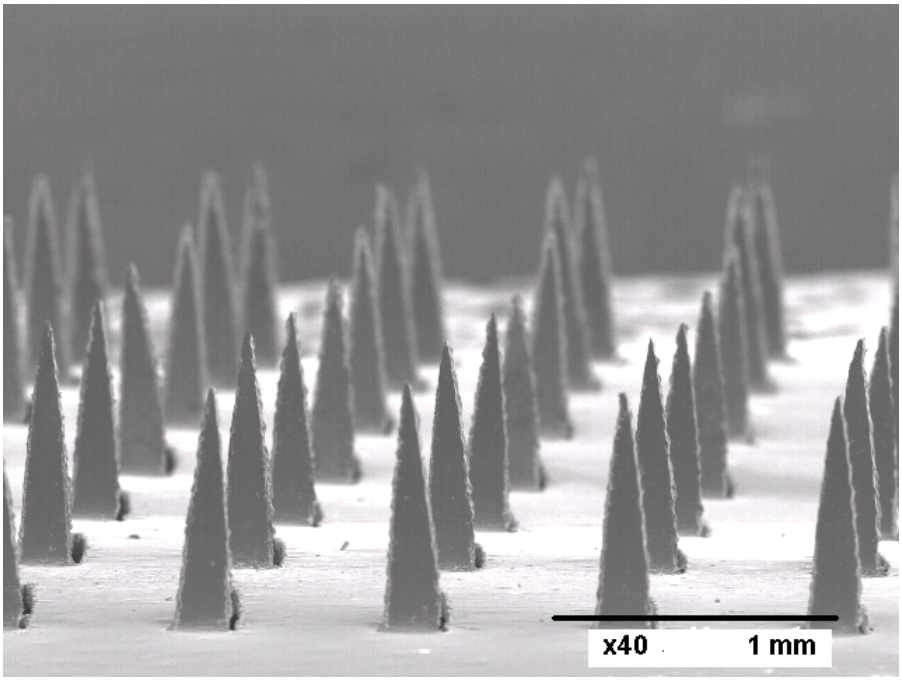

Figure 2.2.4. Solid stainless steel microneedle arrays used in an insulin delivery test using diabetic rats *in vivo* (Martanto, Davis et al. 2004).

Recently, a new delivery method associated with metal microneedles was developed. Using a formulated coating solution, different sized molecular compounds ranging from micro- (sodium fluorescein, sulforhodamine, etc.) to macro- (proteins, DNA, etc.) can be coated onto the shafts of either single metal microneedles or multi-arrays of microneedles as shown in Figure 2.2.5 (Gill and Prausnitz 2006). After insertion into the tissue, the naturally hydrophilic-coating instantly dissolves off the microneedle shafts and creates drug depots within the tissue to provide sustained release.

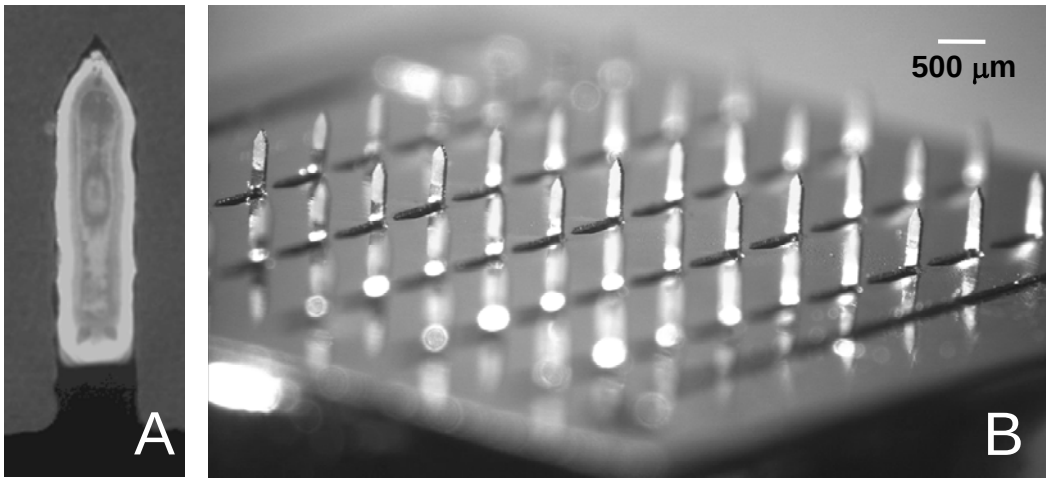

Figure 2.2.5. Images of coated solid metal microneedles. (A) shows a fluorescent image of a single microneedle coated with sodium fluorescein, NaFl, and (B) shows an multi-array of microneedles coated with calcein (Gill and Prausnitz 2006).

2.2.2 Hollow microneedles

Skin permeability can be dramatically increased by the holes created from solid microneedles insertions. However, it is still necessary to have more controlled and reproducible transport pathways to delivery drugs into the tissue. The fabrication of hollow microneedles that allow transport through the hollow shaft of the needle was based on this need. The inclusion of a hollow lumen in a microneedle structure expands its capabilities dramatically and can offer the following advantages: the ability to deliver larger molecules and particles; deliver material in a convective transport fashion (for example, pressure-driven flow) instead of passive diffusion; and minimize the cross-contamination of the deliverables and its surrounding. A variety of hollow microneedles has been fabricated and has demonstrated success in transdermal drug delivery.

2.2.2.1 Silicon hollow microneedles

The most logical technique for the inclusion of a lumen in the silicon spikes presented is the addition of an etching step to form a fluidic channel using standard photolithography and isotropic-anisotropic etching combination (Stoeber and Liepmann 2002). The fabrication steps include coating silicon dioxide on a silicon wafer, patterning the backside of the wafer and etching through the wafer stopping on the upper oxide layer to define the needle lumen. Silicon nitride was then deposited, and a larger circular mask was patterned on the front side and underetched to create the tapering effect of the microneedle. After both silicon dioxide and silicon nitride layers were removed, symmetrical and asymmetrical needle structures can be achieved by adjusting the relative position of the isotropic and anisotropic etching axis. The hollow silicon structures have been created in three-dimensional arrays out of the substrate plane. An extension of the solid pyramids of Hashmi was found to effectively withdraw blood through the lumen by capillary action (Gardnier, Berenschot et al. 2002).

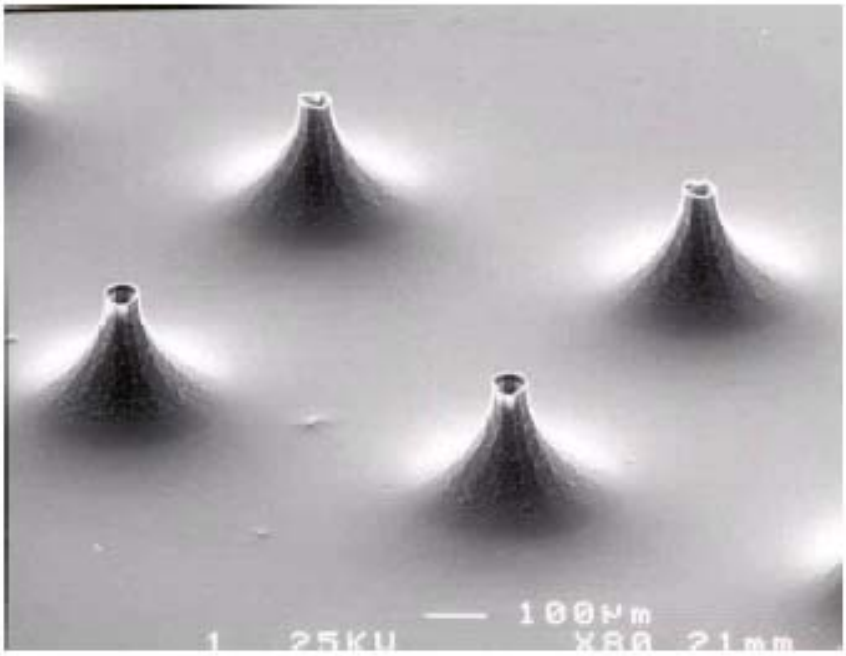

Figure 2.2.6. Arrays of symmetric silicon hollow microneedles used in fluid injection experiments (Stoeber and Liepmann 2000).

Also, an extension to the solid silicon spikes of Henry was found to deliver both larger particles (700 nm Nanospheres) and dye to chicken thighs under pressure driven flow (Stoeber and Liepmann 2000).

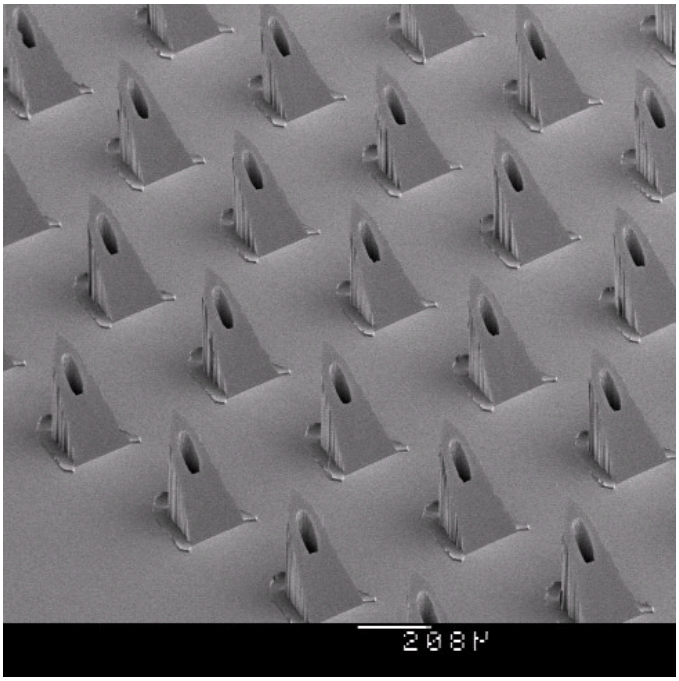

Figure 2.2.7. Arrays of hollow silicon microneedles used for transdermal liquid transport (Gardnier, Berenschot et al. 2002)

2.2.2.2 Metal hollow microneedles

Hollow metal microneedles can be creating using laser micromachining (Davis 2003). Microneedles with straight walls (i.e. that is not tapered) are fabricated using molds with cylindrical holes created either by reactive ion etching (RIE) through silicon wafers or lithographically defining holes in SU-8 photoresist polymer. A thin coating of metal was then electrodeposited onto the molds to produce the desired microneedles. Tapered hollow needle was fabricated either by obtaining a mold from a silicon master or laser drilling tapered holes into polymer sheets, followed by electrodeposition of a thin metal coating onto the mold. Davis et al. (2004) have demonstrated the insertion test using the resulting hollow, metal microneedles as shown in Figure 2.2.8.

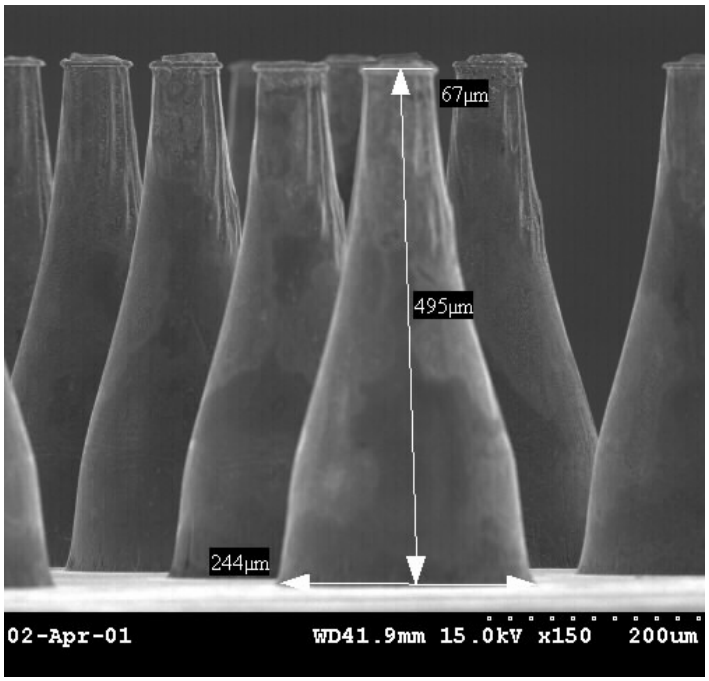

Figure 2.2.8. An array of hollow, metallic microneedles used for skin insertion test (Davis 2003).

The study reported that less insertion force was required since the interfacial area of the needle that is in contact with the skin was reduced. Additionally, these microneedles offered stronger mechanical stability. As a follow-up study, Martanto et al (2004) delivered insulin into hairless, diabetic rats *in vivo* using these hollow microneedle arrays. After 4 hours of delivery, the blood glucose levels of the rats were reduced to 47% of their original value, which indicated the successful transdermal delivery.

2.2.2.3 Glass hollow microneedles

Hollow, glass microneedles can be quickly produced with different geometric parameters for small-laboratory use. These needles are physically capable of insertion into the tissue without breaking, having a larger drug loading dose and permitting

visualization of the deliverables. Thin glass capillaries were placed within a micropipette puller, and could have either a blunt or a beveled tip, which allowed ease of needle insertion into the tissue. Coupling with an insertion apparatus, the insertion depth of the needle into the tissue can be controlled precisely.

McAllister et al. (2003) used single glass microneedles inserted into the skin of diabetic hairless rats *in vivo* to deliver insulin during a 30-min infusion period. The needles had a tip radius of 60 μm and were inserted into the tissue of a depth of 500-800 μm. The results indicated an up to 70% drop in blood glucose level over a 5-h period after the insulin was administered. Using single, beveled-tip microneedles, Martanto et al. (2006) examined the effect of different experimental parameters on microinfusion through hollow glass microneedles into human skin *in vitro*. The study reported that partial retraction of the needle within the tissue increased delivery flow rate 10-fold compared to that without retraction. Infusion rates could also be increased at a greater insertion depth, a larger infusion pressure, a beveled-tip instead of a blunt tip and the addition of hyaluronidase enzyme.

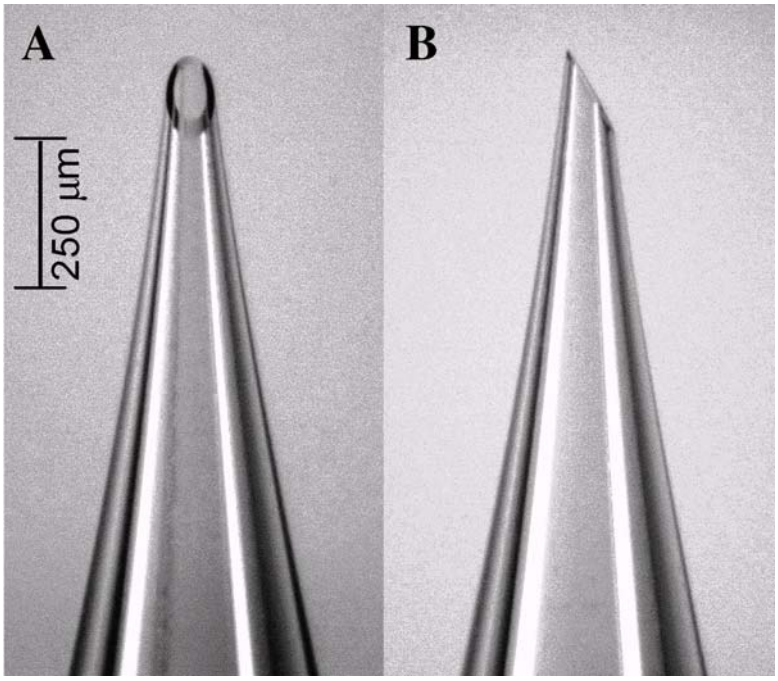

Figure 2.2.9. A single, beveled-tip, hollow glass microneedle used in microinfusion within human cadaver skin (Martanto, Moore et al. 2006).

2.2.3 Other types of microneedles

Besides solid and hollow microneedles, various other types of microneedles were fabricated using different materials such as biodegradable polymers, polysilicon and sugar with additional functionalities. Because of their biocompatible nature with the tissue, biodegradable polymer microneedles were developed (Park, Allen et al. 2006). These needles were fabricated by initially making master structures using lithography-based methods, creating inverse structures from the master molds, and finally producing replicate microneedles by melting biodegradable polymer formulations (i.e. poly-lactic acid, PLA, or poly-lactic-co-glycolic acid, PLGA) into the molds. The resulting microneedles can be loaded with molecules, drugs, DNA or proteins. Unlike solid and hollow microneedles, polymer microneedles themselves serve as the drug implants after

insertion into the tissue. Park et al. (2006) inserted the microneedles loaded with calcein or bovine serum albumin (BSA) into full thickness human cadaver skin. Strong images of the fluorescent model drugs were detected over 200 μm deep from the skin surface. Additionally, the *in vitro* release profiles of calcein and BSA ranged from hours to months depending on the formulations.

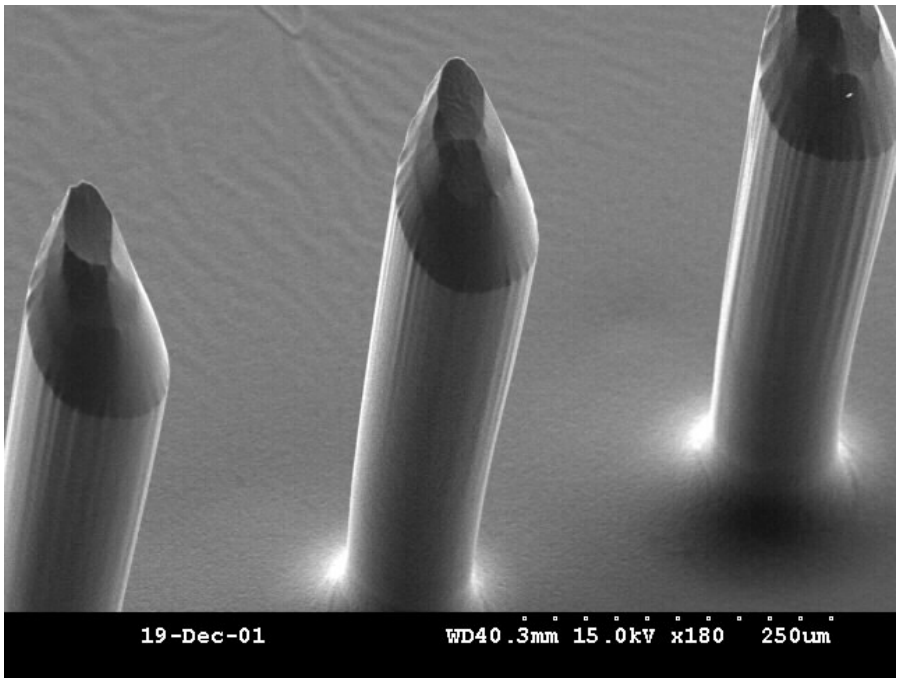

Figure 2.2.10. Solid biodegradable polymer microneedles with calcein encapsulated at the needle tips used for *in vitro* transdermal insertion test (Park, Allen et al. 2006).

Ito et al. (2006) prepared microneedles encapsulated with erythropoietin (EPO) for percutaneous administration of EPO into mice *in vivo*. Under room temperature, EPO solution was added to high concentration of polymer solution (dextrin, chondroitin sulfate or albumin) and microneedle were prepared by forming thread with polypropylene tips.

The results suggested the effectiveness and usefulness of microneedles for administration of EPO.

Microneedles made out of maltose mixed with ascorbate were developed for transdermal delivery of drugs (Miyano, Tobinaga et al. 2005). The lengths of these needles were ranging from 150 μm to 2 mm. A clinical experiment was performed to test the biosafety and basic tolerance of these microneedles. The tests showed the sugar-based microneedles spontaneously dissolved and released ascorbate into epidermis and dermis of human skin. No dermatological problems were reported.

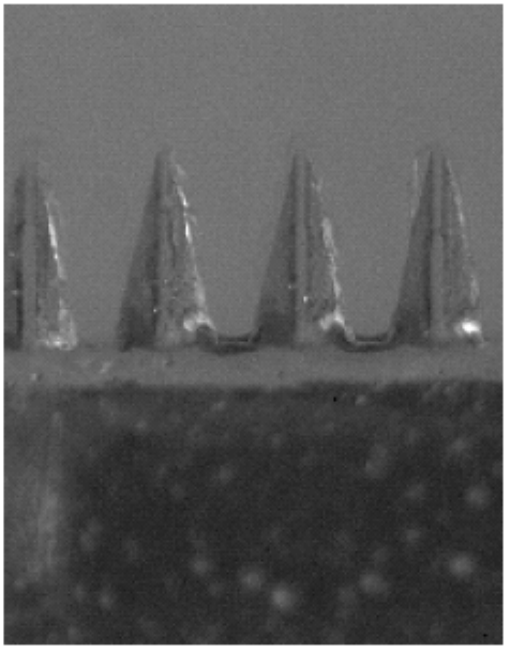

Figure 2.2.11. An array of 500 μm microneedles made out of maltose and used in transdermal insertion test (Miyano, Tobinaga et al. 2005)

Aside from being a drug delivery tool, microneedles can also be used as a biosensor. One major reason for loss of biosensor activity is through the settling of large molecular weight compounds onto the sensor and affecting senor signal stability. A

microdialysis microneedle is fabricated that is capable of excluding large MW compounds (Zahn, Trebotich et al. 2005).

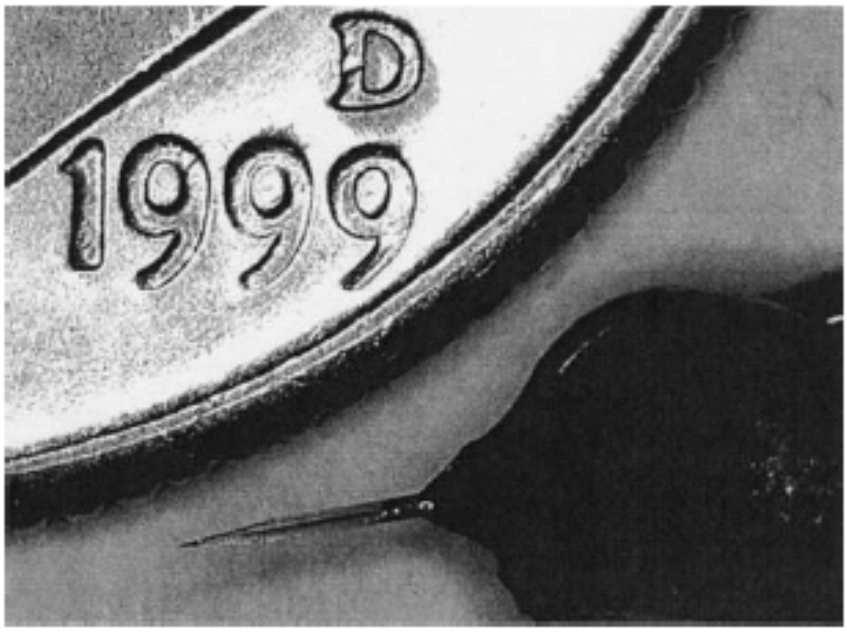

Figure 2.2.12. A microdialysis microneedle next to a dime for size comparison (Zahn, Trebotich et al. 2005).

3 MATERIALS and METHODS

3.1 Lateral diffusion within human sclera

3.1.1 Experimental methods

3.1.1.1 Lateral diffusion measurements

The lateral diffusion profile of a model drug, sulforhodamine (558 Da; Molecular Probes, Eugene, OR), was measured through human cadaver sclera using spectrofluorometry. Human sclera was obtained from the Georgia Eye Bank (Atlanta, GA) and stored in a moist container for 2 – 5 days at 4 ^{o}C. Adherent tissues associated with the retina, choroid and episclera were gently removed with cotton swabs. Strips of full-thickness sclera measuring 10 – 15 mm in length and 3 – 5 mm in width were cut from the globes using surgical scissors and razor blades.

In this study, we used human cadaver sclera, which has the advantage of being human tissue and enabling better control over the experimental system through the *in vitro* environment. Although an *in vivo* animal study would provide an improved physiological environment, this study focused on the process of diffusion within the sclera, which is governed largely by the non-living collagen and extracellular matrix structures, and did not address the effects of, for example, blood flow or other active processes.

A glass vial was filled with 1 ml of donor solution containing 9.0 x 10^{-5} M sulforhodamine in Balanced Salt Solution (BSS; Alcon Laboratories, Ft. Worth, TX). A scleral strip was suspended vertically in the glass vial such that the lower 3 mm of the tissue dipped into the donor solution (Fig. 3.1).

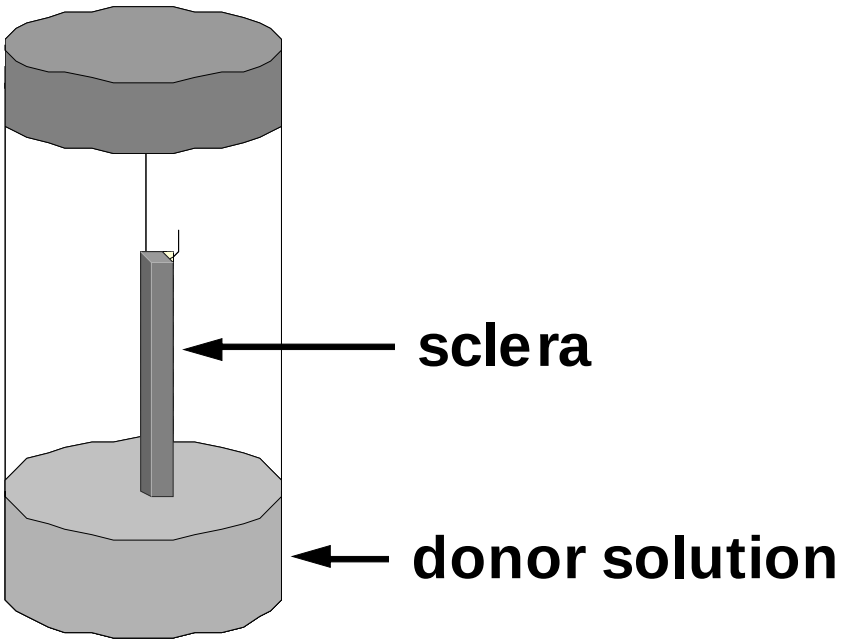

Figure 3.1. Experimental apparatus to measure lateral diffusion profiles within human cadaver sclera. A scleral strip was suspended vertically in a glass vial with the lower end of the tissue submerged in a donor solution of sulforhodamine. At different time points, the tissue was removed, rinsed, snap-frozen, sectioned, and analyzed by calibrated spectrofluorometry to determine sulforhodamine concentration in the sclera as a function of time and position.

The vial was then capped and sealed with parafilm to maintain scleral hydration and placed in a 37 ^{0}C water bath, although some tissue dehydration probably still occurred. After a designated experimental period (4, 24, 48, 72 or 168 h), the scleral strip was removed from the vial, rinsed with BSS, placed into a sample block containing OCT freezing-agent (Sakura Finetechnical, Tokyo, Japan) and snap-frozen using liquid nitrogen.

The scleral tissue was sectioned into 50μm thick pieces using a cryostat microtome (Richard Allan Scientific, Kalamazoo, MI). Every 15 consecutive pieces (750 μm) were collected as one sample. To account for the difference in scleral thickness, the first piece from each sample was examined by brightfield microscopy to determine its cross-

sectional area, which was assumed to be representative of the entire sample. The remaining 14 pieces from each sample were placed into a test tube containing 2 ml BSS and allowed to incubate in the dark at 4 ^{o}C for 12 h to extract the sulforhodamine from the tissue sections.

The solution in each tube was then placed into a cuvette ($V_{cuvette}$ = 1.8 ml) to determine its sulforhodamine concentration by calibrated spectrofluorometry (Photon Technology International, Lawrenceville, NJ) at an excitation wavelength of 565 nm and emission spectra collected at 580 – 620 nm. The sulforhodamine concentration within the tissue, C_{tissue}, was calculated using the following equation:

$$C_{tissue} = \frac{C_{cuvette} \cdot V_{cuvette}}{V_{tissue}} \qquad (1)$$

where $C_{cuvette}$ is the sulforhodamine concentration in the cuvette, determined by spectrofluorimetry, and V_{tissue} is the volume of each tissue sample, which is equal to the measured cross-sectional area multiplied by the total thickness of 14 tissue pieces analyzed per section (i.e. 700 μm). In this way, drug concentration within the tissue was determined as a function of distance along the sclera at each time point.

3.1.1.2 Trans-scleral diffusion measurements

Sulforhodamine diffusion was also measured across the sclera using a flow-through permeation chamber (Figure 3.2).

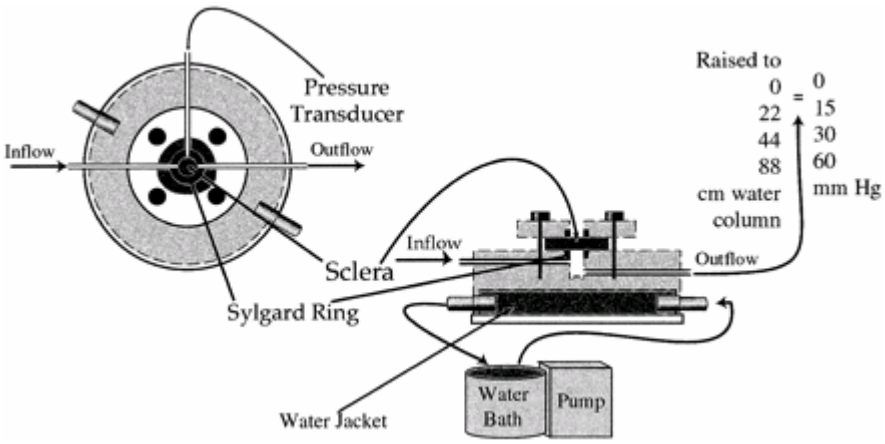

Figure 3.2. Schematic diagram of the perfusion chamber used for measuring trans-scleral permeability under simulated intraocular pressure (Rudnick, Noonan et al. 1999). Sclera is mounted in a horizontal perfusion setup while an intraocular pressure is simulated to create an outflow. The compound to be tested is added to the donor chamber. The receiver chamber has a continual flow and is magnetically stirred using a stir bar

Following the procedure described previously (Rudnick, Noonan et al. 1999), scleral disks of 10 – 15 mm in diameter were excised from human globes and mounted in two-compartment perfusion chambers. A 300 µl depot of 9.0 x 10^{-5} M sulforhodamine donor solution was added to the episcleral surface while perfusing BSS across the choroidal side. Every 1 h, a fraction containing 2 ml of the perfusate was collected over a 24 h period and its fluorescence concentration was measured by spectrofluorimetry. From these measurements, the effective transverse diffusivity (D_{trans}) was calculated as:

$$D_{trans} = \frac{C_{cuvette} \cdot V_{cuvette} \cdot d}{C_{donor} \cdot A \cdot \Delta t} \qquad (2)$$

where d is scleral thickness (0.6 mm) (Olsen, Edelhauser et al. 1995), A is the scleral surface area exposed to donor solution (0.37 cm^2), Δt is sampling time (1 h) and C_{donor} is the sulforhodamine concentration in the donor solution, which was initially at 9.0 x 10^{-5} M and decreased over time; this effect was accounted for by correcting C_{donor} in the

calculation using Eq. 2. The trans-scleral permeability coefficient can be obtained by dividing the transverse diffusivity by scleral thickness (Edwards and Prausnitz 1998).

3.1.1.3 Sclera-to-saline distribution coefficient

An additional experiment was performed to determine the sclera-to-saline distribution coefficient to examine possible binding between sulforhodamine and scleral tissue. A full-thickness scleral strip was submerged in a 9.0 x 10^{-5} M sulforhodamine donor solution for 24 h. After removing the tissue and rinsing with BSS, the tissue was sectioned into 50-μm thick pieces using a cryostat. All tissue pieces were collected and incubated in 20 ml of BSS. The sulforhodamine concentration in the BSS was measured over time using spectrofluorometry until it reached a constant value (after ~1 h). Assuming 100% sulforhodamine extraction efficiency, the sclera-to-saline distribution coefficient (K_D) was obtained as:

$$K_D = \frac{C_{sclera}}{C_{bath}} \qquad (3)$$

where C_{sclera} is the concentration in the sclera determined by extraction, and C_{bath} is the original concentration of the donor solution (9.0 x 10^{-5} M).

3.1.2 Theoretical modeling

A theoretical model was developed to predict the concentration of sulforhodamine as a function of both time and distance during lateral diffusion within human sclera. A one-dimensional model was justified by the geometry of the experimental set-up, which was symmetric in both of the horizontal dimensions of the scleral strip and only provided a concentration-gradient driving force for diffusion in the vertical direction (Fig. 1). We

further recognized that the sulforhodamine could be present within sclera in two forms: (i) free sulforhodamine that can diffuse and (ii) bound sulforhodamine immobilized at binding sites in the scleral tissue. Previous studies have suggested that compounds structurally similar to sulforhodamine bind within sclera (Prausnitz, Edwards et al. 1998).

Transient, one-dimensional diffusion with binding in a semi-infinite slab can be modeled mathematically as (Cussler 1997)

$$\frac{dC_{free}}{dt} = D_{lat}\frac{d^2C_{free}}{dx^2} - k_1(C_{free} - K_{eq}C_{bound}) \qquad (4)$$

$$\frac{dC_{bound}}{dt} = k_1(C_{free} - K_{eq}C_{bound}) \qquad (5)$$

where C_{free} is the free sulforhodamine concentration in the sclera, C_{bound} is the bound sulforhodamine concentration in the sclera, k_1 is the binding rate constant, D_{lat} is the effective lateral diffusivity of free sulforhodamine in the sclera, x is the lateral position in the sclera, and K_{eq} is the ratio of free-to-bound sulforhodamine at equilibrium in sclera

$$K_{eq} = \frac{C_{free}}{C_{bound}} \qquad (6)$$

To evaluate bound versus free sulforhodamine in the sclera, the sclera-to-saline distribution coefficient (Eq. 3) can be re-expressed as

$$K_D = \frac{C_{sclera}}{C_{bath}} = \frac{C_{free} + C_{bound}}{C_{bath}} \qquad (7)$$

Because the liquid phase of sclera is composed of saline of similar composition to that of the surrounding bath, we can assume C_{free} is equal to C_{bath}. Thus,

$$K_D = 1 + \frac{C_{bound}}{C_{free}} = 1 + \frac{1}{K_{eq}} \qquad (8)$$

Using Eq. 8, as well as the assumption that sulforhodamine binding in the sclera is at equilibrium ($C_{free} = K_{eq} \cdot C_{bound}$), Eqs. 4 and 5 can be rewritten as:

$$\frac{d(C_{free} + \frac{C_{free}}{K_{eq}})}{dt} = D_{lat} \frac{d^2 C_{free}}{dx^2} \tag{9}$$

Rearranging Eq. 9 yields the following expression:

$$\frac{dC_{free}}{dt} = D_{lat} \frac{K_{eq}}{1 + K_{eq}} \frac{d^2 C_{free}}{dx^2} \tag{10}$$

To solve Eq. 10, the initial and boundary conditions are:

$$\begin{aligned} C_{free}(x,0) &= 0 \\ C_{free}(0, t) &= C_{donor} \cdot K_D \\ C_{free}(z, t) &= 0 \end{aligned} \tag{11}$$

where z is the length of the scleral strip above the donor solution. Solving Eq. 10 subject to the conditions in Eq. 11, yields the final expression for sulforhodamine concentration in the sclera as a function of time and position (Cussler 1997):

$$C_{free}(x,t) = C_{donor} \cdot K_D \cdot [1 - erf \frac{x}{\sqrt{4 \cdot D_{lat} \cdot t \frac{K_{eq}}{1 + K_{eq}}}}] \tag{12}$$

where *erf* is the error function.

3.1.3 Statistical analysis

Mean absolute percent error (MAPE) was used to statistically analyze the difference between theoretical predictions and experimental data. MAPE is calculated by averaging the percentage difference between fitted (predicted) values and experimental data.

$$MAPE = \sum \left| \frac{C_{\exp} - C_{theor}}{C_{\exp}} \right| \cdot \frac{1}{n} \cdot 100\% \qquad (13)$$

where C_{exp} is the experimentally measured concentration, C_{theor} is the theoretically predicted concentration, and n is the number of measurements.

3.2. Ocular drug delivery using coated solid microneedles

3.2.1 Microneedle fabrication

Single solid metal microneedles were fabricated using an infrared laser (Resonetics Maestro) to cut needle structures from stainless steel sheets (SS 304, 75 μm thick; McMaster-Carr, Atlanta, GA). The shape and orientation of microneedle structures were initially drafted in a CAD file (AutoCAD; Autodesk, Cupertino, CA), which was converted to the file type required by the laser control software (Oregon Microsystems, Beaverton, OR). The laser beam traced the desired pattern of the needle that ablated the metal sheet and created the microneedles within the plane of the sheet.

To deburr and sharpen the microneedle edges, electropolishing was applied after laser cutting. The metal sheet with needles on it was cleaned using hot soapy water (Alconox, White Plains, NY) and rinsed with DI water. Each needle was then manually bent out of the sheet at 90^{o}. The sheet was then placed into a 1:3:6 v/v mixture of water, phosphoric acid and glycerin (Fisher Scientific) to remove debris. The mixture was maintained at 70 ^{o}C and stirred at 150 rpm using a magnetic stirring bar, while the sample sheet was manually agitated during the electropolishing process. After 20 minutes of polishing, the sheet was rinsed in DI water for 10 seconds followed by another 10 seconds each in 20% nitric acid (VWR, West Chester, PA) and in hot water. This rinsing

cycle was repeated 3 times. After electropolishing, each microneedle was manually detached from the metal sheet using a pair of scissors.

3.2.2 Microneedle coating

Using a previously described coating method (Gill and Prausnitz 2006), single, solid stainless steel microneedles could be coated with different molecular compounds in a formulated coating solution. The coating dose onto each microneedle is dependent on various factors, including the composition of coating solution, the number of needle dips into the solution and the duration of leaving the needle within the solution. Each single microneedle was mounted individually onto a micropositioner in a manually assembled coating apparatus, and dip-coated horizontally into a large-orifice pipette tip containing the coating solution. Each dipping step lasted for 3 seconds and the coating procedure was repeated 5 times for each microneedle coating. The entire procedure was performed under a stereomicroscope. In this study, the coating solution was comprised of 10% (w/v) poly-vinyl-pyrrolidone (PVP) (1300 kDa; Sigma-Aldrich, St. Louis, MD) and a coating compound. For *in vitro* experiments, the coating compound was 0.05% (w/v) sulforhodamine (558 Da; Molecular Probes, Eugene, OR), 1% fluorescein-labeled bovine serum albumin (Molecular Probes) and 0.05% gWiz^{TM} luciferase plasmid DNA (6732 base pairs, Aldevron, Fargo, ND). DNA was made fluorescent by incubating with YOYO-3 (Molecular Probes) at a dye:base pair ratio of 1:4 for 1 h at room temperature in the dark. For *in vivo* experiments, the coating compounds were 0.5% (w/v) sodium fluorescein, NaFl, (376 Da; Sigma-Aldrich, St. Louis, MO) and 10% (w/v) pilocarpine hydrochloride (243 Da; Sigma-Aldrich).

To determine the dose of compound coated onto the microneedle, coated microneedles were placed into cuvettes containing 2 ml of phosphate-buffered saline, PBS, (Mediatech, Inc., Hernodon, VA), which allowed the coating solution to dissolve off the needle shaft. The compound concentration in each cuvette was then measured using either spectrofluorometry (Photon Technology International, Lawrenceville, NJ) for fluorescein-labeled molecules or UV spectrometry (Molecular Devices, Sunnyvale, CA) for pilocarpine molecules. The coating dose was then calculated as following:

$$\text{Coating dosage} = C_{cuvette} * V_{cuvette} * MW_{compound} \qquad (14)$$

where $C_{cuvette}$ is the measured molar compound concentration in the cuvette, MW is the molecular weight of the compound and $V_{cuvette}$ is the volume of PBS solution in the cuvette.

3.2.3 In vitro coated microneedle insertion

Human sclera was obtained from the Georgia Eye Bank (Atlanta, GA). Pieces of sclera tissue (0.7 x 0.7 cm) were cut from scleral globe using surgical scissors, rinsed with water, and adherent tissues associated with the retina, choroid and episclera were removed with cotton swab. The scleral tissue was placed on top of a hemi-sphere surface (0.6 cm in radius), which simulated the curving ocular shape. Even though solid metal microneedles showed successes in previous transdermal insertion tests, they have never been tested in ocular tissues. To examine whether solid microneedles are strong enough to penetrate into the sclera, single non-coated microneedles were manually pierced into human cadaver sclera. The insertion site was then stained with blue tissue dye (tissue marking Dye; Shandon, Pittsburg, PA) for visual examination. In the later

phase, single sulforhodamine-coated microneedles were manually pierced into the sclera. The needles were left within the tissue for 20 sec after insertion to allow the coating solution to dissolve off. Upon needle removal, the excess sclera tissues around the insertion site were trimmed away using a surgical blade. The resulting tissue pieces were placed in sample blocks containing OCT freezing-agent (Sakura Finetechnical, Tokyo, Japan) and snap-frozen using liquid nitrogen. Each scleral tissue was sectioned into 10-μm thick pieces using a cryostat microtome (Richard Allan Scientific, Kalamazoo, MI). Histological pieces were collected onto glass slides, and examined using a fluorescent microscope (Olympus X70).

3.2.4 In vivo coated microneedle insertion

3.2.4.1 Fluorescein-coated microneedle

A single New Zealand white rabbit (1.8-2.2 kg) was used in this study. The animal was kept in the cage and fed with food and water on a daily basis. Prior to microneedle insertion, the animal was anesthetized using intramuscular injection of 5 mg/kg xylazine (Butler, Columbus, OH) and 35 mg/kg ketamine (Bedford laboratories, Bedford, OH). A single NaFl-coated solid microneedle (500 μm in length, 45^{o} in tip angle) coated with 0.3 μg of NaFl was manually inserted half-way into the upper region of the rabbit cornea, to prevent possible leakage of the aqueous solution from the rabbit eye. The needle was held steady within the cornea tissue for 2 minutes before removal. The fluorescein concentration in the anterior part (cornea, aqueous humor and lens) of the eye was measured periodically using a fluorometer (Ocumetrics, Mountain View, CA) at 0, 0.5, 1, 2, 3, 4, 5, 6 and 24 hours after insertion. This fluorometer delivered a

specifically focused excitation beam of blue light using an optic head into the ocular cavity and then received the resulting fluorescent green light and directed it into a photodetector. By changing the focal plane every 0.25 mm, sequential readings of the fluorescein concentration were obtained along an axis from the lens in the eye to a position anterior to the cornea.

The fluorescein concentration in the non-inserted eye was also monitored as the negative control. The animal was brought back to the cage, given a 24 h recovery period, and same experiment was applied to the other eye. As the positive control, a drop of NaFl solution that used for coating was applied topically to the rabbit eye, and the fluorescein concentration in the eye was measured over same time periods.

3.2.4.2 Theoretical estimation of microneedle delivery efficiency

To estimate the delivery efficiency by a single, fluorescein-coated microneedle in the *in vivo* animal study, a mass balance of fluorescein in the aqueous humor of the rabbit eye was performed as shown in Eqn. (15):

$$M_{in} = M_{out} + M_{accumulated} \tag{15}$$

where M_{in} is the mass inflow rate of fluorescein, M_{out} is the mass outflow rate of fluorescein, and $M_{accumulated}$ is the mass of fluorescein accumulated within the aqueous humor over each time increment. Assuming the volumetric fluorescein outflow rate is as same as the aqueous humor production rate, M_{out} can be calculated as:

$$M_{out} = C_{fluo} * v_s \tag{16}$$

where C_{fluo} is the fluorescein concentration leaving the aqueous humor, which is equivalent to the experimental measurement assuming the fluorescein concentration is

uniform throughout the aqueous humor, and v_s is the aqueous humor production rate, which is reported as 0.0042 – 0.0045 ml/min in the rabbit eye (Fatt and Wissman 1992). The fluorescein accumulation term can be estimated as

$$M_{accumulated} = \frac{dM_{fluo}}{dt} = \frac{d(VC_{fluo})}{dt} \cong \frac{V\Delta C_{fluo}}{\Delta t} \qquad (17)$$

where ΔC_{fluo} is the change of fluorescein concentration in the aqueous humor between two time points, V is the aqueous humor volume, which is about 0.3 ml in the rabbit eye (Girgis, Reed et al. 2005) and Δt is the time change.

By substituting Eqn. (16) and (17) into Eqn (15), the mass in-flow rate of fluorescein, M_{in}, at each measurement time is estimated as

$$M_{in} = C_{fluo} * v_s + \frac{V\Delta C_{fluo}}{\Delta t} \qquad (18)$$

and the total amount of fluorescein entered the aqueous humor is equal to

$$M_{in,total} = \sum_{n}^{i} M_{in_n} * t_n \qquad (19)$$

in which i is the total number of measurement points, n is the corresponding measurement point and t is the time of the measurement.

3.2.4.3 Pilocarpine-coated microneedle

To assess whether microneedle can deliver drug molecules into the eye, we coated microneedles with a commercially used drug, pilocarpine, which causes pupil contraction and is used to treat glaucoma (Lee and Higginbotham 2005; Uva, Longo et al. 2006). All the insertion experiments were carried out in a bright room with consistent light intensity. After anesthetizing the rabbit, five single pilocarpine-coated solid microneedles (500 μm

in length, 45^{o} in tip angle, each needled coated with 1.1 ± 0.5 μg pilocarpine) were inserted halfway into the rabbit cornea individually. The needles were spaced radially with an even pattern of spacing between the insertion points. Each needle was left within the cornea 20 seconds before removal. The diameter of the rabbit pupil was then measured every minute for half an hour, continued on an hourly basis for 4 hours after microneedle insertion, and the corresponding image was captured with a digital camera (Canon U.S.A. Inc.). The pupil sizes of the other eye were measured at the same time points as the untreated control. As another control, a drop of pilocarpine (Sigma-Aldrich) solution at equivalent dose to the microneedle coating was topically applied to the eye. In addition, a positive control consisted of one drop of 1% ophthalmic pilocarpine solution (Falcon Pharmaceuticals, Ltd., Fort Worth, Texas) applied to the rabbit eye.

3.2.5 Safety examinations

Single uncoated solid microneedles were inserted into the rabbit cornea after the animal was anesthetized. A slit-lamp examination was used to examine the microneedle insertion site. Before each measurement, a droplet of fluorescein solution (0.5% w/v) was applied topically to the insertion site of the eye, which helped to identify the insertion gap. The rabbit eye was examined for cell and flare responses for any possible inflammation at 0, 1, 2 3, 4 and 24 hr after insertion.

3.3. Microinfusion using hollow microneedles

3.3.1 Tissue preparation

Human cadaver eyes were obtained from the Georgia Eye Bank (Atlanta, GA) and stored in moist container at 4 ^{o}C for 2-7 days before use. A piece of sclera tissue (1 x 1 cm) was cut from the globe using surgical scissors. Adherent tissues associated with the retina, choroid and episclera were gently removed with cotton swabs. The sclera tissue was soaked in water for 5 min prior to each infusion experiment to retain its physiological hydration level. The scleral piece was placed onto a hemi-spherical surface (0.6 cm in radius) that was obtained by cutting off the end of a polystyrene round-bottom flow tube (BD Falcon^{TM}, Bedford, MA), which mimics the ocular curvature.

3.3.2 Microneedle fabrication

Single, hollow, glass microneedles were used in this study. Using a previously described method (Martanto, Moore et al. 2006), these microneedles were fabricated using a micropipette puller. Fire-polished borosilicate glass pipettes (o.d. 1.5 mm, i.d. 0.86 mm, B150-86-15, Sutter Instrument Co., Novato, CA) were pulled using a micropipette puller (P-97, Sutter Instrument) and detached into two halves at desired settings. These blunt-tip microneedles were then beveled at a setting of 20^{o} tip angle using a glass grinder (BV-10, Sutter Instrument). Each needle was connected to a 3 ml syringe by a small piece of tubing, dipped into a chromic acid bath (Mallinckrodt, Hazelwood, MO) while blowing air through the needle shaft for 15 sec, and followed by the same procedures using DI water and acetone (J.T. Baker, Phillipsburg, NJ) for 15 sec each. The resulting microneedles were examined using bright field microscopy (Leica

DC 300; Leica Microsystems, Bannockburn, IL) and image analysis (Image Pro Plus, Media Cybernetics, Silver Spring, MD).

3.3.3 Experimental apparatus

A 1-ml glass syringe (Gastight Syringe, Hamilton Company, Reno, NV) was used as the delivering solution reservoir. One end of the syringe was connected to a high-pressure CO_2 tank (Airgas, Radnor, PA), and the other end was connected to a 2.1-mm-i.d. metal tubing line, which was connected to the end of a glass microneedle by a flexible tube linker. A pressure regulator (Two-Stage Regulator, Fisher Scientific, Hampton, NH) was used to adjust pressure during the delivery. A custom-made device (Wang, Cornwell et al. 2005) was designed to hold the needle. In a controllable fashion, the microneedles could be inserted into and retracted within the scleral tissue by rotations (i.e., 1 full rotation equals 1440 μm in microneedle displacement). The entire assembly was held by a stainless-steel adapter mounted to a Z-stage (Graduated Knob Unislide, Velmex, Bloomfield, NY) to control the vertical motions of the microneedle holder.

3.3.4 Infusion of sulforhodamine solution

Sulforhodamine (558 Da; Molecular Probes, Eugene, OR), which serves as a model drug and a visual marker for fluid flow, was added to phosphate buffered saline (PBS) to make a 1 x 10^{-3} M sulforhodamine solution to be delivered into the human sclera tissue. The solution was loaded into the glass syringe of the apparatus using a 5-ml syringe. Single, bevel-tipped, microneedles were then inserted and delivered

sulforhodamine solution into human cadaver sclera at a constant pressure (5, 10, 15, 20 and 25 psi).

In the human eye, the sclera is relatively thick near the limbus (0.53 ± 0.14 mm); it thins at the equator (0.39 ± 0.17 mm) and becomes substantially thicker near the optic nerve (0.9 to 1.0 mm) (Olsen, Aaberg et al. 1998). To examine the effect of scleral thickness on volume delivery, the sclera was divided into 3 different regions around the globe: front (near the limbus), middle (at the equator), and back (near the optic nerve). The microneedles were initially inserted into the tissue at a depth of 700 – 1080 μm, and retracted out of the tissue in increments of 60 μm. Throughout the experiments, the volumetric delivery of sulforhodamine solution was monitored by the movement of the gas-fluid meniscus in the glass syringe, and the differences were recorded between each retraction. The infusion was immediately stopped when a retraction caused leakage of sulforhodamine solution to be first seen on the surface of the tissue.

3.3.5 Delivery of nanoparticles

To determine if hollow microneedles can deliver nanoparticles into the sclera, nanospheres were added to 1 ml PBS solutions at solid contents of 0.5, 1, 5 and 10 wt %, and delivered into the sclera at 15 psi. Provided courtesy of Dr. Uday Kompella (University of Nebraska), these nanospheres, made out of poly-lactic acid (PLA), had an effective diameter of 278 ± 13 nm and encapsulated Nile Red within the particle. A previous study reported that only 0.4% Nile Red was released from PLA nanoparticles over 28 days (Bourges, Gautier et al. 2003). The particles were dispersed in PBS solution and vortexed for further suspension. Due to the limited quantity of nanospheres available,

each microneedle was then preloaded with just 20 μl nanosphere solution, inserted into each region on the sclera and delivered into the tissue using same insertion and retraction procedures described above for sulforhodamine solution infusion.

3.3.6 Delivery of microparticles

Solid latex, fluorescein-labeled microspheres (1.0 micron in diameter, Polysciences Inc., Warrington, PA) were added to 1 ml PBS solutions at solid contents of 0.3, 1.3 and 2.6 wt% for infusion delivery. A drop of 5 μl polyoxyethylenesorbitan monooleate (Tween 80, Sigma Chemical Co., St. Louis, MO) was then added to each solution to reduce the surface tension and enhance the microparticle stability within the solution. The mixture was then vortexed and ultrasonicated to ensure the microspheres were suspended without clumping within the solution. Single hollow glass microneedles, preloaded with 20 μl microsphere solution, were inserted into each region on human sclera tissue for delivery as described above.

3.3.7 Effect of collagenase and hyaluronidase

Two types of experiments were performed to examine the effect of hyaluronidase, an enzyme known to break down the glycosaminoglycans (GAGs) in the scleral extracellular matrixes, on scleral delivery using hollow microneedles: first, the scleral tissue was soaked in a 200 U/ml hyaluronidase solution (Vitrase, 200 U/ml, ISTA Pharmaceuticals, Irvine, CA) for 1 h prior to microneedle injection and later infusion experiments were performed; and second, hyluronidase solution was mixed with the injectable solution and delivered into the sclera by hollow microneedles. Collagenase

type I (Sigma Aldrich, St. Louis, MO), which is known to break down type I collagen fibers, was also tested for possible enhancement of particle delivery within the sclera. Same experimental procedures were carried out.

3.3.8 Histological and microscopic image analysis

After each microneedle infusion experiment, the backside of each scleral tissue was examined under bright-field microscope (Leica DC 300) to ensure that no solution leakage occurred on the back of the tissue. To visualize the microneedle penetration pathways and the distribution of solution within the sclera, histology was used. Scleral tissues after microneedle infusions were immediately rinsed with water to wash off the residue solution on the tissue surface. Tissues were then placed into sample blocks containing freezing agent (OCT; Sakura Finetechnical, Tokyo, Japan) individually, and snap frozen with liquid nitrogen. Each tissue sample was sectioned into 10 μm thick pieces using a cryostat microtome (Richard Allan Scientific, Kalmazoo, MI) and was collected into consecutive sections onto glass slides. Each histological section was then examined using both bright-field (Leica DC 300) and fluorescence microscopy (Eclipse E600W, Nikon, Melville, NY).

3.3.9 Statistical Analysis

Replicates of microneedle infusion experiments were performed at each different condition (scleral position and pressure), from which the mean and standard deviation were calculated. A one-way analysis of variance (ANOVA, $\alpha = 0.05$) was used to

examine the impact of scleral position and pressure on the dose delivery. In all cases, a value $p < 0.05$ was considered statistically significant.

4 RESULTS

4.1 Lateral diffusion within human sclera

4.1.1 Introduction

Targeted administration of drugs to the posterior segment of the eye remains a significant challenge in ocular drug delivery. Current treatment strategies include systemic delivery, by oral or parenteral routes, and local delivery using topical drops, subconjunctival and peribulbar injections, intravitreal injections, and implants (Lang 1995; Geroski and Edelhauser 2000). However, none of these approaches provide fully satisfactory ocular delivery to the posterior part of the eye.

Systemic delivery is often accompanied by side effects because of the high drug doses needed to reach the target tissues within the eye. Topical drops through cornea generally cannot achieve adequate drug concentrations in the posterior segment due to slow diffusion across the cornea to the back of the eye, blinking and counterproductive convection of tear fluid and aqueous humor (Lang 1995; Tasman 1995). While intraocular injection and implants can provide delivery targeted to the posterior segment, they can lead to complications such as retinal detachment, hemorrhage, endophthalmitis and cataract, especially when repeated injections are required (Tasman 1995; Maurice 2001).

Because of these limitations, there is growing interest in drug delivery across the sclera, which avoids the complications associated with penetrating the globe and the diffusional barrier of the cornea (Geroski and Edelhauser 2000). The sclera's large surface area, which averages 17 cm^2 on the human eye (Olsen, Aaberg et al. 1998), is approximately 20-fold larger than cornea. Moreover, sclera is much more permeable,

especially to large and hydrophilic drugs (Maurice and Polgar 1977; Olsen, Edelhauser et al. 1995). Conventional subconjunctival and peribulbar injections provide access to the trans-scleral route. Novel delivery systems, involving implants, gels and patches applied to the scleral surface and intrascleral injections are being developed to enable extended-release and better-targeted drug delivery via the sclera (Geroski and Edelhauser 2000).

Motivated by these opportunities, a number of studies have examined rates of diffusion across the sclera as a function of molecular size and other parameters (Prausnitz, Edwards et al. 1998; Ambati, Canakis et al. 2000; Cruysberg, Nuijts et al. 2002; Gilbert, Simpson et al. 2003; Mora, Eperon et al. 2005). However, little attention has been given to diffusion within the sclera in the lateral direction parallel to the scleral surface, which could affect drug distribution caused by lateral spread of drug released, for example, from an extraocular implant or intrascleral injection. The non-isotropic architecture of collagen lamellae and other features of scleral microanatomy (Fatt and Weissman 1992) suggest that lateral diffusion may behave differently from trans-scleral diffusion.

To address this issue, this study presents the first experimental measurements of lateral diffusion within the sclera using sulforhodamine as a model drug and provides a theoretical model that predicts the diffusion profile as a function of both time and distance along the sclera. Lateral diffusivity values are also compared to transverse diffusivity across sclera to identify possible differences.

4.1.2. Imaging lateral diffusion within the sclera

An initial experiment was carried out to provide visual images showing the progression of sulforhodamine diffusion along the sclera as a function of time and

position. Fig. 4.1 shows representative cross-sectional views of sclera frozen after 24 h of sulforhodamine diffusion and then sectioned for viewing by fluorescence microscopy. Within each scleral slice, the sulforhodamine concentration appears uniform, which indicates that vertical diffusion occurred at the same rate, independent of position in the horizontal direction. This observation is consistent with modeling sulforhodamine diffusion as a one-dimensional process. Scleral sections collected further from the sulforhodamine donor solution show progressively lower sulforhodamine concentrations over the ~1 cm scleral strip.

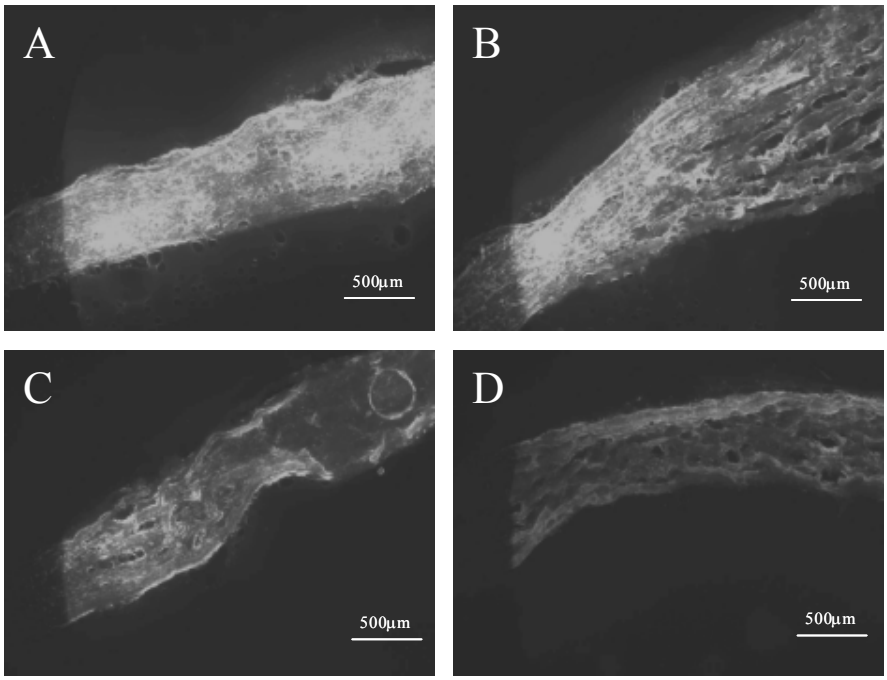

Figure 4.1.1. Representative cross-sectional views of human cadaver sclera containing sulforhodamine imaged by fluorescence microscopy. One end of the sclera (A), which had been submerged in a sulforhodamine donor solution for 24 h, contains a large concentration of the model drug. Progressively less sulforhodamine is seen in scleral sections located further away at distances of (B) 3.25 mm, (C) 6.50 mm and (D) 9.75 mm from the donor solution.

4.1.3. Quantifying lateral diffusion within the sclera

To quantify the lateral diffusion profile within the sclera, sulforhodamine concentration was measured in the scleral sections as a function of both time and distance along the sclera. Figure 3 shows the resulting concentration profiles over a distance of 11 mm along the sclera at time points between 4 h and 1 week (i.e., 168 h). After 4 h, sulforhodamine diffusion was detected at a distance up to 5 mm along the sclera. After 1 week, sulforhodamine diffused further than 1 cm along the sclera. At each time point, concentration decreased with increasing distance (analysis of variance ANOVA, $p < 0.0001$), which is consistent with the pattern seen in Figs. 2 and 3. Over time, the sulforhodamine concentration at each position increased with time (ANOVA, $p < 0.0001$).

4.1.4. Determining lateral diffusivity

To determine the effective lateral scleral diffusivity of sulforhodamine from the data in Fig. 3, we employed a theoretical model of one-dimensional diffusion (Eq. 12). As parameters for this model, we measured the sclera-to-saline distribution coefficient, $K_{D,}$ experimentally to be 13.6, which indicates a strong binding between sulforhodamine molecules and the sclera tissue. The free-to-bound sulforhodamine ratio, K_{eq}, was then calculated to be 0.08 using Eq. 8. This left sulforhodamine diffusivity, D_{lat}, as the only unknown variable. The diffusion model was then fitted to the experimental data, as shown in Fig. 4, which yielded an effective sulforhodamine diffusivity of $D_{lat} = 3.82 \times 10^{-6}$ cm^2/s.

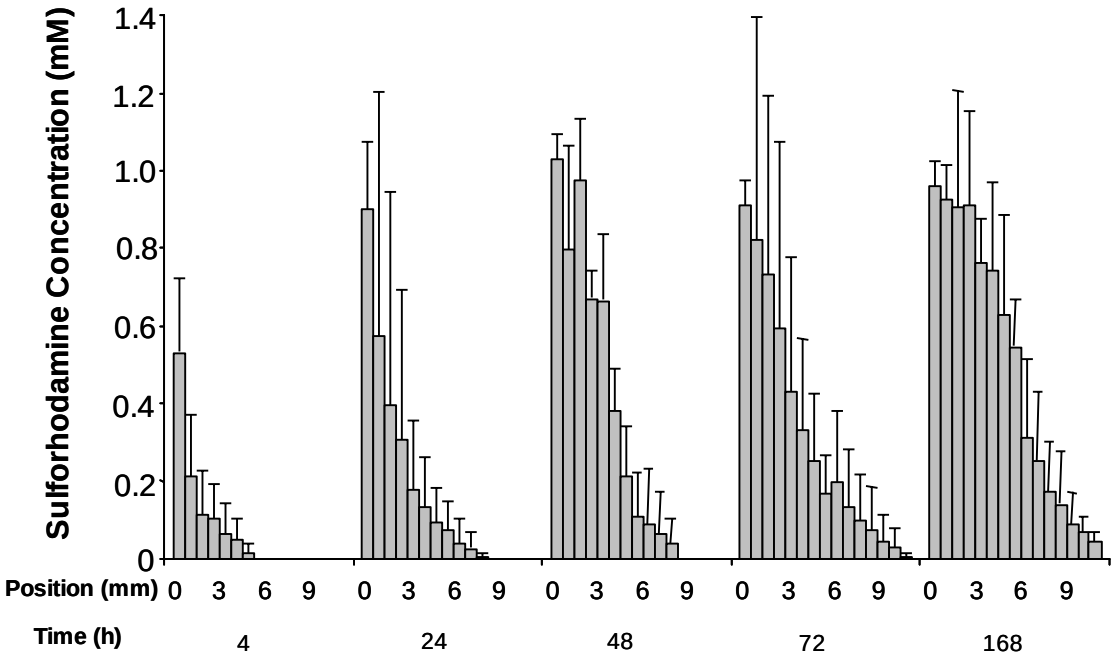

Figure 4.1.2. Lateral diffusion profiles of sulforhodamine in human cadaver sclera as a function of time and position. At each time point, the spatial distribution of sulforhodamine is shown, where the bar on the left of each set corresponds to sclera bathed in the donor solution and each consecutive bar to the right corresponds to 750 μm increments in position away from the donor solution. Average values with standard error bars are shown for n = 3 replicates.

Visually, the predicted curves in Fig. 4.3 capture the trend of the data, but show some disagreement. The quality of this fit can be gauged quantitatively by its mean absolute percent error of MAPE = 39%, which indicated that predicted values were on average within 39% of experimental values. This uncertainty can be compared to the average standard error associated with experimental measurement (i.e., average of error bars in Fig. 4.2), which was calculated to be 60%. Thus, the error associated with the experimental measurements is greater than the disagreement between the theoretical model and the experimental data. This means that the theoretical model predictions are as good as possible given the uncertainty in the data.

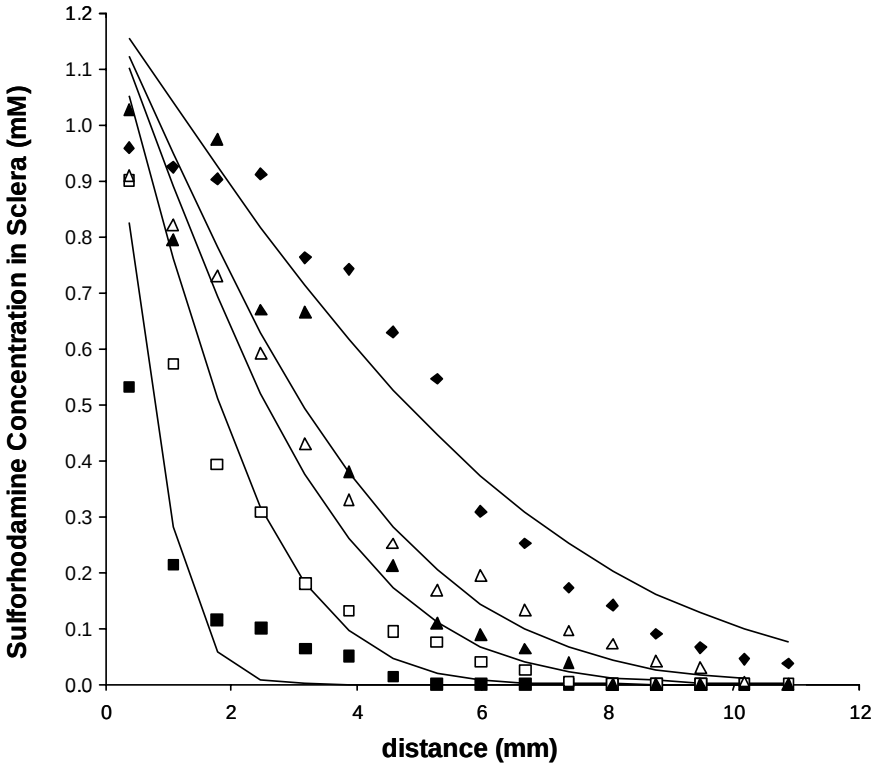

Figure 4.1.3. Experimental measurements and theoretical predictions of sulforhodamine concentration in human cadaver sclera as a function of time and position. Experimental data points show good agreement with theoretically predicted curves (Eq. 12) using experimentally determined values for K_D = 13.6 and K_{eq} = 0.08 and a fitted value for diffusivity, D = 3.82 x 10^{-6} cm^2/s at 4 h (■), 24 h (□), 48 h (▲), 72 h (Δ) and 168 h (♦). The experimental data are the same as shown in Fig. 4.1.2.

Further examination shows that at early times (e.g., 4 h), the model generally underpredicted the data, whereas at later times, the model generally overpredicted the data. This can be explained by a changing diffusivity, which was initially larger than the overall fitted value and later was smaller. Diffusivity might have changed over time due to changes in tissue hydration. Although the sclera was maintained in a humid environment, some tissue de-hydration could have occurred over the course of the 1-week experiment. Decreasing tissue hydration could progressively decrease diffusivity in the sclera as the aqueous diffusion pathways decrease in number and size. In addition, decreased water content of the sclera could also decrease average tissue sulforhodamine

concentrations by decreasing the aqueous regions containing sulforhodamine relative to the collagen, GAG and other insoluble regions.

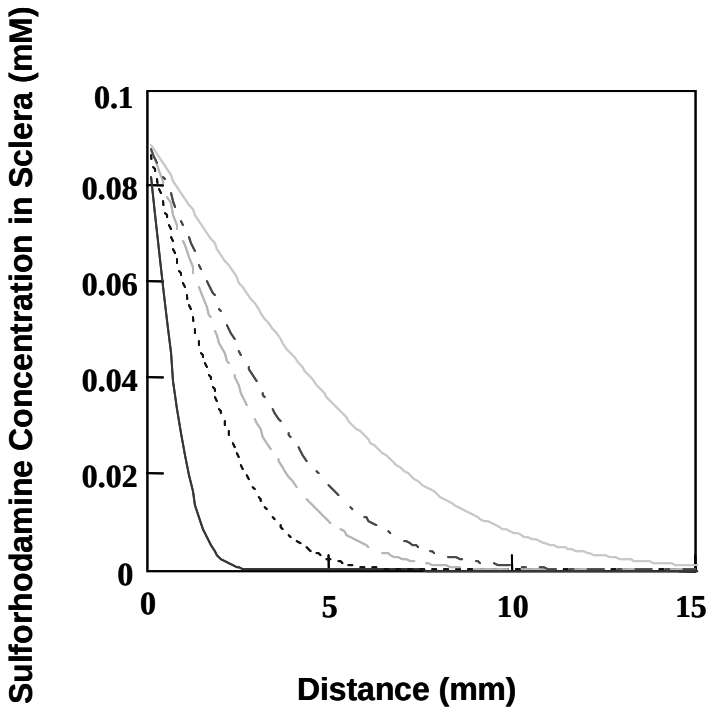

Figure 4.1.4. Theoretical prediction curves of sulforhodamine concentration in human cadaver sclera with the sclera-to-saline distribution coefficient, $K_D = 1$, as a function of time and position at 4 h (———), 24 h (……...), 48 h (– – – – –), 72 h (– · – · –) and 168 h (————).

As a modification o the model, the sclera-to-saline distribution coefficient, K_D, was set equal to 1 in Eq. 12 to assess the significance of binding on the prediction model. The resulting predicted curves still displayed a similar trend of the diffusion length of sulforhodamine along the sclera tissue over each time period; however, the model greatly underpredicted the sulforhodamine concentrations within the tissue by a factor of 13.6, which was equivalent to K_D. This shows that without K_D, the model will still qualitatively predict the time dependent of the diffusion profile, but quantitatively it will

underpredict the concentrations by an order of magnitude. This further shows the importance of explicitly considering possible binding o drugs to sclera when predicting their lateral diffusion.

4.1.5. Comparing lateral and transverse diffusivities

To compare lateral and transverse diffusion in the sclera, we measured the rate of transverse diffusion of sulforhodamine across the sclera, which provided an effective diffusivity of D_{trans} = 1.28 ± 0.22 x 10^{-6} cm^2/s, which corresponds to a permeability of 2.15 ± 0.37 x 10^{-5} cm/s. These values compare well with previously reported experimental data for scleral permeability of other molecules of similar molecular weight (Prausnitz and Noonan 1998) and to a predicted diffusivity value of 2.5 x 10^{-6} cm^2/s for sulforhodamine generated using an independent theoretical model described previously (calculation not shown) (Edwards and Prausnitz 1998).

Comparing the lateral (D_{lat} = 3.82 x 10^{-6} cm^2/s) and transverse (D_{trans} = 1.28 x 10^{-6} cm^2/s) diffusivity values generated in this study indicates that diffusing in the lateral direction occurs three times faster than in the transverse direction. Although a rigorous analysis of statistical significance is difficult due to the way that lateral diffusivity was determined, this three-fold difference may be insignificant due to experimental variability. If there is a significant difference, then the larger diffusivity of lateral diffusion might be explained by the lateral orientation of collagen fibers in the sclera. Diffusion parallel to these fibers might encounter less hindrance than diffusion across the fibers, which might be more tortuous. However, the importance of the collagen fibers is not clear, since diffusion in the sclera is expected to be governed by the extracellular glycosaminoglycan

matrix (Edwards and Prausnitz 1998), which is randomly oriented (Fatt and Weissman 1992) and thus should not favor diffusion in any particular direction.

4.1.6. Discussion

This study provides the first measurements of lateral diffusion in the human sclera. As new modalities for the treatment of age-related macular degeneration and other retinal diseases become available, drug diffusion across and within the sclera to target the posterior segment will become increasingly important. For example, after peribulbar or other periocular injection, drug may diffuse across the sclera to reach targets in the choroid or retina. Because retinal diseases are often disseminated, it may be desirable for drug to diffuse laterally to cover a larger area of retina beyond the site of injection. This may be especially important in the case of localized, slow-release drug delivery devices placed on the sclera, such as a scleral buckle or other implanted devices

Data from this study showed that after just 4 h, measurable concentrations of sulforhodamine were present at a distance of 5 mm from the donor solution, but measurable concentrations at 10 mm required 3 days. This is consistent with a calculation using the value of lateral diffusivity determined in this study: at a distance of 1 cm, the characteristic diffusion time is $(1\ \text{cm})^2 \times (3.82 \times 10^{-6}\ \text{cm}^2/\text{s})^{-1} = 2.6 \times 10^5\ \text{s} = 3.0$ days. Based on a similar calculation, it should take at least 6 weeks for sulforhodamine to diffuse from a localized source throughout all of the sclera in a human eye (using a characteristic distance of 3.75 cm, which is half the circumference of a human eye (Fatt and Weissman 1992).

Although only validated using one compound, the model developed in this study for scleral diffusion is general. It should be valid for both hydrophilic and lipophilic compounds, as well as small drugs and macromolecules, given knowledge of their effective diffusivity, distribution coefficient and binding constant in the sclera, as shown in Eq. 12. Effective diffusivity should be strongly reduced by increases in molecular size, but only weakly affected by lipophilicity. Binding constant and distribution coefficient (which is strongly influenced by the binding constant) should be strongly influenced by molecular properties, such as lipophilicity.

Measurements and calculations of lateral diffusion in this study have assumed that diffusion is one-dimensional and no drug exits the sclera along its choroidal or episcleral surfaces. In the *in vivo* scenario, from a drug implant source within the sclera, some drug might be lost due to the "early leakages" of drug into various escaping routes, such as the choroid, periocular space and tear film; therefore the lateral distribution of drug within the sclera is expected to be even slower. A further modified model will then be needed to address these drug escaping routes. Moreover, because diffusion in sclera is known to be a strong inverse function of molecular size (Prausnitz, Edwards et al. 1998), lateral diffusion of proteins and other macromolecules is expected to be one or more orders of magnitude slower than sulforhodamine.

This slow lateral distribution indicates that if delivery localized on the millimeter length scale is desirable, then drug administration to a particular site in or on sclera will remain highly localized on a timescale of hours to days. Conversely, if lateral distribution of drug over a larger area with faster kinetics is required, then a less localized injection or implant that covers a larger area of scleral surface may be needed. Moreover, drug

distribution by the vasculature in the choroid has not been considered in this analysis and may provide a means for additional drug distribution over larger areas.

4.1.7. Conclusion

Lateral diffusion of sulforhodamine, a hydrophilic model drug, was studied in human cadaver sclera. Measurable amounts of drug were detected at distances of 5 and 10 mm from the drug donor reservoir at 4 h and 3 days, respectively. Experimental data were used to calculate an effective lateral diffusivity of 3.82×10^{-6} cm^2/s. This calculation enabled the prediction that a point source of sulforhodamine would require 6 weeks to diffuse throughout all of the sclera in a human eye. Comparison of experimental measurements of lateral diffusion within the sclera to transverse diffusion across the sclera indicated similar effective diffusivities, although lateral diffusion was approximately three times faster. A theoretical model for one-dimensional diffusion in the sclera was developed and shown to match experimental data with a mean absolute percent error of 39%. This model can be used to predict rates of lateral diffusion in the sclera for various drug delivery scenarios. Altogether, this study shows that lateral diffusion in the sclera is a slow process that localizes drug distribution on the millimeter length scale for hours to days; lateral diffusion over larger surface areas could occur over longer times, for example, during extended release drug delivery from an implant.

4.2 Ocular drug delivery using solid coated microneedles

Drug delivery to the eye is notoriously difficult, especially delivery of macromolecules and delivery to the back of the eye. In this study, we propose that microneedles can be used as a minimally invasive method to deliver drugs into the eye via either intrascleral or intracorneal routes. This work leverages existing technology to fabricate microneedles and was guided by existing experience using microneedles for drug delivery across the skin. These microneedles can be inexpensively mass-produced by adapting the technology of the microelectronics industry. Given that microneedles have not been previously studied for ocular drug delivery, this study sought to design, fabricate and test microscopic needles that penetrate just hundreds of microns into ocular barrier tissues and deliver drugs into the eye.

4.2.1 Characterization of coated microneedles

Single solid microneedles were made by laser-cutting needle structures from stainless steel sheets. Fig. 4.2.1 shows the size comparison of a single stainless steel microneedle to a penny. Guided by the average human sclera thickness of 600 ± 49 μm (Lee, Geroski et al. 2004) and possible tissue deformation during the needle insertion, the microneedles used in scleral *in vitro* insertion tests were 750 μm in length, 200 μm at needle base and 55^{o} in tip angle. For *in vivo* experiments, the microneedles were modified to 500 μm in length and 45^{o} in tip angle, to avoid the penetration through the thinner cornea tissue. To handle these microneedles using forceps during the insertion, an extended metal substrate attached to the needle base, which normally was 1 cm in length and 4 mm at the base, was included in the needle design.

Figure 4.2.1. Bright field microscopy image of a single solid stainless steel microneedle used in *in vivo* insertion experiments shown next to a penny. A close view of the needle, which is 500 µm in length and 45^{o} in tip angle, is shown at the upper left corner of the figure

Using a formulated coating solution, different drug molecules, sizing from fluorescein to DNA, were coated onto the shafts of the microneedles as shown in Fig. 4.2.2. After tissue insertion, these hydrophilic coatings were designed to rapidly dissolve off the needle. In addition, using a modified coating apparatus, arrays of multiple microneedles were coated with compound solutions. Development of these methods, formulations and coating device has been carried out by others and is beyond the scope of this thesis.

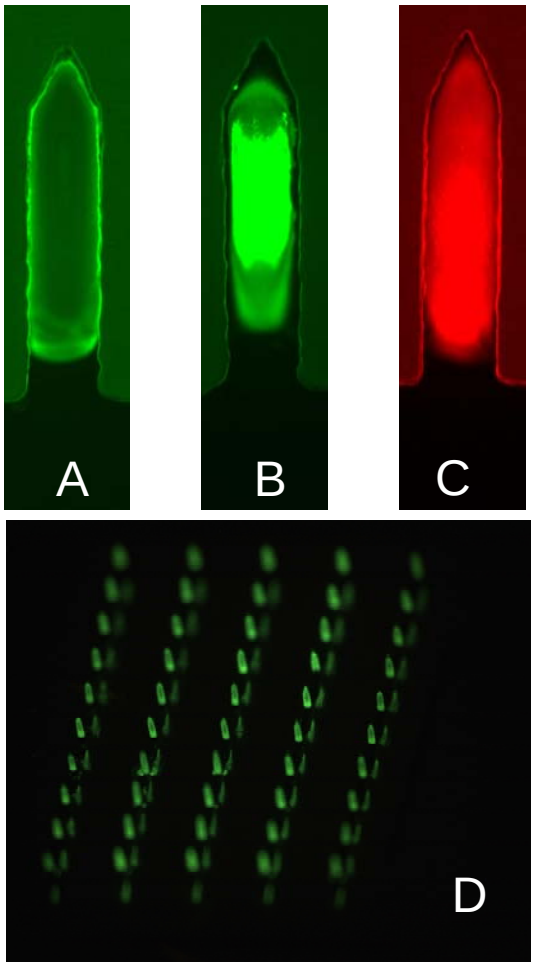

Figure 4.2.2. Solid stainless steel microneedle coated with different molecules, such as sodium fluorescein (A), fluorescein-labeled bovine albumin (B), and fluorescein-labeled plasmid DNA (C) using dip-coating method. Similarly, arrays of SS microneedles can also be coated and used in delivery experiments (D).

4.2.2 *In vitro microneedle insertion*

After coating the microneedles, we tested their ability to insert into human cadaver sclera *in vitro.* To qualitatively visualize the insertion site created by the insertion, single, clean, microneedles were manually pierced half-way into the sclera tissues to avoid full penetration, and immediately after needle removal, blue tissue dye was applied on top of the tissue and then wiped off. The histological image was shown in Fig. 4.2.3A. Using bright field microscopy, the top surface of the sclera was stained by the blue dye while the insertion gap created by the microneedle was evident within the tissue. The measured gap distance of 300 μm is similar to the half microneedle length, which also indicates only partial needle penetration into the sclera, due in part to tissue deformation during insertion.

Sulforhodamine-coated microneedles were also tested. After each insertion, the microneedles were left within the tissue for 20 sec, allowing the dissolution of the coating the needle. The representative histological image shown in Fig. 4.2.3B indicates that the sulforhodamine coating was deposited through the microneedle hole, as well as some deposition on the tissue surface. The sulforhodamine fluorescein intensity appears much brighter around the needle insertion site compared to the scleral regions away from the insertion. This image shows that the sulforhodamine coating was able to instantly dissolve off the needle shaft and diffuse within the tissue. Similar results were obtained from BSA-coated microneedle insertion (Fig. 4.2.3C).

After each insertion experiment, the microneedles were examined using bright-filed microscopy for any mechanical defects. No observations of either needle breakage

or bending were reported, which suggested that these microneedles were sufficiently strong and sharp to penetrate into rigid scleral tissues.

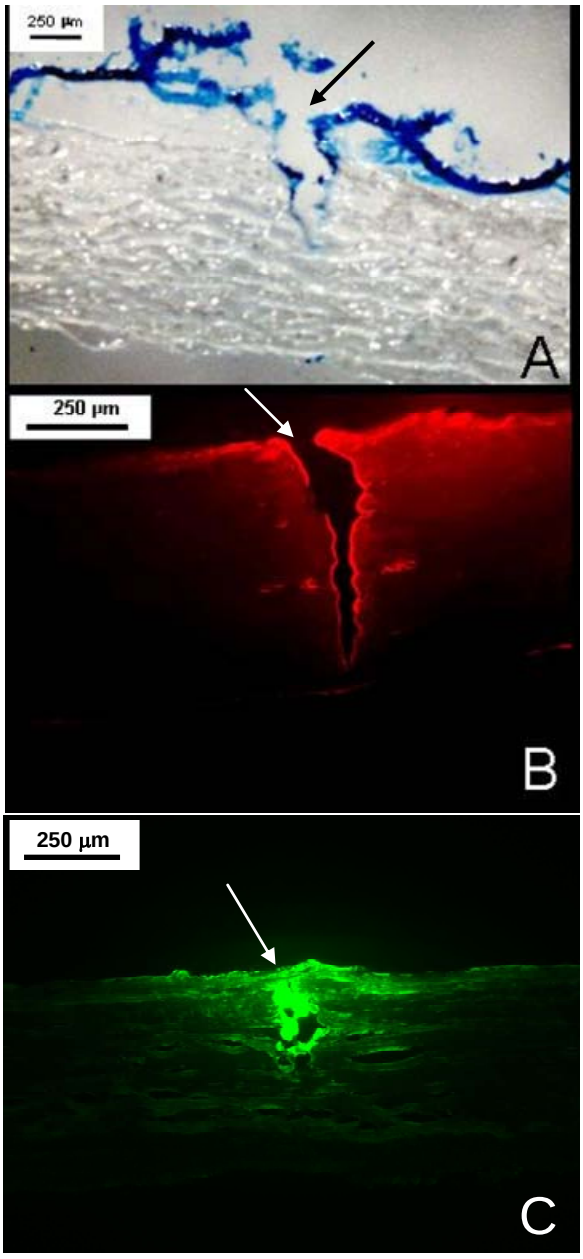

Figure 4.2.3. Histological sections of human cadaver sclera pierced with single solid SS microneedles and subsequently stained with a blue tissue marking dye (A), using sulforhodamine-coated needles (B) and using FITC-labeled BSA-coated needles (C). The arrow in each image indicated the direction of microneedle insertion.

4.2.3 In vivo fluorescein delivery

We next tested the ability of using coated microneedles to deliver drugs into the eye in a rabbit model *in vivo*. Using calibrated spectrofluorometry, each solid microneedle was coated with 280 ± 14 ng of NaFl. In initial experiments, we inserted 10 NaFl-coated needles into the rabbit sclera and attempted to deliver the molecules into the vitreous body of the rabbit eye. However, the amount of fluorescein delivered by microneedles was insufficient to be detected in the vitreous body due to dilution in its relatively large volume. To facilitate fluorometric analysis and imaging, we chose to deliver fluorescein into the rabbit cornea, rather than the sclera. After a single NaFl-coated microneedle insertion, the fluorescein concentration in the anterior segment of the rabbit eye was monitored for 24 h.

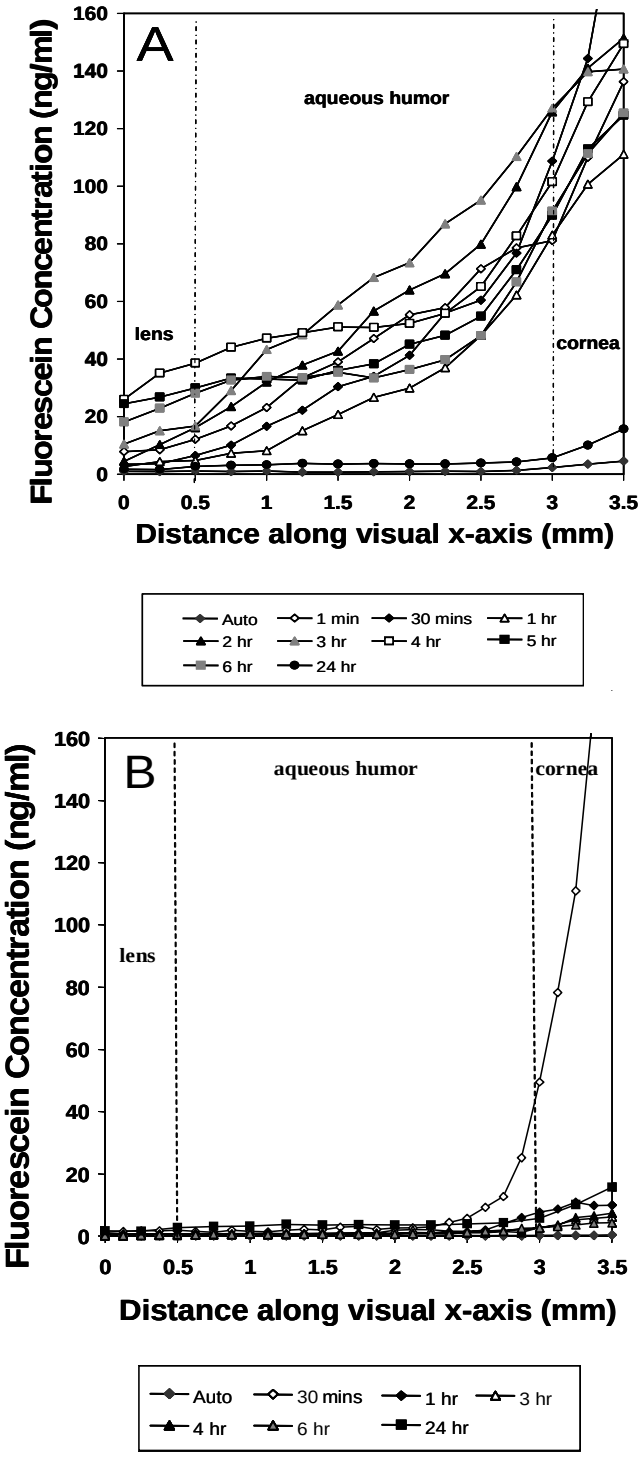

Figure 4.2.4. Fluorescein concentration profiles in the rabbit eye as a function of position in the anterior chamber after NaFl-coated microneedle delivery (A) and topical administration of equivalent dose (B).

As shown in Fig. 4.2.4, fluorescein concentration was measured over time as a function of the distance along the visual axis from the cornea to the lens in the rabbit eye. Prior to the microneedle insertion, almost no fluorescein was detected in both the aqueous humor and the lens of the eye. Immediately after the needle insertion, a sharp increase of the fluorescein concentration was observed in both regions compared to the background fluorescein reading. The measured concentration reached to the peak after 3 h, and gradually decreased to the background level within 24 h. The fluorescein concentration profile in Fig. 4.2.4A suggested that after the fluorescein coating dissolved off the microneedles, a depot was formed within the cornea that steadily released fluorescein for hours. For comparison, we performed a control experiment using a conventional topical application of equivalent fluorescein dose, and similarly measured the fluorescein concentration in the eye over time. As shown in Fig. 4.2.4B, only small amount of fluorescein was detected in the aqueous humor 30 min after topical administration, and essentially all the fluorescein on the cornea was washed away by tear flow afterward.

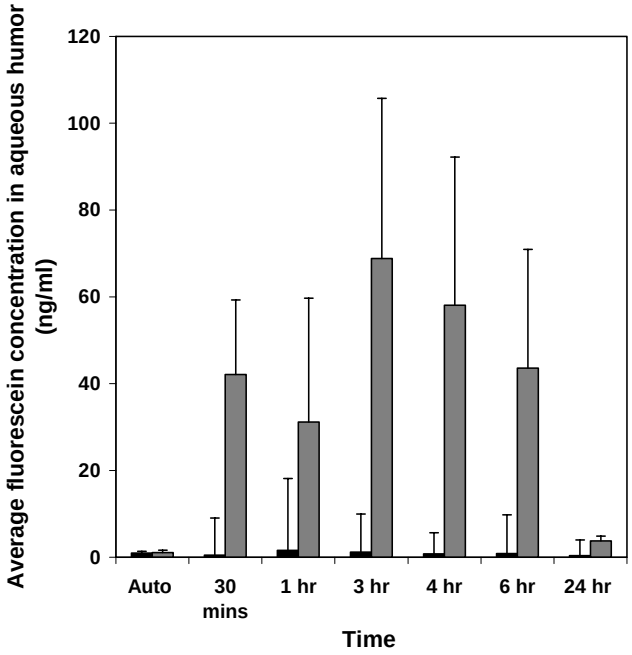

Figure 4.2.5. Average fluorescein concentration in the anterior chamber of the rabbit eye delivered by microneedle insertion (gray bars) and topical administration of equivalent dose (black bars). Single coated microneedle delivered more than 60 times higher amount of fluorescein over a prolonged time comparing to topical administration.

To compare microneedle delivery and topical application delivery, Fig. 4.2.5 shows average measured fluorescein concentration in the aqueous humor at each time point for each delivery method. The improved efficiency of microneedle delivery is evident, showing that microneedle delivered a significantly larger amount of fluorescein into the eye over a longer period. 3 h after application, the dose delivered by a single coated microneedle was 60-fold higher than that of topical delivery.

A useful control experiment would be to make a single, un-coated microneedle insertion into the rabbit cornea, topically apply the fluorescein solution on the cornea, and then measure the fluorescein concentration in the anterior segment of the eye to examine whether microneedle insertion would improve the topical drug delivery efficiency by

locally increasing corneal permeability at the site of needle insertion. Even though this experiment has not been done yet, theoretically we can estimate both mass fluxes through the cornea and through the hole made by microneedle insertion. We hypothesize that the flux through the microneedle insertion hole will be much less than the flux through the cornea.

The fluorescein flux across the cornea can be estimated as:

$$flux = P * C * A \qquad (20)$$

where A is the surface area of rabbit cornea at 1.6 cm^2 (Mietz, Addicks et al. 1994), C is the applied drug concentration, which is assumed as 300 ng/ml, and P is the corneal permeability to fluorescein that is $5.0x10^{-6}$ cm/s (Hale and Maurice 1969). The mass flux across the cornea is then calculated as $2.4x10^{-3}$ ng/s. The mass flux of fluorescein through the microneedle insertion gap can be estimated as:

$$flux \cong \frac{D * C * A_{pore}}{d_{epith}} \qquad (21)$$

where A_{pore} is the surface area of microneedle insertion gap of $8.5x10^{-5}$ cm^2, C is the applied drug concentration at 300 ng/ml, D is the diffusivity of fluorescein in water that is reported as $6.4x10^{-6}$ cm^2/s (Galambos and Forster 1998) and d_{epith} is the thickness of corneal epithelium layer, which is reported as 45 μm (Reiser, Ignacio et al. 2005). The fluorescein mass flux through the hole created by microneedle insertion is then obtained as $3.6x10^{-5}$ ng/s, which is 150-fold less compared to the flux through the cornea. This finding agrees with our hypothesis and shows that the microneedle insertion by itself has an insignificant impact on drug delivery to the eye. In order to improve drug delivery efficiency using topical application, hundreds of single microneedle insertions will be

needed, which is not ideally suitable for clinical applications due to safety concerns and patient convenience.

4.2.4 Microneedle delivery efficiency

In order to assess bioavailability of microneedle delivery, we determine the total dose of fluorescein delivered into the eye. Using Eqn. 19 described in the Method Section to analyze the experimental data shown in Fig. 4.2.5, the estimated fluorescein delivered into the aqueous humor was calculated to be 196 μg, which is equal to 69% of the dose of fluorescein coated on the microneedle. To further investigate the delivery efficiency of microneedle, an additional experiment was carried out. We inserted NaFl-coated microneedles into rabbit cadaver cornea, and measured the fluorescein content within the cornea tissue and that remaining on the needle. This analysis determined that on average 74 ± 27% of the needle coating was delivered into the cornea *in vitro*, which is similar to the result obtained from the *in vivo* estimation. Combining the two findings, these data also suggested that most fluorescein was released from the needle to form the depot in the cornea tissue to provide further release with a bioavailability of approximately 70%. The remaining fluorescein might have been washed away by the tear fluid before entering the aqueous humor.

4.2.5 In vivo pilocarpine delivery

To further demonstrate the capability of using microneedles to deliver drugs into the eye, pilocarpine, a drug known to cause pupil contraction and used in treatment of glaucoma, was coated onto 5 single solid microneedles, which were later inserted into

rabbit cornea *in vivo*. The size of the rabbit pupil was both measured as a function of time and imaged at each time point, as shown in Fig. 4.2.6 & Fig. 4.2.7. Microneedle delivery caused a much more rapid and prolonged pupil contraction compared to a topical application of equivalent dose. The pupil size after microneedle insertion was reduced from 8 mm down to 5 mm, where topical application only reduced the pupil to 7 mm. In another control experiment, a drop of ophthalmic solution, which containing a pilocarpine dose at 10 times greater than that administered by microneedles, was applied topically to the eye. Despite the large drug dose difference, this topical delivery gave only a modestly increased pupil constriction response compared to microneedle delivery.

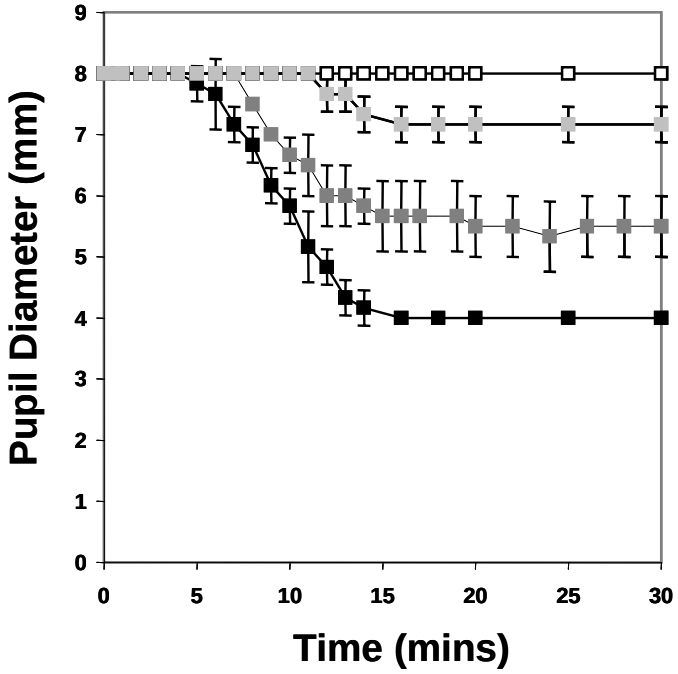

Figure 4.2.6. The measured diameter of rabbit pupil changes over time of negative control (—□—), topical application of a dose equal to microneedle coating dose (—■—), pilocarpine-coated microneedles delivery (—■—), and topical application of 1% ophthalmic solution (—■—). Average measurements with the standard errors are presenting in each set of experiments ($n \geq 3$).

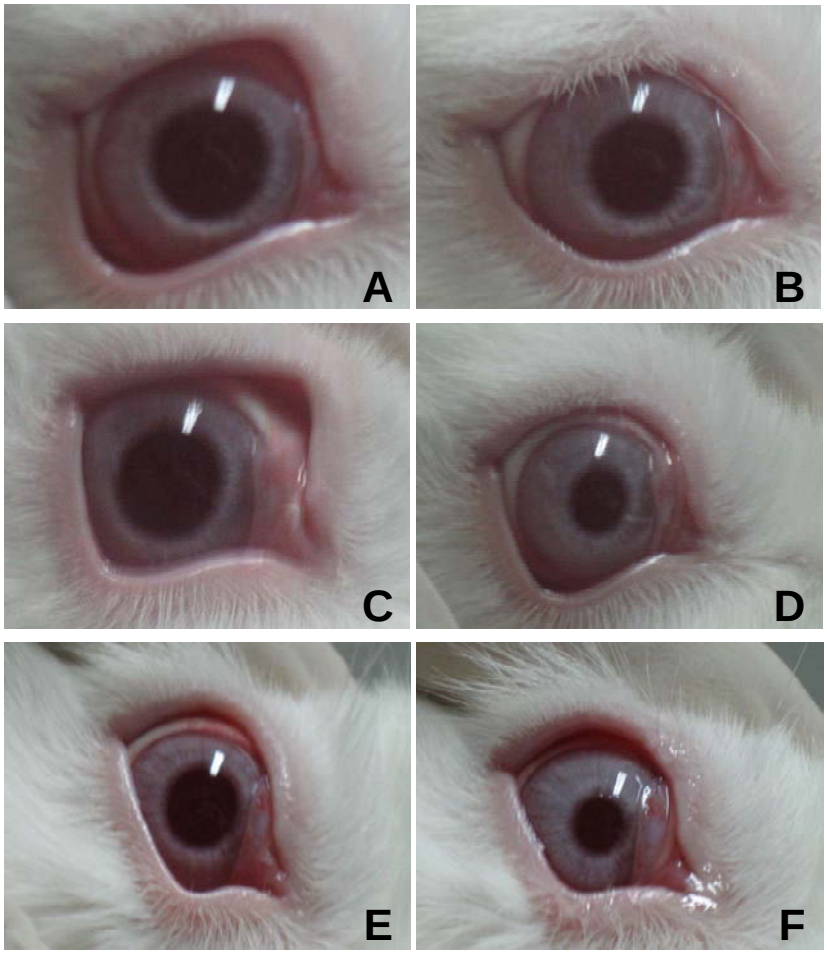

Figure 4.2.7. Representative images of rabbit pupil before and 20 min after and topical application of pilocarpine solution of a dose equivalent to microneedle coating dose (A and B), five pilocarpine-coated microneedles delivery (C and D) and topical application of 1% ophthalmic solution (E and F).

4.2.6 Safety Exam

A final experiment was carried out to assess safety of microneedle insertion into the eye. Based on three replicate experiments, a single, non-coated microneedle was inserted into rabbit cornea *in vivo*. As a standardize clinical test, inflammatory response in the eye can measured by the degree of cells and flare, using a grading system from 1 to 4, in the anterior chamber (Soheilian, Karimian et al. 1997), These experiments

indicated that the insertion wound was no longer visible after 3 h and no cell-and-flare response was reported, which suggested there was no inflammatory response. This analysis suggests that microneedle insertion into the eye may be well tolerated.

4.2.7 Implications for ocular drug delivery

Many inflammatory and proliferative diseases in the posterior segment of the eye, such as macular degeneration and diabetic retinopathy, require long-term pharmacological treatment. However, it is difficult to deliver effective drug doses to the back of the eye using conventional delivery methods such as topical application, which has poor efficacy. Systemic administration often causes significant side effects (Geroski and Edelhauser 2000). Direct injection into the eye is often effective, but requires professional training and safety is a major concern (Maurice 2001).

Because of their small size, microneedles can be inserted into the tissue with minimized physiological damage, which would be an asset in ocular drug delivery. In this study, we demonstrated that microneedles are capable delivering drug particles into the eye via the cornea or the sclera in a minimally invasive way. Coupled with a coating formulation, these needles can be coated with a broad range of drug molecule with sizes varying from the small (fluorescein) to the large (DNA). As a convenient and effective procedure, this study showed that ocular tissues could be partially penetrated by microneedles and followed by the deposition of drug formulations within the tissue to provide treatment for hours. Compared to topical application and intraocular injection, microneedle delivery offered a much improved efficiency without causing significant tissue damage.

With the consideration of combining with additional systems, such as biodegradable polymers or hydrogels, the application of microneedles can provide a controlled and prolonged drug delivery. In addition, the patient compliance should also be improved, since this microneedle treatment lasts only for seconds and could provide longer-term effect. With further optimization, microneedles may be a broadly applicable technology for ocular drug delivery.

4.2.8 Conclusion

This study demonstrated that coated microneedles can deliver model drugs into the human sclera *in vitro* and the rabbit cornea *in vivo*. Additional analysis indicated sustained delivery from a depot in the cornea for many hours after microneedle delivery with increased bioavailability. Slit lamp examination of microneedle-treated eyes showed no adverse events. This study shows for the first time that microneedles might be used for ocular drug delivery that microneedles may be applicable in treating diseases of the posterior segment of the eye.

4.3 Microinfusion using hollow microneedles in sclera

For the first time, hollow microneedles were used to deliver molecules and particles into scleral tissues in this study. To examine various parameters affecting the microinfusion into sclera using hollow microneedles, we microinjected flowed sulforhodamine solution into human cadaver sclera and measured the delivered volumetric dosage as a function of scleral thickness, needle retraction depth and infusion pressure. Additionally, we delivered nano- and micro-particles into the tissue, and examined the effect of hyaluronidase and collagenase on particle delivery. This study was motivated by the goal of using hollow microneedles as a novel ocular drug delivery tool to deposit drugs within the sclera to provide controlled release in treating diseases in the back of the eye.

4.3.1 Characterization of microneedles

The microneedles used in this study were fabricated using a micro-pipette pulling technique. Practically the desired clinical applications of microneedles are envisioned to be using multineedle arrays made of metal that are mass-produced by microfabrication using tools from the microelectronic industry. We chose to use glass micropipettes to make the needles due to the easy fabrication process. Despite the long shafts these needles have, the needle tip geometric dimensions (i.e. tip opening length, diameter, and angle) are similar to those of desired microfabricated metal microneedles. A representative glass microneedle used in this study is shown in Fig. 4.3.1, which has a tip opening of 100 μm in length and 40 μm in diameter, and an angle of 25^{o}. The sharp tip allowed these microneedles to repeatedly pierce into the sclera without breaking.

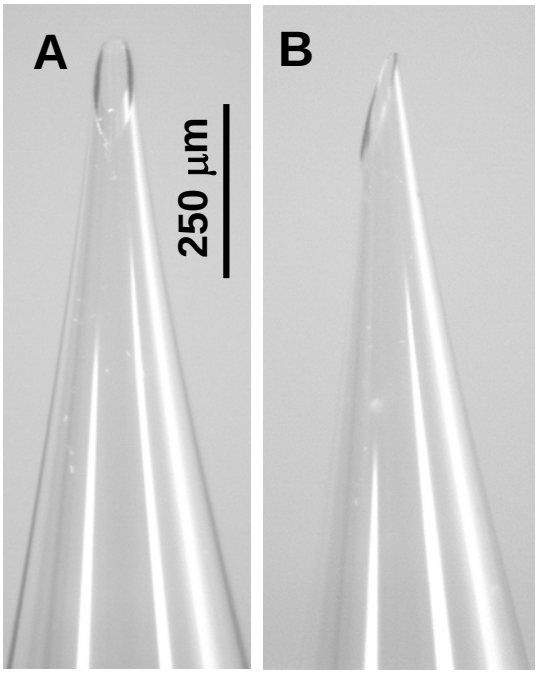

Figure 4.3.1. (A) Front and (B) side views of a representative hollow glass microneedle. The microneedle shown has a tip opening radius of 20 μm and length of 100 μm with a bevel tip angle of 25°.

Single, hollow microneedles were inserted into human cadaver sclera *in vitro* to a controlled depth and then partially retracted. Sulforhodamine solution was infused into the sclera tissue through the hollow shaft of the needle using pressure-driven flow. Fig. 4.3.2a shows the top view of the sclera after microinfusion of sulforhodamine solution. In a typical experiment, the distribution of the solution appeared in a circular shape, which has a diameter measured from millimeters up to one centimeter, depending on infusion conditions. When the tissue was viewed from the backside, the distribution of sulforhodamine showed similar pattern. A previous study showed a delicate architecture of criss-crossed lamellae that was aligned in the innermost layers of the sclera, but moving further towards the surface, larger, less regular bundles became evident (Raspanti,

Marchini et al. 1992). The solution distribution within the sclera was, therefore, governed by the alignment of the lamellae.

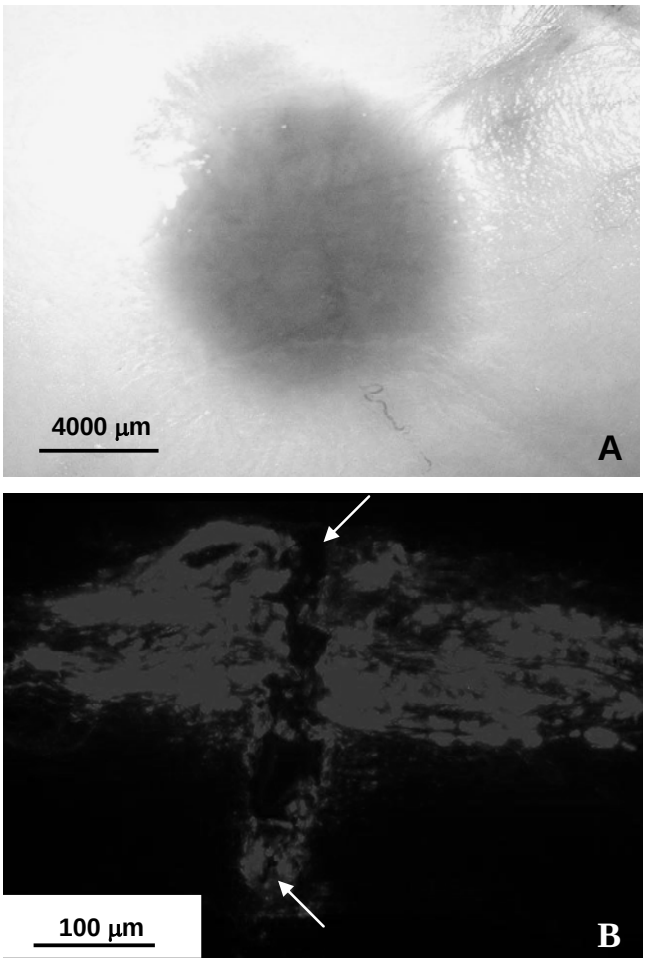

Figure 4.3.2. Top view of a representative human cadaver sclera tissue after a single hollow microneedle infusion of sulforhodamine solution as shown in (A) and a representative histological, fluorescent image of the microneedle insertion site within the tissue (B). A single hollow microneedle with a beveled tip angle of 25^{o} was inserted 720 μm into the sclera and then retracted 200 μm out. Sulforhodamine solution was infused into the tissue at a pressure of 15 psi.

Fig. 4.3.2b shows a fluorescein image of a 10 μm-thick histological cross-section of scleral tissue after infusion. A single microneedle was inserted 720 μm into the middle region of a scleral piece, and retracted 200 μm to infuse sulforhodamine solution into the tissue. The insertion pathway created by the microneedle is evident, measured at 300 μm deep and the shape of the insertion gap retained that of the needle tip. There was no clear evidence of tissue deformation due to microneedle compression at the scleral surface, although this may have occurred during insertion, but recovered after needle removal and imagining. A lack of compression could be explained by the tightly packed fiber arrangements in the upper layers of sclera, which the impact force of the needle insertion did not distort the fiber arrangement. The surrounding tissues around the needle insertion site were stained by infused sulforhodamine solution, and showed a significant difference compared to a control tissue without sulforhodamine injection, and the section appeared completely black by fluorescence microscopy.

4.3.2 Effect of scleral thickness and retraction depth

The human sclera thickness varies from 0.3 to 1.0 mm with respect to the position along the scleral globe (Fatt and Wissman 1992). To examine the effect of the thickness gradient on microneedle infusion, the sclera was divided into three different regions around the scleral globe: front (near the limbus), middle (at the equator), and back (near the optic nerve). Guided by the previous observations that subsequent needle retraction can induce flow into the tissue (Wang, Cornwell et al. 2006), microneedles were inserted into each region of the sclera at a controlled depth (720-1080 μm), and then partially retracted. Each retraction displacement was 60 μm and lasted 3 minutes.

The results showed that essentially no solution was delivered into the tissue after the initial insertion in all experiments as shown in Fig. 4.3.4. The delivery did not start until a certain retraction distance, normally ranging from 200 to 300 μm depending on the scleral region, was achieved. Fig. 4.3.3 shows the volume delivery as a function of retraction distance of a representative experiment.

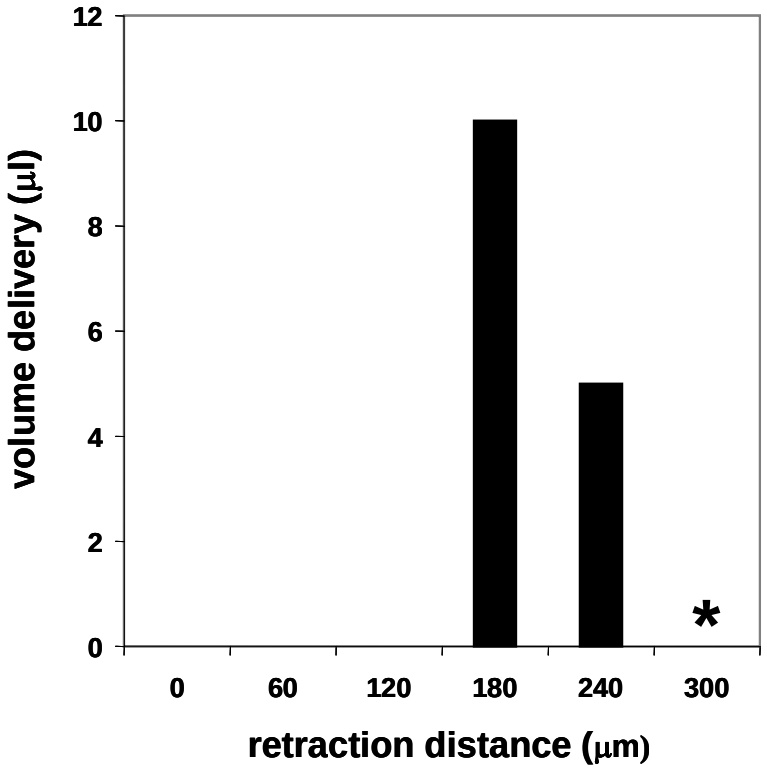

Figure 4.3.3. Effect of microneedle retraction on solution volumetric delivery from a representative experiment, in which a single, bevel-tipped, glass, hollow microneedle was inserted 720 μm into the middle region of a scleral tissue. Retractions were made at an increment of 60 μm, and the delivery did not start after the needle was retracted 180 μm. A total of 15 μl of sulforhodamine solution was delivered into the tissue in this experiment after retraction of 150 μm and 240 μm. After 300 μm retraction, solution leaking was observed on the scleral surface; and thus no further solution was delivered into the sclera (*).

Since the scleral tissue at the equator is thinner compared to that near the limbus and the optic nerve, typically less retraction (209 ± 92 μm) in the middle region was needed compared to that in the front region (287 ± 182 μm) and in the back region (262 ± 145 μm). The scleral fibers are known to be elastic (Fatt and Wissman 1992), and the elastic system appears to be largely confined to the deeper layers in the sclera (Raspanti, Marchini et al. 1992), which could explain the zero volumetric delivery at the initial phase. After the needle penetrated into inner layers of the sclera, the fibers were deformed due to the compression of needle tip and blocked the needle tip opening. As the needle was retracted back into the upper layer, where the fibers were less elastic, larger openings between the needle and collagen fibers were formed and allowed the solution to spread within the tissue.

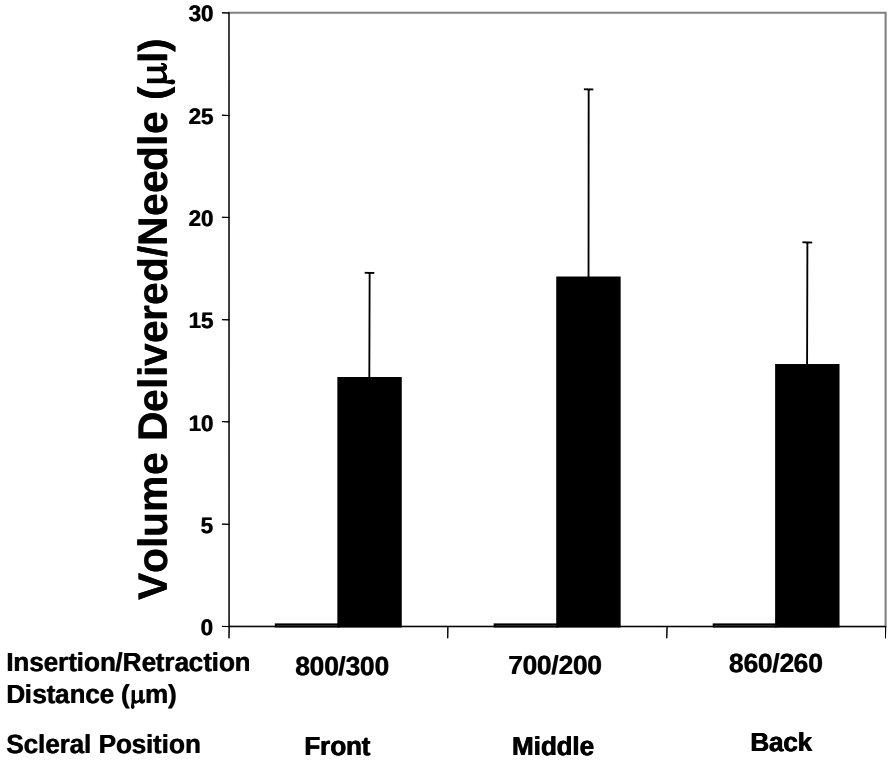

Figure 4.3.4. Effect of microneedle retraction on volumetric delivery into different regions of human cadaver sclera, which on average up to 18 μl solution was delivered into the tissue at a pressure of 15 psi using a single, glass, hollow microneedle with a beveled tip of 25°. Data are expressed at mean value ($n \geq 17$) with standard deviation bars.

On average in the middle region, a larger volume of sulforhodamine solution (18 ± 6 μl) was delivered into the tissue comparing to the amount delivered into the front (12 ± 4 μl) and the back (13 ± 5 μl) regions upon needle retraction. Statistics showed that even though a difference was observed among the sulforhodamine dose delivered into scleral regions with different thickness, this difference was not significant and the scleral thickness did not have a significant impact on volumetric delivery (ANOVA, $p = 0.074$).

4.3.3 Effect of infusion pressure

Guided by previous results in a transdermal study (Martanto, Moore et al. 2006), we hypothesized that by increasing the infusion pressure we should increase the flow rate, which should result in an increase in total volume delivery of the solution. However, our results indicated that pressure had an insignificant effect on the delivery (ANOVA, $p = 0.83$) as shown in Fig. 4.3.5, and the flow rates did not change with increased pressure. This suggested that the limiting factor in determining the amount of flow with the sclera could be the tight-packed collagen fibers. The elevated pressure was not sufficient enough to distort the fiber arrangement to open up the pathways allowing the solution to spread.

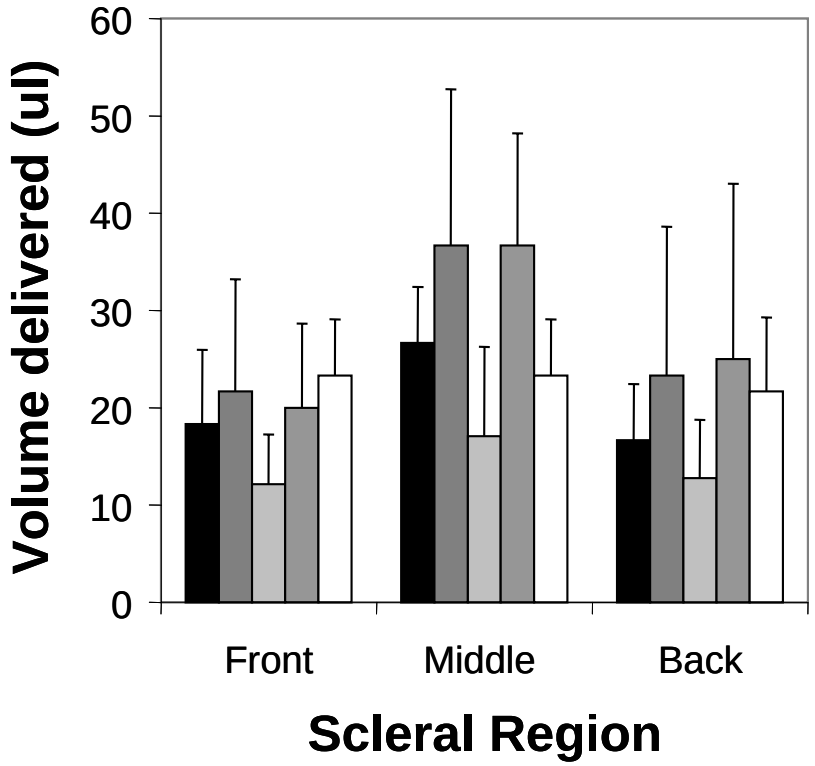

Figure 4.3.5. Effect of pressure on volume of delivery by single hollow glass microneedles. Experiments were carried out at pressure of 5 (■), 10 (■), 15 (□), 20 (■) and 25 (□) psi. Single hollow microneedles with a beveled tip angle of 25° were inserted 720 μm into each region of the sclera and retracted 140-300 μm out from the tissue. Data are expressed as mean values ($n \geq 3$) with standard deviation bars.

4.3.4 Delivery of nanoparticles

Fig. 4.3.6 shows a bright-field histological image of a human cadaver scleral tissue after infusion of 1.0 wt% nanosphere suspension using a hollow microneedle using bright field microscopy. The insertion depth was measured to be 500 μm, and the distribution of the particles is clearly present within the tissue. Unlike the results from sulforhodamine infusion experiments, the nanoparticles did not spread widely within the tissue. Concentrated particle regions were evident around the microneedle insertion gap, which suggested that the particles filled the spaces between collagen fibers.

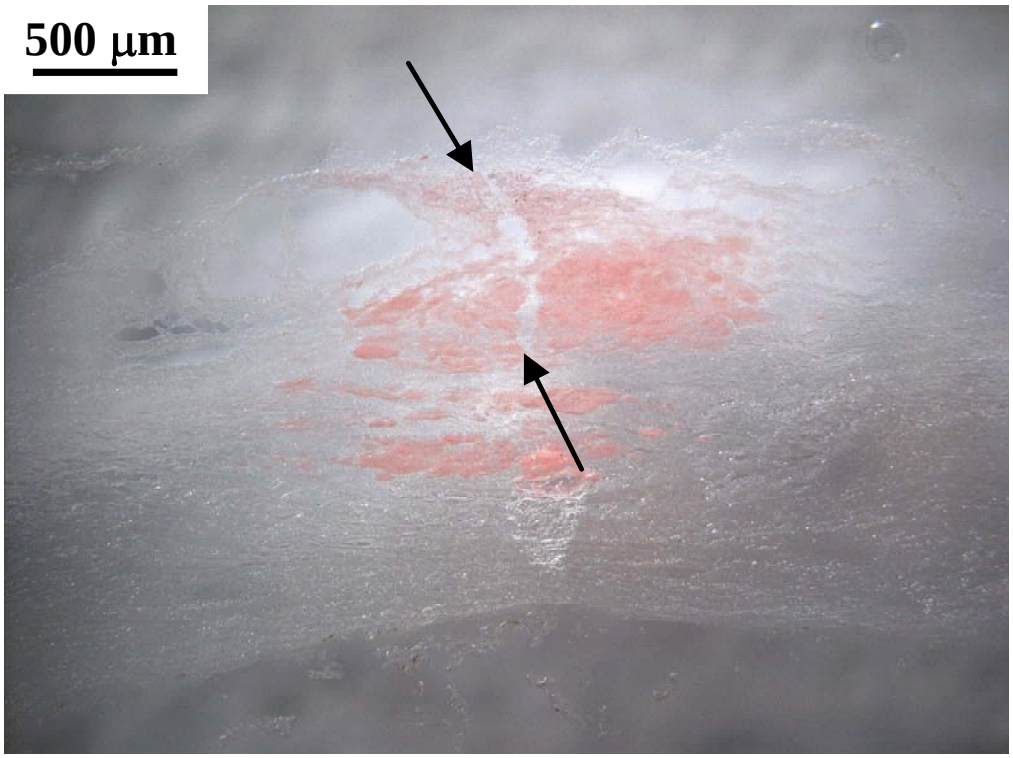

Figure 4.3.6. A representative histological image of human cadaver sclera after 1.0 wt% nanosphere suspension infusion using a single, beveled-tip, hollow glass microneedle. The needle was inserted 720 μm into the front region of sclera, and then retracted 240 μm. The nanosphere suspension was infused into the tissue at a pressure of 15 psi. The top arrow indicates the site of the microneedle insertion, and the gap between both arrows represents the insertion depth, which is about 500 μm.

Fluorescent images showed that the amount of nanoparticles infused into the scleral tissue increased as the concentration of particles in the donor solution increased in each region of the sclera as shown in Fig. 4.3.7. Larger fluorescent areas were detected with more concentrated nanoparticle solutions.

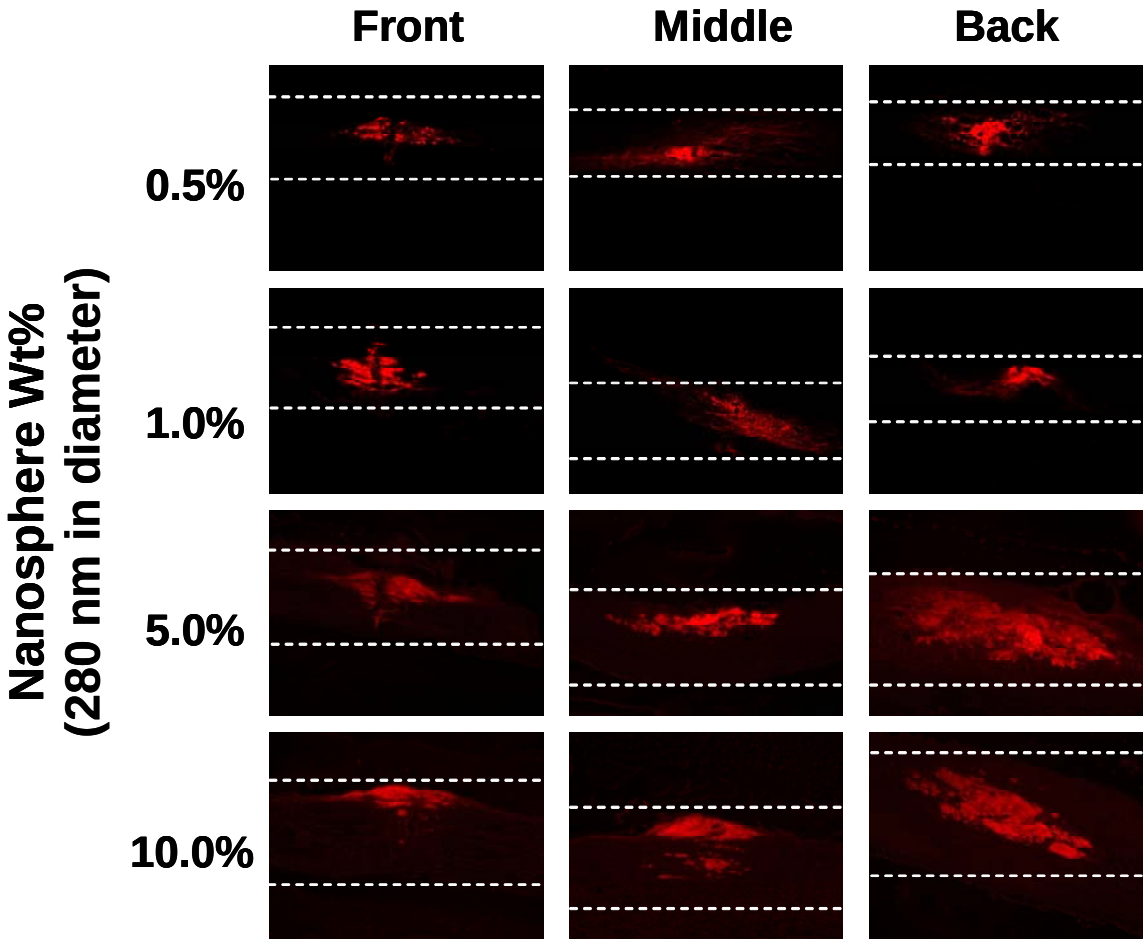

Figure 4.3.7. Representative histological fluorescent images of human cadaver sclera after infusion of various nanosphere suspensions with single hollow glass microneedles. The nanosphere mixtures had solid contents of 0.5, 1, 5 and 10 %. Microneedles were inserted 720-1080 μm respective to the scleral thickness in each region of the sclera, and then retracted 240-360 μm. In each experiment, 20 μl nanosphere suspension was infused into the tissue at a pressure of 15 psi. The dotted lines in each image represent the scleral thickness.

4.3.5 Delivery of microparticles

Another goal of this study was to deliver microparticles into the sclera tissue using hollow microneedles. The microparticles had diameters of 1 μm, and we failed to deliver any significant number of the larger particles into the tissue in a majority of the experiments. The microparticles appeared to clog the tip of the hollow microneedles (data not shown). A control experiment was performed to determine whether the clogging was caused by the size of the microspheres relative to the small needle bore size. We loaded single, hollow microneedles with 20 μl microsphere solution each, and infused the solution into the air, such that there was no physical tissue barrier induced. We did not experience any needle clogging and therefore concluded that the presence of scleral tissue played a critical role in blocking flow. The collagen fibers in the human sclera are reported to vary from 160 to 220 nm in diameters (Raspanti, Marchini et al. 1992), and their center-to-center spacing varies between 250 and 280 nm (Edwards and Prausnitz 1998). Therefore, we hypothesize that the nanometer-scale spacing between scleral collagen fibers might serve as the main barrier during the microparticle delivery, which restricted large-sized microspheres to pass.

Previous analysis (Ethier 1983) also demonstrated the importance of the noncollagenous proteins in determining the molecule transport in the sclera. These proteins make up 10% of the scleral dry weight (Fatt and Wissman 1992), and some of them are associated with GAGs and together form proteoglycan complexes (the GAGs form side chains that are chemically linked to a core protein) ((Edwards and Prausnitz 1998). The junctions of these proteoglycan complexes might also play an important role in microparticle particle delivery.

4.3.6 Effect of hyaluronidase

Hyaluronidase is a spreading or diffusing enzyme, which modifies the permeability of connective tissue through the hydrolysis of hyaluronic acid, a polysaccharide found in the intercellular ground substance of connective tissue. Previous studies have shown the use of it to reduce flow conductivity of dermis during injection (Bruera, Neumann et al. 1999; Kreil 1999; McGuire and Yuan 2001). We therefore hypothesized that this enzyme could similarly enhance microsphere delivery into sclera by breaking down the GAGs in the scleral extracellular matrixes.

Using a purified ovine testicular hyaluronidase, Vitrase, which is commercially available and is FDA-approved for human use, we carried out two sets of tests as described in the Methods Section. Compared to the histological images of the control experiment in which no hyaluronidase was used, a significantly larger dose of microspheres was delivered into each region of the scleral tissue that was soaked in the hyaluronidase solution prior to the infusion experiment as shown in Fig. 4.3.8. The same effect also took place in the hyaluronidase-mixed infusion tests showing that the effect of hyaluronidase is extremely rapid. This finding supported our hypothesis that by breaking down the ground substance in the sclera matrix, we can deliver bigger particles into the tissue.

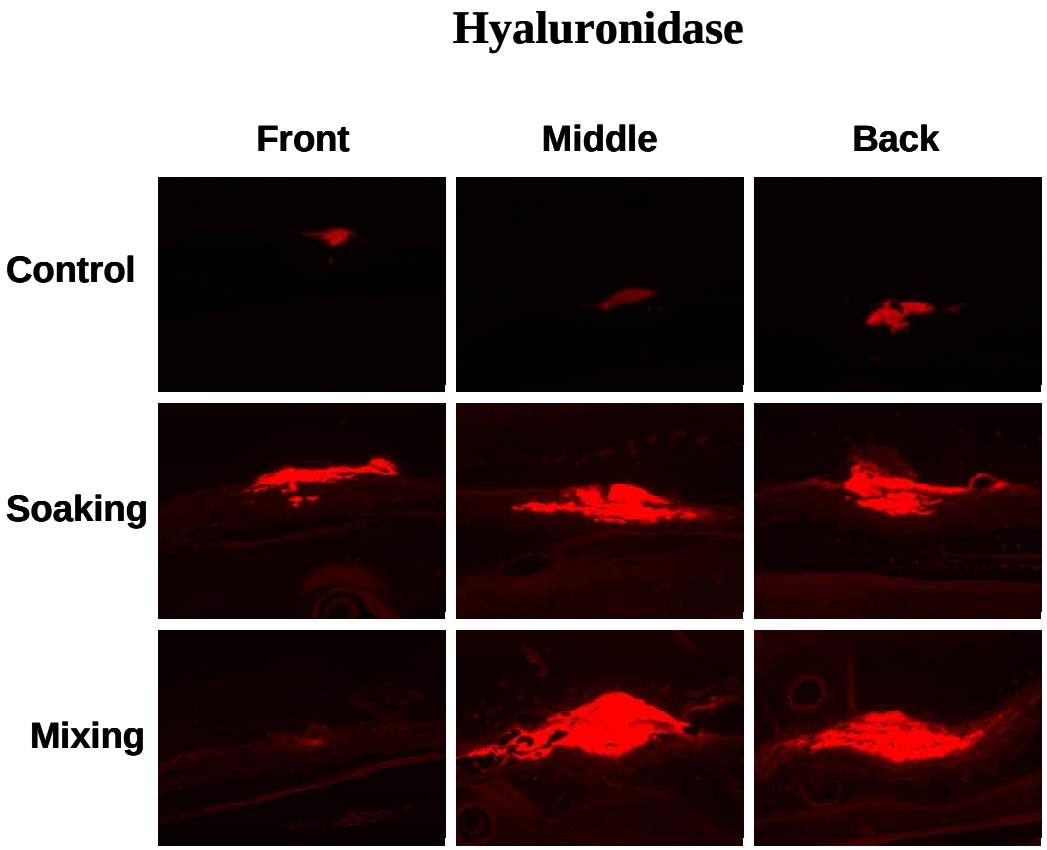

Figure 4.3.8. Representative histological images of the effect of hyaluronidase on delivery of 1.3 wt% microsphere suspension using hollow glass microneedles into human cadaver sclera. Two types of experiments were performed: first, sclera was presoaked in a hyaluronidase solution for 1 h prior to microinfusion, and second, the microparticle suspension was mixed with hyaluronidase and infused into sclera. In each experiment, a single, beveled-tip, hollow, glass microneedle was inserted 720-960 μm into the sclera and then retracted 250-300 μm depending on the scleral thickness in the region. 20 μl of microsphere suspension was infused into the tissue at a pressure of 15 psi.

Additionally, we also repeated the sulforhodamine solution infusion experiments with the addition of hyaluronidase and we did not observe any noticeable change in the volumetric delivery. This suggested that the spacing in the scleral extracellular matrices affects the delivery of micron-sized particles, but not small molecules.

4.3.7 Effect of collagenase

Collagens are defined as molecules contributing to the structure of extracellular tissue matrices (Kielty and Grant 2002). The collagen fibers within the human sclera are arranged in a very complex way: in the innermost layers a delicate architecture of criss-crossed lamellae is easily seen, but moving further towards the surface larger, less regular bundles become evident (Raspanti, Marchini et al. 1992). This fiber arrangement could affect particle delivery within the sclera. Type I, III, V and VI collagen are presented in the sclera, although both biochemical analyses (Keeley, Morin et al. 1984) and light microscopy immunolocalization (Tengroth, Rehnberg et al. 1985; Thale, Tillmann et al. 1996) have shown that type I predominates.

Collagenase, an enzyme that breaks down the native collagen that holds animal tissues together, was also used in this study to examine its effect on microparticle delivery within the sclera. Similar to the results from the hyaluronidase tests, the histological images in Fig. 4.3.9 showed that either pre-soaking the tissue in collagenase solution or adding collagenase to the microparticle suspension increased the amount of microspheres infusing into the scleral tissue. This finding also agreed with our hypothesis that the tight architecture of the collagen fibers served as a critical barrier in micron-sized particle delivery.

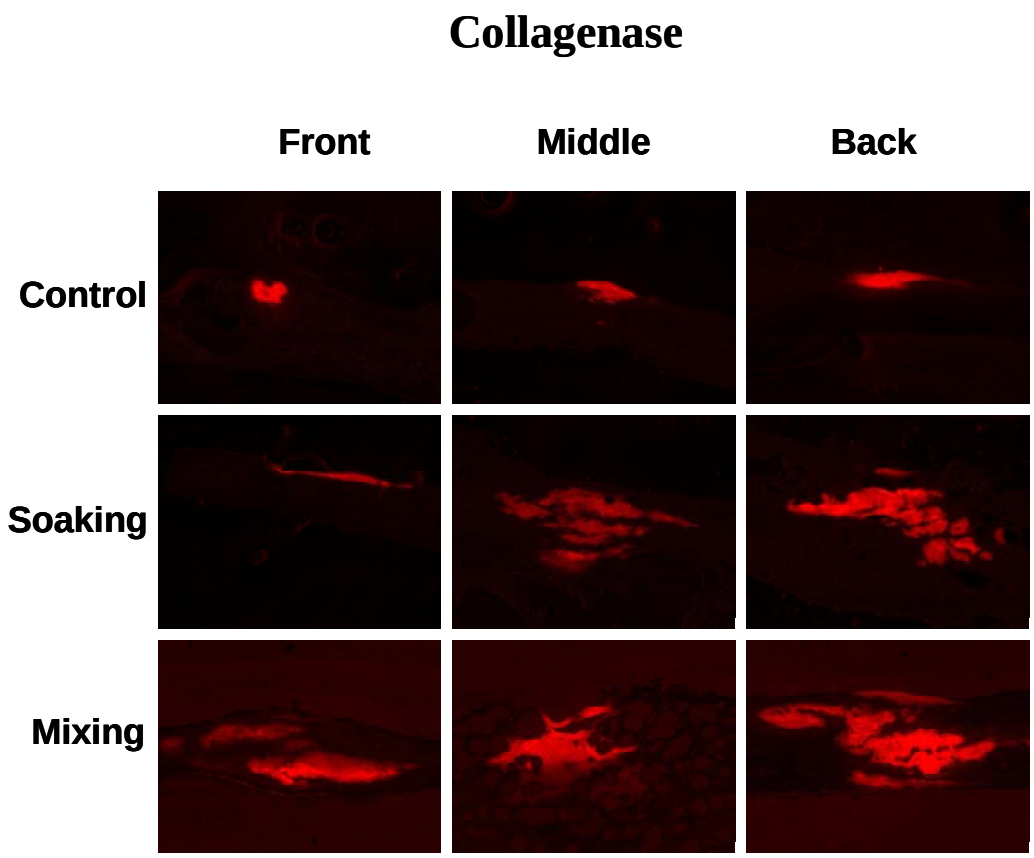

Figure 4.3.9. Representative histological images of the effect of collagenase on the delivery of 1.3 wt% microsphere suspension using hollow glass microneedles into human cadaver sclera. Two types of experiments were performed: first, sclera was presoaked in a collagenase solution for 1 h prior to microinfusion, and second, microparticle suspension was mixed with collagenase and infused into sclera. In each experiment, single, beveled-tip, hollow glass microneedle was inserted 720-960 μm into the sclera and then retracted 250-300 μm depending on the scleral thickness in the region. A 20 μl microsphere suspension was infused into the tissue at a pressure of 15 psi.

4.3.8 Implications for ocular drug delivery applications

This study shows that hollow microneedles can infuse fluid solutions containing particles varying from small-sized molecules (about 500-600 Da) to micron-sized particles (about 1 μm in diameter) into sclera after partial needle retraction within the tissue. Unlike previous results showing in transdermal delivery, the volumetric delivery was independent to the infusing pressure possibly due to the complex alignment of the scleral collagen fibers. Microspheres were only delivered into the sclera with the presence of either hyaluronidase or collagenase. These effects can be explained by the overall hypothesis that microinfusion through hollow microneedles into sclera is limited by the resistance to flow offered by the naturally tightly packed collagen fibers. Needle retraction may induce flow by creating open pathways between the needle and the fibers. Both hyaluronidase and collagenase attack extracellular matrix structures within the sclera to break down collagen and GAG fibers to allow microspheres to flow through.

This study is significant because for the first time, hollow microneedles have been used to deliver solution and particles into the ocular tissue in a controlled fashion. In contrast to hypodermic injection, the microneedle system can deposit drug particles within the sclera with minimized tissue damage. The mechanistic interpretation that fiber alignment serves as the rate-limiting barrier in scleral delivery provides a rational guideline to design new approaches for *in vivo* applications.

Single microneedles were shown to infuse on average up to 30 μl of fluid into sclera, which is sufficient for many short-term applications. In order to provide a therapeutic delivery dose, an array containing multiple microneedles is envisioned. In this way combining with drug-encapsulated microspheres, up to hundreds of microliters

solution can be delivered into the eye and provide a sustained drug delivery depending on the biodegradation of the particles. Microneedles could be coupled with a user-friendly device, such as a commercially available infusion pump, in a potential scenario of clinical application. Aside from drug delivery, we hypothesize that hollow microneedles may also be used for fluid extraction; such as removing fluid from the vitreous body of the eye to lower intraocular pressure. Future studies will be needed to assess this possibility.

There are limitations to infusion using microneedles. Typically glass is not the ideal material for microneedles for *in vivo* applications, since breakage of the needle will cause additional complications. Alternative materials, such as stainless steel or biodegradable polymers, can be investigated to replace single, hand-drawn, glass needles. In addition, the minutes-long duration of the microneedle application suggests that this system is not suitable for scenarios required rapid drug delivery. Finally, the current microneedle is designed for laboratory use only; therefore, further modifications and adjustments must be needed targeting toward *in vivo* studies and low cost manufacturable devices.

4.3.9 Conclusions

In this study, we demonstrated the ability of using hollow microneedles to deliver fluid into the human cadaver sclera, guided by the hypothesis that the infusion is mainly limited by the tight alignment of the collagen or GAG fibers. In a typical experiment, a single microneedle can deliver up to 20 μl of solution into the tissue upon needle retraction. Infusion pressure has an insignificant effect on delivery. By adding either hyaluronidase or collagenase, we also delivered micron-sized particles into the sclera.

Altogether, this study shows that hollow microneedles can be used as a novel approach to deliver drug particles or solutions into the eye in a minimally invasive manner contrasted to hypodermic injections.

4.4 Therapeutic drug application using microneedles

In this study, we have demonstrated the capability of using either solid microneedles or hollow microneedles to deliver molecules into the sclera. Our next goal is to assess this microneedle system for possible delivery of therapeutic agents such as Macugen, pilocarpine and methotrexate to treat diseases in the anterior and posterior segments of the eye via the sclera.

Topical application remains the most common method to deliver drugs into the eye. Pilocarpine (e.g. Timolol) is used to lower the intraocular pressure to treat glaucoma (Asseff, Weisman et al. 1973). Typically a drop of 0.25% Timolol eye drop solution is applied twice per day, which suggests that approximately 250 μg drug is delivered onto the cornea of the eye on a daily basis (DrugBank). Previous study (Asseff, Weisman et al. 1973) reported that only 1-3% or less of an instilled pilocarpine dose gains access to the internal eye structures. Assuming 2% drug bioavailability, only 5 μg drug will reach to the back of eye. Base on this calculation, a total of 150 μg drug is needed for a 30-days treatment. In our study, a single solid microneedle can be coated with up to 3 μg of drug, which suggests that 50 microneedles will be needed to meet the dose requirement for 30 days. On average, a single hollow microneedle delivered up to 30 μl drug solution into the sclera tissue. Using a solution of pilocarpine at it solubility limit (2.74 mg/ml), 2

hollow microneedles are needed to provide the therapeutic dose requirement by infusion of 30 μl of solution each.

A similar calculation has been done for methotrexate, an anti-inflammatory agent to treat uveitis in the eye (Bom, Zamiri et al. 2001). A topical drop of 0.1% methotrexate solution normally is needed for application twice per day, which suggests that only 1 μg drug will enter the eye (DrugBank). Using the same bioavailability assumption of 2%, for a 30-day therapeutic treatment, 60 μg methotrexate is needed. This means 20 solid microneedles are required while only a single hollow microneedle injection of 30 μl solution of methotrexate at its solubility limit (2.6 mg/ml) is needed.

Ideally a controlled drug release is favored in the eye, and to achieve this goal, our microneedle system can be coupled with biodegradable polymer systems, such as microspheres and nanospheres. Assuming a 10% drug encapsulation efficiency in the microsphere, 500 solid microneedles will be needed for Timolol delivery and 200 needles will be needed for methotrexate treatment. In the hollow microneedle needle delivery, using a donor solution containing 1 wt% of drug-encapsulated microparticles with the same encapsulation efficiency, 5 hollow microneedle injections each loaded with 30 μl solution are needed for pilocarpine delivery and the number of hollow microneedle needed for methotrexate injection is 2.

Macugen (Pegatanib sodium injection) is a therapeutic agent used to treat macular degeneration in the eye (Pfizer). Typically, a dose of 300 μg must be injected intravitreally every 6 weeks. On a 30-day period, 210 μg drug is needed. Based on this information, a need of 70 solid microneedles or 2 hollow microneedles, each loaded with 30 μl of 0.3% Macugen solution, is suggested. Coupled with the microparticle system of

10% encapsulation efficiency, 700 solid microneedles or 7 hollow microneedles, each loaded with 30 μl of microparticle solution, will be needed for drug administration.

Drug	Dose (μg/day)	30 days Application (μg)	30 days App. (μg)	30 days App. (μg)	30 days App. (μg)	30 days App. (μg)
			# of Solid MN	# of Hollow MN	# of Solid MN w/ MS	# of Hollow MN w/ MS
Pilocarpine*	5.0	150	50	2	500	5
Methotrexate*	2.0	60	20	1	200	2
Macugen**	7.0	210	70	2	700	7

Table 4.1. The number of microneedles (solid and hollow) required for a 30-day period of therapeutic drug (Timolol, Methotrexate and Macugen) administration.
* indicates topical administration of Timolol (0.25%) and Methotrexate (0.1%) with a bioavailability assumption of 2 percent
** indicates intraocular injection of Macugen
MN = microneedle and MS = microsphere with a drug encapsulation efficiency of 10%

Based on these estimates, the hollow microneedle system seems to be more suitable to treat ocular diseases that need a large amount of therapeutic drug, where solid microneedles can be used in the cases that only require modest drug dose (e.g. single-day application) or rapid treatment.

5 CONCLUSIONS

Current treatment of ocular disorders in the back of the eye is constrained by inadequate drug delivery methods, since topical application can only deliver small molecules into the eye and intraocular injections lead to safety concerns. In this study, microneedles were tested to provide targeted drug delivery into the eye guided by their previous success in transdermal drug delivery.

To better interpret subsequent microneedle studies, we first quantified lateral drug diffusion profile within the sclera, by carrying out a diffusion study of a model compound, sulforhodamine, through human cadaver sclera, and developing a theoretical model for prediction of drug delivery kinetics and distribution. Experimental results showed that the lateral diffusion of sulforhodamine depended significantly on both time and distance along the sclera. After 4 h, sulforhodamine was observed 4 mm along sclera and to diffuse as far as 1 cm after 1 week. Equilibrium experiments further showed a sclera-to-saline partition coefficient of 13.6, indicating a significant binding between sulforhodamine particles and scleral tissue. Coupling with the theoretical prediction, an effective diffusion coefficient was found to be 3.82e-6 cm^2/s. Comparison with trans-scleral diffusion indicated similar diffusion coefficients, although lateral diffusion was approximately 3 times faster. Based on an average human scleral surface area of 16.7 cm^2, these data suggest that it would require up to 7 weeks for sulforhodamine or molecules with similar sizes to diffuse from a localized source throughout the scleral globe, which is useful to estimate the drug distribution over time from an implantation delivery device. This study presented the first experimental measurements of lateral

diffusion within the sclera, and showed this diffusion is a slow process that localizes drug distribution on the millimeter scale for hours to days.

To examine if microneedles can insert into sclera and deliver drug particles, solid metal microneedles of 500-750 μm in length coated with different molecules (small drugs, proteins and DNA) were manually pieced into human cadaver sclera. The tests showed that these microneedles were sufficiently strong and sharp to penetrate into the sclera without bending or breaking, and were able to rapidly deposit water-soluble drug coatings within the tissue after insertion. Guided by these *in vitro* results, we assessed the system to deliver drugs into an animal model *in vivo*. To facilitate imaging and fluorometric analysis, fluorescein was delivered to the rabbit cornea. The measured fluorescein concentration profile in the anterior segment of the rabbit eye suggested that a drug depot was formed within the cornea and steadily released fluorescein molecules for hours. Microneedle delivery exhibited elevated fluorescein levels in the aqueous humor 60 times greater than that delivered by topical application of the equivalent dose. Similarly, microneedle delivery of pilocarpine caused rapid and extensive pupil constriction. We also investigated the efficiency of microneedle –based delivery and the analysis indicated that more than 70% of coated fluorescein was released from the needle, but a large fraction did not reach the aqueous humor and possibly was washed away by the tear fluid, which suggested that further optimization of the system must be needed. Additionally, slip lamp exams showed that the insertion site created by the microneedle was no longer visible after 3 h and no inflammation or cell-and-flare responses were reported. This study showed for the first time that microneedle can be used to deliver

small drugs and macromolecules into the eye in a minimally invasive manner for potential treatments of anterior segment diseases, as well as posterior segment diseases.

Since hollow microneedles offer extended delivery capabilities, we inserted bevel-tipped, hollow glass microneedles into human cadaver sclera for infusion test. Despite the thickness variance around the scleral globe, on average 18 μl of sulforhodamine solution and a solution containing nanoparticles was delivered into the sclera upon retraction of the microneedle. Due to the densely aligned scleral collagen fibers, varying infusion pressure did not have a significant impact on the volumetric delivery. Elevated pressure was not sufficient to distort the fiber arrangements to open pathways for solutions to pass through. Successful delivery of micron-sized particles into the sclera could be improved by breaking down tightly packed collagen fibers in the sclera. With the presence of either hyaluronidase or collagenase, we were able to achieve microsphere delivery using hollow microneedles. After encapsulating drugs into the microparticles, the delivery can be managed in a controlled fashion. Altogether, this study demonstrated the promise of using hollow microneedles to microinfuse therapeutically useful amount of drug solutions into the ocular tissue for various clinical applications.

6 RECOMMENDATIONS

This study presented the first results of using microneedles to deliver drugs into the eye either through cornea or sclera. While building off these results, further investigations are recommended to optimize this novel ocular drug delivery system, especially for the scenarios of *in vivo* studies. Both diffusion-based solid microneedles and injection-based hollow microneedles showed the promise of providing targeted and controlled drug delivery, especially when coupling with biodegradable polymer systems. The ultimate goal of the study is to efficiently deliver therapeutic drug doses using single or multiple microneedles into the posterior segment of the eye through sclera and conjunctiva to treat diseases such as diabetic retinopathy, retinitis, pigmentosa, and macular degeneration.

Single coated microneedle insertion demonstrated its capability of delivering various sized molecules into the human cadaver sclera *in vitro*, and drugs into the front of the rabbit eye *in vivo*. However, in order to deliver a large amount of drugs, typically ranging from tens to hundreds of micrograms for therapeutic treatment on a weekly basis, multi-arrays of microneedles are recommended. Due to the curving scleral surface, further optimization of the needle array, such as the geometric design and numbers of needles, will be needed. One possibility is to have variable microneedle lengths in the needle array such that needles at the ends are preferably longer than these in the center, which corresponds to the scleral curvature.

In order to provide controlled drug release, coating solid microneedles with biodegradable, drug-encapsulated, polymer microspheres is suggested. After maximizing both drug encapsulation efficiency and particle loading efficiency onto the needle shaft, a

short-term *in vitro* insertion test should be carried out to examine the insertion effects, followed by *in vivo* applications in living animals. Aside from scleral insertion, conjunctiva can also used be used as a route for drug delivery to the posterior part of the eye.

Hollow microneedles can deliver larger drug capacities into the sclera compared to solid microneedles; however, the current insertion setup is not ideally suited for use in the *in vivo* delivery experiments. Needed modifications of the apparatus include: shortening the length of the infusion tubing, redesigning the microneedle holder targeting *in vivo* delivery scenarios, and using a constant flow rate source (i.e. syringe pump) instead the pressure source. The use of microneedles is envisioned to be in an arrangement of multiple needles; thus, a device containing multi hollow microneedles should be considered, extending and augmenting the results of single glass needle infusion. In clinical applications, glass is not the ideal material for tissue insertions; therefore, alternative material for hollow microneedles, such as stainless steel or biodegradable polymers, needs to be looked into. Ultimately, a compact and user friendly hollow microneedle-based device should be built to deliver sufficient drug dosage into the eye. Besides using hollow microneedle as a delivery tool, it can also be used in other applications, such as extracting fluids in the vitreous body to lower the intraocular pressure.

Appendix A.

MathCAD programming of theoretical lateral diffusion modeling

semi-infinite diffusion model for lateral diffusion within human sclera

$C_0 := 8.96 \times 10^{-5}$ initial donor concentration

$P := 13.6$ exprimentally determined partition coefficient

$k := \frac{1}{P - 1}$ binding coefficient

$D := 3.82 \times 10^{-6}$ fitted diffusion coefficient for sulforhodamine MW=558.5, cm^2/s

$i := 1 .. 150$ creating a loop for the distance along sclera

$z_i := \frac{i}{100}$ distance along the sclera

For a diffusion period of 4 hours

$t := 4 \cdot 60 \cdot 60$ $t = 1.44 \times 10^4$ seconds

$$C_{4hr_i} := P \cdot \left[C_0 - C_0 \cdot \operatorname{erf}\left[\frac{z_i}{\sqrt{4 \cdot D \cdot \left(\frac{k}{1 + k} \right) \cdot t}} \right] \right]$$

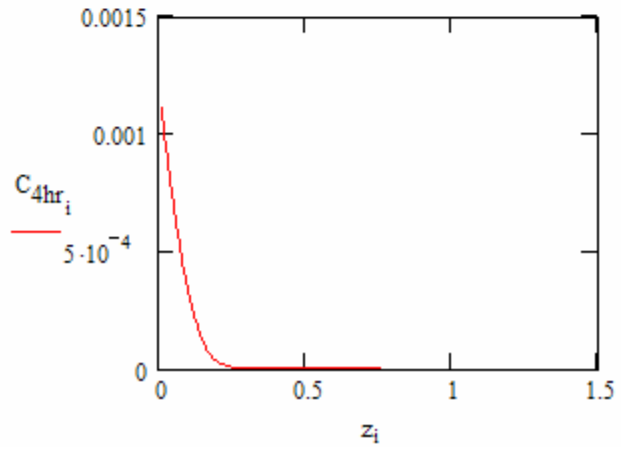

For a diffusion period of 24 hours

$t := 24 \cdot 60 \cdot 60 \qquad t = 8.64 \times 10^{4}$ seconds

$$C_{24hr_i} := P \cdot \left[C_0 - C_0 \cdot \operatorname{erf}\left[\frac{z_i}{\sqrt{4 \cdot D \cdot \left(\frac{k}{1+k} \right) \cdot t}} \right] \right]$$

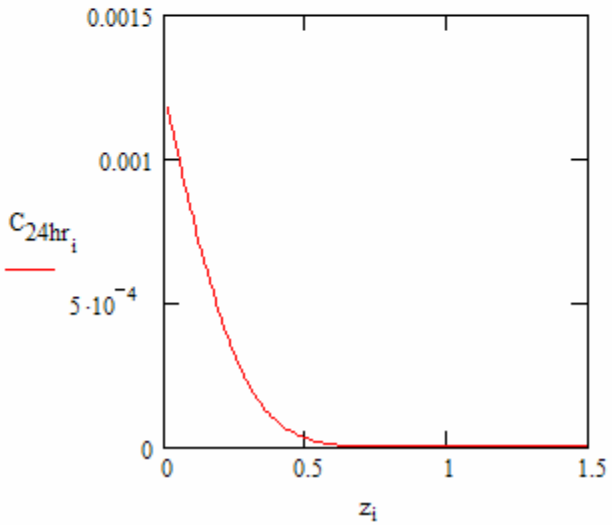

For a diffusion period of 48 hours

$t := 48 \cdot 60 \cdot 60 \qquad t = 1.728 \times 10^{5}$ seconds

$$C_{48hr_i} := P \cdot \left[C_0 - C_0 \cdot \operatorname{erf}\left[\frac{z_i}{\sqrt{4 \cdot D \cdot \left(\frac{k}{1+k} \right) \cdot t}} \right] \right]$$

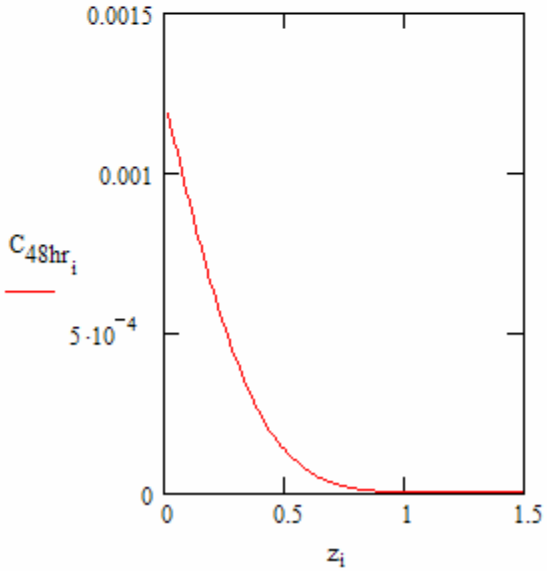

For a diffusion period of 72 hours

$t := 72 \cdot 60 \cdot 60 \qquad t = 2.592 \times 10^{5}$ seconds

$$C_{72hr_i} := P \cdot \left[C_0 - C_0 \cdot \operatorname{erf}\left[\frac{z_i}{\sqrt{4 \cdot D \cdot \left(\frac{k}{1+k} \right) \cdot t}} \right] \right]$$

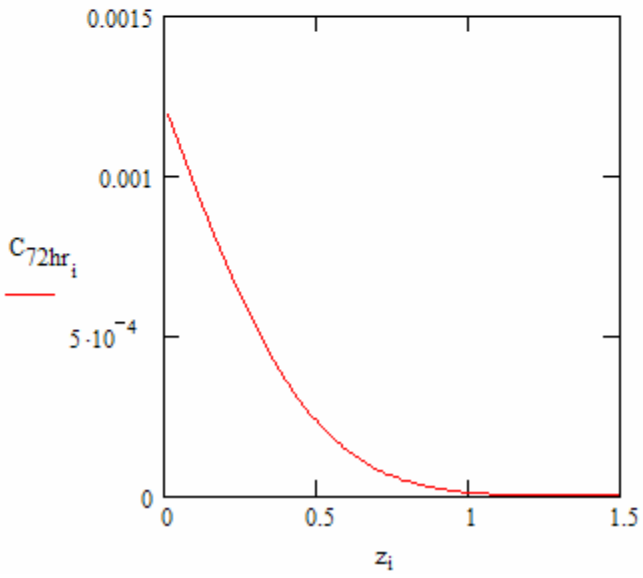

For a diffusion period of 168 hours

$t := 168 \cdot 60 \cdot 60 \quad t = 6.048 \times 10^{5}$ seconds

$$C_{168hr_i} := P \cdot \left[C_0 - C_0 \cdot \operatorname{erf}\left[\frac{z_i}{\sqrt{4 \cdot D \cdot \left(\frac{k}{1+k} \right) \cdot t}} \right] \right]$$

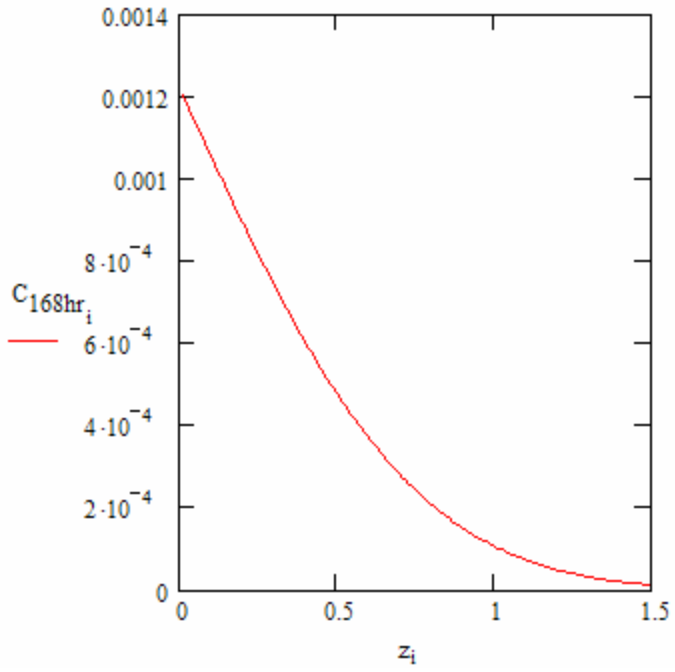

Appendix B

MEMS device for controlled drug delivery

B.1 Introduction

It is desirable to control the release of drug compounds from within an implantable device to the external environment. The method by which a drug is released can have a significant impact on the drug's therapeutic effect (Bakken and Heruth 1991). Conventional drug delivery typically produce a sharp initial increase in drug concentration to a peak above the therapeutic range, followed by a rapid decrease in concentration to a level below the therapeutic range (Huang and Brazel 2001). However, this initial concentration burst can induce a serious risk of toxicity, and the total time, which the released drug spent in the desired therapeutic range, is also short. Therefore, a constant release of drug over long periods is often desirable. In recent years, a new focus in the area of controlled release is pulsatile drug delivery. For example, insulin (Matthews, Lang et al. 1983) and hormones of the anterior pituitary gland such as growth hormone and gonadotropin-releasing hormone (GnRH) are secreted by the human body in a pulsatile fashion (Santini, Richards et al. 2000). Various polymer systems have been developed for pulsatile controlled drug release that can respond to ultrasound (Kost, Leong et al. 1989), changes in pH (Kim, Kim et al. 1992; Lowman, Morishita et al. 1999) or temperature (Hoffman, Afrassiabi et al. 1986), electric (Kwon, Bae et al. 1991) and magnetic field (Edelman, Kost et al. 1985).

In this study, we designed, developed and tested a Micro-Electro-Mechanical Systems (MEMS) device made out of biodegradable polymers, which is suitable for implantation to provide controlled and possible pulsatile drug delivery from weeks up to

months. This device consists of two different parts: a lower mold containing drug reservoirs and an upper covering polymer film of variable thickness. The device is designed to release drugs at different times depending on the degradation rate of the covering film, which depends on the film local thickness along its thickness gradient. Ideally, as the film degrades, drugs release from the thinnest end to the thickest end.

B.2 Material and methods

B.2.1 Fabrication of the master structure and the device

By adapting the fabrication process of the microelectronic industry (Park, Allen et al. 2006), a device for controlled drug delivery was made. A master structure of the device was first created using lithography-based methods, followed by the creation of an inverse mold using the master structure, and the final device was obtained by melting biodegradable polymers into the inverse molds as shown in Fig. B1.

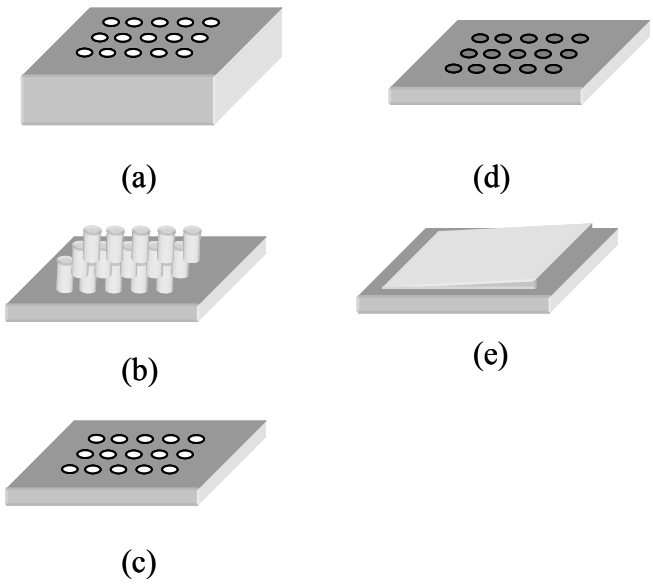

Figure B1. The fabrication steps for a MEMS device that provides controlled drug delivery. (a) A SU-8 master structure fabrication using inclined UV lithography, (b) an inverted PDMS mold made from the master structure, (c) a PLA mold with built-in reservoirs, (d) a PLA mold encapsulated with molecules, and (e) the final MEMS device made of a PLA base mold covered with a PLGA film that has a thickness gradient.

The master structure was fabricated out of SU-8 epoxy using inclined UV-lithographic techniques (Choi, Rajaraman et al. 2006) to form negative concave shaped structures. Each structure was a cylindrical well of 125 μm in radius and 600 μm in length. The center-to-center distance between two wells was 640 μm. SU-8 epoxy (SU-8 100; MicroChem, Newton, MA, USA) was coated onto a silicon substrate and lithographically patterned into desired cylindrical holes to make the master mold. While varying both the mask dimension and the incident angle of UV light, the depth of the mold can be controlled.

After obtaining the master structure, poly (dimethylsiloxane) (PDMS; Sylgard 184, Dow Corning, Midland, MI, USA) was poured into the mold, applied with vacuum at 100 kPa for 1 h to remove the gas bubbles in the solution, and placed inside an incubator at 37 ^{o}C overnight. The solidified PDMS was then peeled off to make an inverse mold.

Since PLA is a FDA-approved polymer that is biocompatible with the human tissue and has a relatively slow degradation rate (Miller, Brady et al. 1977), it was chosen as the material for our base mold. Solid, poly-L-lactide (L-PLA, 1.0 dl/g; Birmingham Polymer) pellets were placed on top of the inverse mold and placed in an oven at 190 ^{o}C. After all the pellets were melted, vacuum suction was applied at 100 kPa for 5 minutes every half hour to remove the air bubbles trapped beneath. This vacuuming procedure normally lasted for 2-3 hours. The final PLA structure was taken out of the oven, compressed against a silicon wafer resting on the table to maintain a flat backside, allowed to cool down and finally was peeled off from the inverse PDMS mold.

B.2.2 Encapsulation of molecules in mold reservoirs

In this study, sulforhodamine (558 Da; Invitrogen, Eugene, OR, USA) and polyethylene glycol (PEG, 1500 Da, Acros Organics, New Jersey, USA; a hydrophilic and biocompatible polymer) were used to fill the reserviors. 50 mg Sulforhodamine powder were dissolved in 1 ml DI water, and solid PEG pellets (500 mg) were then added to the solution. The mixture was stirred at 300 rpm at 40 ^{o}C on a magnetic hot plate for 1 h to remove all the water molecules, which resulting in a solidified PEG cake mixed with sulforhodamine. This PEG cake was re-melted at 50 ^{o}C , and 200 μl of the melted

solution was pipetted on top of the reservoirs of the PLA mold inside a vacuum oven, applied with vacuum suction for 30 min to encapsulate the compounds within the reservoirs. Any residue solution left on the surface of the mold was gently removed using a cotton tip. Because of the presence of PEG, the filling solution was solidified in each reservoir at room temperature.

B.2.3 Fabrication of covering polymer film

An aluminum mold with a surface thickness gradient (slope = 0.013) was made by the machine shop in the School of Chemical and Biomolecular Engineering at Georgia Tech. Compared to PLA, the degradation of poly (lactide-co-glycolide) acid (PLGA), which is also a FDA-approved polymer, occurs at a faster rate (Witschi and Doelker 1998; Lu, Peter et al. 2000). PLGA is chosen as the material for the covering film. Solid PLGA (50:50; Sigma-Aldrich Inc., St. Louis, MO) pellets were placed in between two Nylon films (BASF) on top of the aluminum mold. A Nylon slab (0.25 in. thick; McMaster, Atlanta, GA, USA) was placed above the top Nylon film, while clamps were used to tighten the contact between the films and the slab with the structure. The entire apparatus was placed in an oven at 100 ^{o}C to melt the PLGA pellets. After an hour of heating, the apparatus was taken out and allowed to cool down to the room temperature overnight. The resulting PLGA film with a thickness gradient at the surface, typically from 20 to 100 μm, was then detached from the nylon films.

B.2.4 Binding of the PLA mold and the PLGA film

Using a solvent binding method (Vinter 1996), the PLGA covering film was attached onto the PLA mold. The PLA mold and a vial containing 10 ml of chloroform were placed inside a vacuum oven at 40 ^{o}C, and followed by 30 min of vacuuming. The PLGA film was then placed on top of the PLA mold inside oven. After another 30 min of vacuuming, the film was manually pressed onto the mold using a paint brush to complete the binding between the film and the mold.

We tested two other methods to enhance the binding between the film and mold: addition of an extract sealing layer and ultrasonic welding. For the first methd, solid PLA pellets were mixed with methylene chloride (J.T. Baker, Phillipsburg, NJ, USA) at an m/v ratio of 50:50. Using cotton swabs, this mixture was carefully applied onto the four edges of the film, as an additional sealing layer at the interface. An ultrasonic machine (VC 505; Sonic & Materials, Inc., Newton, CT, USA) was also used as an alternate method to enhance the film binding. The MEMS device was placed on a flat surface, while the ultrasound probe was in contact with the covering film. The ultrasound was applied at a frequency of 20 kHz for 1 s.

B.2.5 In vitro release test

The sulforhodamine-encapsulated MEMS device was submerged into a 20 ml phosphate buffered saline solution (PBS) bath and placed inside an incubator maintained at 37 ^{o}C and 100% humidity. At each desired experimental period (1 h, 2 h, 4 h, 1, 2, 3, 7, 10, 14, 17, 21 and 24 days), a 2 ml sample was withdrawn from the bath and pipetted into a cuvette while 2 ml of PBS solution was added back into the bath. The sulforhodamine

concentration inside the cuvettte was measured by calibrated spectrofluorometry (Photon Technology International, Lawrenceville, NJ, U.S.A.) at an excitation wavelength of 565 nm and emission spectra collected at 580 to 620 nm. The amount of sulforhodamine presented in the sample was calculated using the following equation:

$$m_{cuvette} = C_{cuvette} * V_{cuvette} * MW_{sulf} \quad (1)$$

where $C_{cuvette}$ is the measured molar concentration in the cuvette, V is the sample volume in the cuvette and MW_{sulf} is the molecular weight of sulforhodamine. Assuming the measured concentration is equal to the concentration in the bath, the total dose of sulforhodamine presenting in the donor bath at each experimental time was then calculated as:

$$m_{bath} = m_{cuvette} * 10 + \sum_{i}^{n} m_{cuvette_i} \quad (2)$$

where n is the total number of days, i is the sample number and the summation term accounts for the total amount of sulforhodamine samples withdrew from the bath. In addition, at each experimental period, a corresponding bright-field (Leica DC 300) image of each device was captured, which provided the visual indication for the particle releasing pattern within the mold.

B.2.6 Drug encapsulation efficiency

Using a filling solution of 100 mg/ml, 3 μg of drug can be encapsulated in each reservoir in the device based on its volume; therefore, a single MEMS device of 100 reservoirs can contain 300 μg drug. The actual total amount of drug encapsulated in the device can be estimated using Eqn. 2 when the maximum sample concentration is

detected in each experiment. The drug encapsulation efficiency can then be calculated as:

$$D.E. = \frac{m_{experimental}}{m_{theoretical}} * 100\% \qquad (3)$$

where $m_{experimental}$ is the total amount of drug determined by experimental measurements, and $m_{theoretical}$ is the theoretical estimation of total amount of drug encapsulated in the device.

B.3 Results and discussions

B.3.1 Fabrication of master structure

The first step to make our MEMS device for controlled- drug delivery involved fabricating a master structure using microelectromechanical systems (MEMS) techniques. This master structure was then used to make inverse molds, which were used to make replicate polymer base molds for the device. The basic layout of the master structure is a 2 x 2 cm square, with a 10 x10 array of reservoirs built-in at its center. Each reservoir is in cylindrical shape that has a radius of 125 μm and a depth of 600 μm, and is able to hold up to a few micrograms of drugs. The center-to-center spacing between the reservoirs is 640 μm. The entire array occupies an area of 6 x 6 mm. The final PLA mold had the same geometric parameters as the master structure.

B.3.2 *Effect of covering PLGA film*

In order to establish a controlled drug release, a thin layer of PLGA film of variable thickness was placed on top of the PLA mold. The particle release was intended to be continuously changing guided by the degradation of the PLGA film, where the

earliest release came from the reservoirs covered by the thinnest end of the film and gradually proceeding to the thickest end. On average the film thickness gradient was measured at 80 ± 12 μm. The thickness at the thinnest end was 20 ± 8 μm and at the thickest end was 100 ± 10 μm.

As a positive control, a PLA mold encapsulated with sulforhodamine without a covering PLGA film was placed into a PBS bath. Immediately afterwards, the drug diffused out from the reservoirs and one hour later, all the reservoirs were depleted as shown in Fig. B2B. By comparison, after 1 week, there was still a significant amount of sulforhodamine present in the reservoirs of a device that was covered by a PLGA film as shown in Fig. B2D.

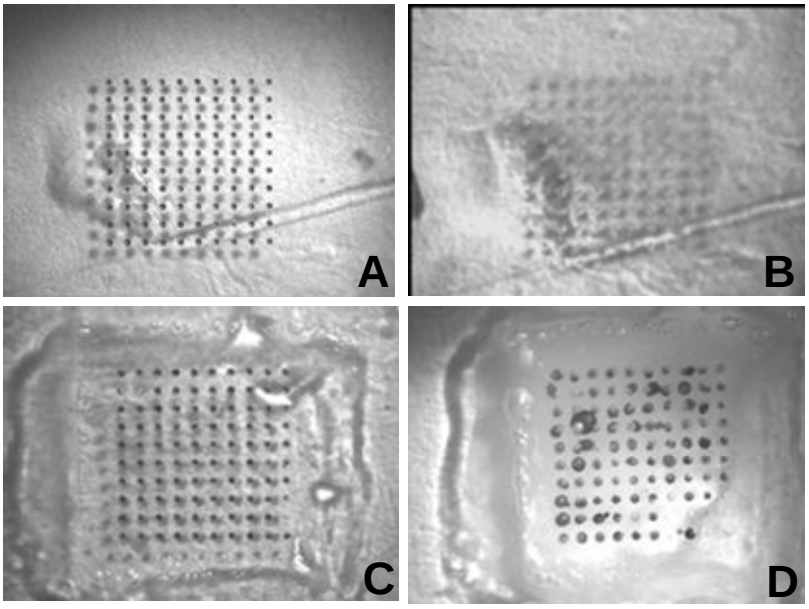

Figure B2. (A) A MEMS device without a covering polymer film serves as the positive control. (B) 1 h after the control device was placed into the release bath, all the reservoirs were depleted. (C) A MEMS device covered with a PLGA film varying in thickness, from the thinnest end on the right of the mold to the thickest end on the left (D) 1 week into the release test, most of the sulforhodamine was still remaining in the reservoirs.

B.3.3 Initial release test results

In the first trial, sulforhodamine was mixed with melted PEG solution and filled into the reservoirs of three PLA molds. The covering films were then manually pressed onto the molds; however, after the film binding, sulforhodamine leakage from several reservoirs in the molds was observed. This could have been caused by the elevated temperature inside the vacuum oven, where the binding process took place. Since the oven temperature operated near the melting point of PEG, the filling compounds inside the reservoirs were melted again. Due to the manual compression of the PLGA film, some liquefied filling solutions were forced out of the reservoirs.

The release test was carried out over a 30 day period, and the results showed that a maximum sulforhodamine concentration measured in the PBS bath was reached after 3 weeks in each case (Fig. B3). The normalized sulforhodamine release profile indicated an initial sharp boost in the concentration, followed by a gradual concentration increase and eventually a leveling concentration. The initial sharp concentration could be explained by the non-uniformity of the film binding using the manual-pressing method. At the interfaces between the film and the mold, there were small opening gaps that allowed water to enter beneath the film. The bright field images also agreed with our hypothesis, and indicated the early release of sulforhodamine from the reservoirs covered by the thicker portion of the film (images not shown).

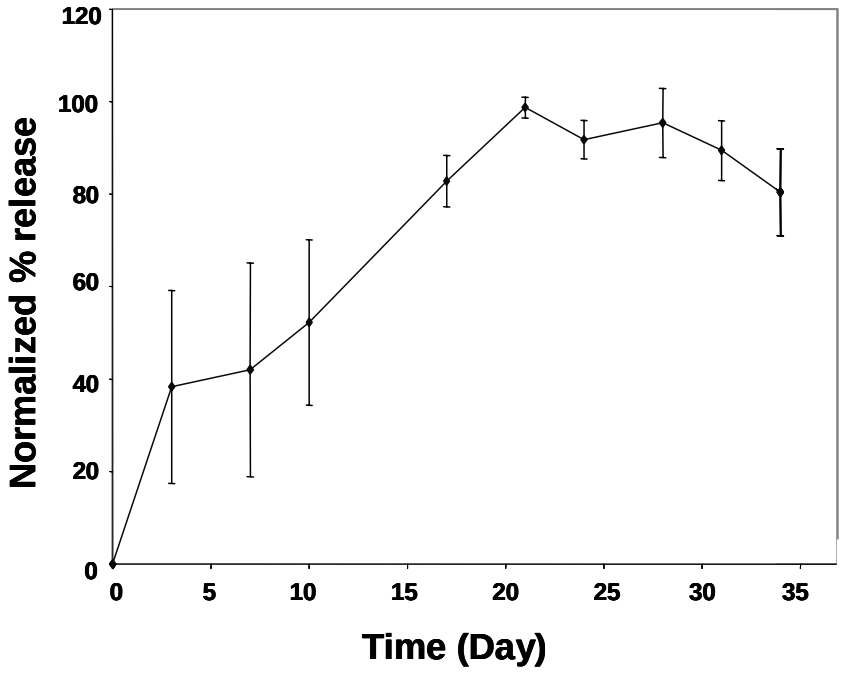

Figure B3. Normalized sulforhodamine percentage release profile of the MEMS devices (n=3). Each data point was normalized with respect to the maximum sulforhodamine concentration measured in the release bath, which was determined at Day 21, in each mold.

A drug encapsulation efficiency of 20% was reported. This relatively low efficiency was caused by the heterogeneous mixture of the filling solution. After solid PEG pellets were melted, it was difficult to dissolve all the sulforhodamine particles in the highly viscous PEG solution. To improve the encapsulation efficiency, in the later studies we dissolved sulforhodamine in water first, mixed with PEG and evaporated all the water molecules to make a homogenous mixture. Using this approach, the encapsulation efficiency was improved to 33.4±10.3%.

B.3.4 Effects of various film binding enhancements

The initial release test indicated an imperfect binding between the covering PLGA film and the PLA base structure, which caused early leakage of drug from the reservoirs

covered by the thicker parts of the film. To fix this problem, two other binding enhancement methods, ultrasonic welding and addition of a polymer sealing layer, were used after the film was manually bound. The normalized percentage releasing profiles obtained over time are shown as in Fig. B4, where two molds using enhancement methods showed longer release periods of 3 weeks.

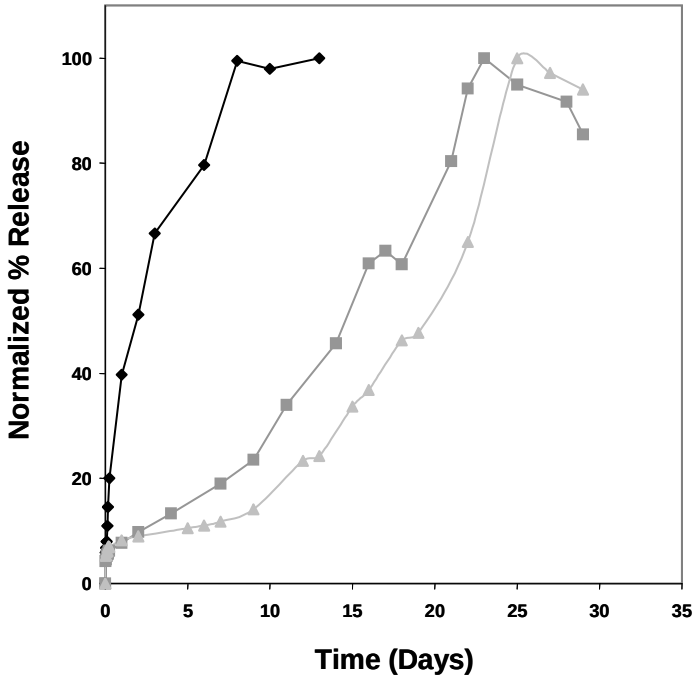

Figure B4. Normalized sulforhodamine percentage release profiles of three MEMS devices, each using a different film binding method. Using the manual pressing method only (—◆—), all the sulforhodamine depleted from the reservoirs after one week. Both enhancement methods using an additional PLA sealing layer (—■—) and ultrasonic welding (—▲—) extended the drug release periods to 3 weeks.

The mold that only used manual-press binding method showed a relatively shorter release period of 7 days compared to the others. The images in Fig. B5 show that water went underneath the binding film 30 min into the release test. At Day 3, a large cluster of

sulforhodamine was evident at the lower left corner in the mold, where the covering film was thickest. A week later most of the drugs had diffused out of the reservoirs.

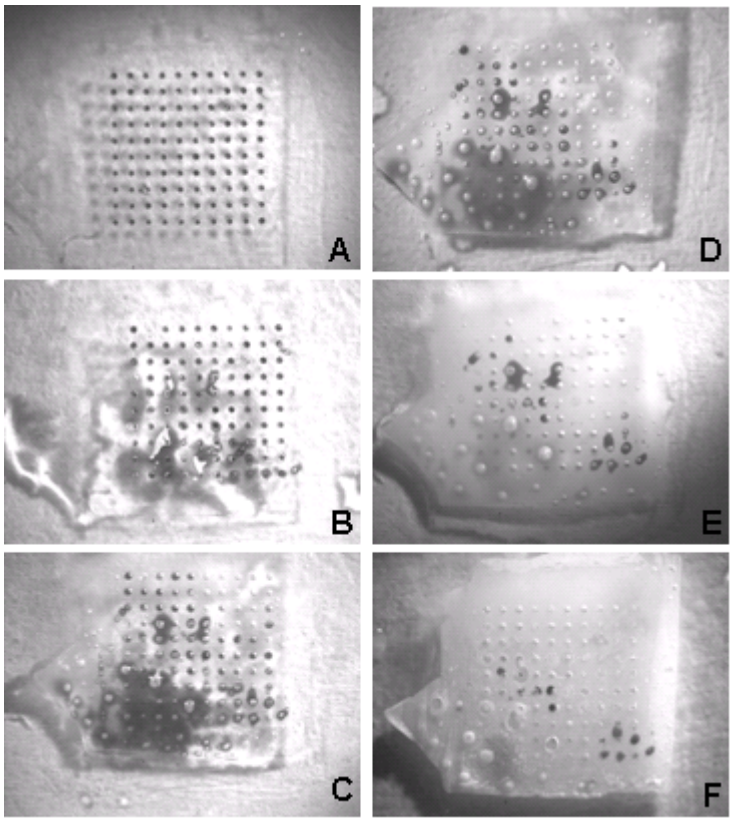

Figure B5. Images of a MEMS device covered with a PLGA layer using hand pressed method at the experimental release periods of (A) 0, (B) 30 min, (C) 1, (D) 3, (E) 8 and (F) 13 days. The leakages of sulforhodamine at the thicker region of the covering film were evident, which indicated an imperfect film binding.

Ultrasonic welding is an industrial technique whereby high-frequency ultrasonic acoustic vibrations are used to weld objects, such as plastics and polymers, together. This method was used to enhance the interface binding between the reservoirs and the polymer film, which caused local melting of the polymers due to absorption of vibration energy. By comparison, the mold using ultrasonic enhancement had a longer release period of 3 weeks with a gradual increase in the concentration profile. Even though some

reservoir leaks were still detected, it was not as significant as the case using manual-pressing method only.

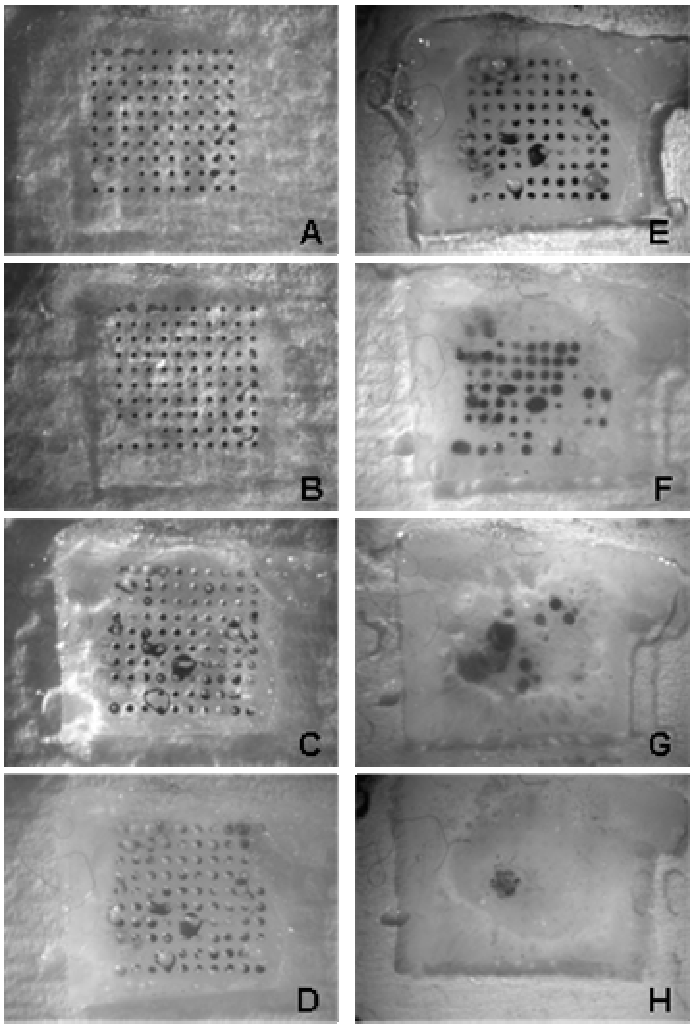

Figure B6. Images of a MEMS device covered with a PLGA layer using ultrasonic binding enhancement method at the experimental release periods of (A) 30 min, (B) 1, (C) 3, (D) 7, (E) 11, (F) 14, (G) 21 and (H) 24 d. Less sulforhodamine leakage was evident and after 3 weeks, most of the sulforhodamine was depleted from the reservoirs.

An additional set of experiments was performed using three MEMS devices fabricated using the same binding enhancement method, and release data are shown in Fig. B7. Unfortunately, in 2 of 3 molds we experienced early sulforhodamine leakage,

which shortened the total release time as a result. We hypothesize that this leakage could be caused by microfractures on the surface of the film created during ultrasonic welding. One solution is to reduce the contact time between the ultrasound probe and the film while using a lower intensity in the future experiments. A bigger-sized ultrasound probe is also recommended, so that the entire surface of the film will be covered during the ultrasound application.

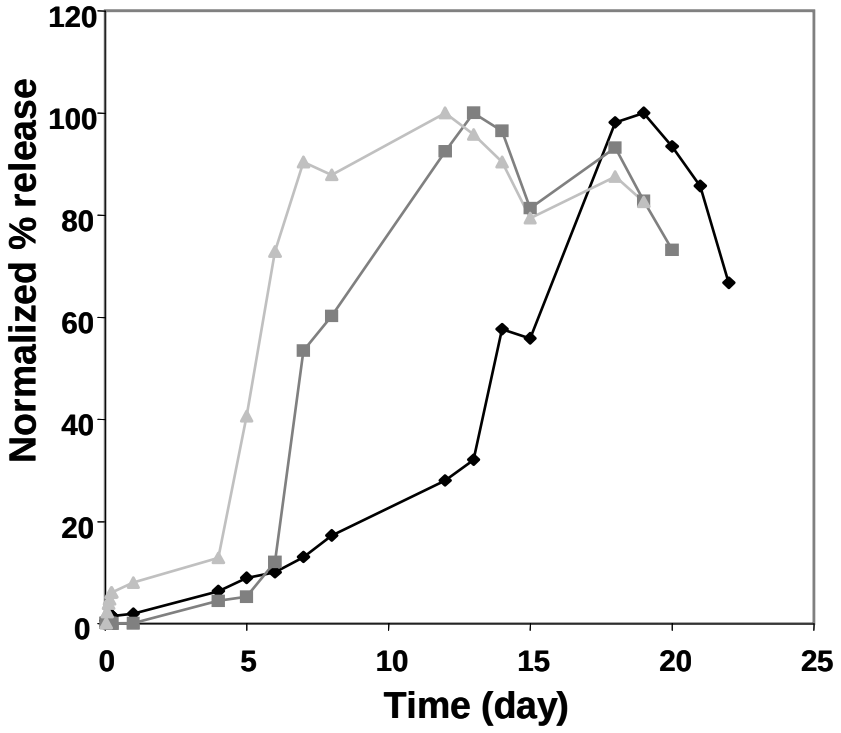

Figure B7. Normalized sulforhodamine percentage release profiles of three MEMS devices fabricated using ultrasonic binding enhancement. Mold 1 (—◆—) showed a release period of 3 weeks. Both mold 2 (—■—) and mold 3 (—▲—) experienced the reservoir leakages, which shortened the release period to 2 weeks.

A second binding enhancement was also tested, which was adding a PLA layer at the edges of the film to prevent water entering at the interfaces. A similar release profile was obtained compared to that of using ultrasonic welding. The images showed fewer

leaks occurred during the study, and the release profile also showed a steady increase in the sulforhodamine concentration over time.

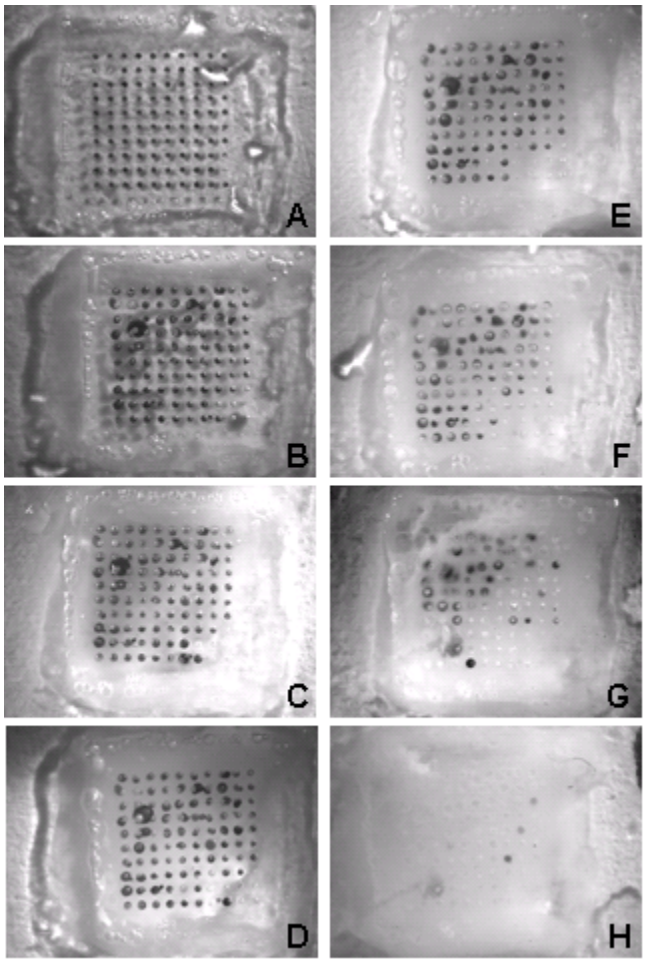

Figure B8. Images of a MEMS device covered with a PLGA layer using a PLA sealing layer at the experimental release periods of (A) 30 min, (B) 1, (C) 3, (D) 7, (E) 11, (F) 14, (G) 21 and (H) 24 d. After 3 weeks, most of the sulforhodamine was depleted from the reservoirs.

B.3.5 Encapsulation of multiple compounds in the device

We attempted to encapsulate two different molecules, sulforhodamine and fluorescein (376 Da, Sigma, St. Louis, MO, USA), into the device. While half of the reservoirs were covered with masking tape, the other half was filled with sulforhodamine

using vacuum suction. The same filling technique was then repeated to encapsulate fluorescein particles into the other half of the reservoirs. The PLGA film was attached to the mold afterwards for completion. A resulting MEMS device is shown in Fig. B9.

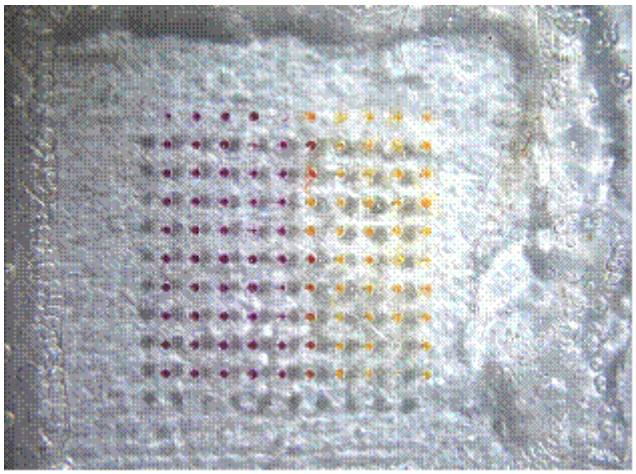

Figure B9. A MEMS device encapsulated with two different compounds, fluorescein, which are filled into the right half of the reservoirs, and sulforhodamine, which are filled into the right half.

B.4 Conclusions

We demonstrated the fabrication of a MEMS device with built-in multiple-arrays of drug reservoirs that can provide controlled drug release depending on the degradation of a covering polymer film. This device could be implanted in the body, for instance underneath the skin or adjacent to tissues such as the eye. By varying the film thickness, we can achieve a drug releasing period from weeks up to a month. Multiple drug formulations can also be encapsulated within the device.

B.5 Recommendations

One of the biggest challenges we faced in this study was to efficiently bind the covering polymer layer onto the base mold to avoid reservoir leakage. Our study suggested that a better binding method could be a combination of ultrasonic welding and addition of a sealing layer around the contact edges. However, besides using a degradable polymer film with a thickness gradient, removing the covering of the reservoirs can be controlled by other mechanisms also. One possibility is to have a uniform covering film with various channels of different geometric design (length, pattern, etc.) to guide the drug release. The channels can also be filled with another material that may further slow the drug transport and release. Another method is to fabricate the covering with different materials that undergo inductive heating in the presence of an alternating electromagnetic field. By applying a certain electromagnetic frequency, the corresponding inductive heating material would then be excited to get hot, whereas other inductive materials, with a different characteristic frequency, would not. Encapsulated particles would then be released depending on this frequency exposure.

REFERENCES

Ahmed, I. and T. F. Patton (1985). "Importance of the noncorneal absorption route in topical ophthalmic drug delivery." Invest Ophthalmol Vis Sci **26**(4): 584-7.

Ahmed, I. and T. F. Patton (1987). "Dispostion of timolol and insulin in the rabbit eye following corneal versus non-corneal absorption." Int. J. Pharm. **38**: 9-21.

Ambati, J., C. S. Canakis, et al. (2000). "Diffusion of high molecular weight compounds through sclera." Invest Ophthalmol Vis Sci **41**(5): 1181-5.

Asseff, C. F., R. L. Weisman, et al. (1973). "Ocular penetration of pilocarpine in primates." Am J Ophthalmol **75**(2): 212-5.

Bakken, E. E. and K. Heruth (1991). "Temporal control of drugs: an engineering perspective." Ann. N.Y. Acad. Sci. **618**: 422-27.

Bom, S., P. Zamiri, et al. (2001). "Use of methotrexate in the management of sight-threatening uveitis." Ocul Immunol Inflamm **9**(1): 35-40.

Bourges, J. L., S. E. Gautier, et al. (2003). "Ocular drug delivery targeting the retina and retinal pigment epithelium using polylactide nanoparticles." Invest Ophthalmol Vis Sci **44**(8): 3562-9.

Bruera, E., C. M. Neumann, et al. (1999). "A randomized controlled trial of local injections of hyaluronidase versus placebo in cancer patients receiving subcutaneous hydration." Ann Oncol **10**(10): 1255-8.

Chabri, F., K. Bouris, et al. (2004). "Microfabricated silicon microneedles for nonviral cutaneous gene delivery." Br J Dermatol **150**(5): 869-77.

Choi, S. O., S. Rajaraman, et al. (2006). 3-D Patterned Microstructures using Inclined UV Exposure and Metal Transfer Micromolding. Solid-State Sensos, Actuators, and Microsystems Workshop. Hilton Head Island, South Carolina.

Cruysberg, L. P., R. M. Nuijts, et al. (2002). "In vitro human scleral permeability of fluorescein, dexamethasone-fluorescein, methotrexate-fluorescein and rhodamine 6G and the use of a coated coil as a new drug delivery system." J Ocul Pharmacol Ther **18**(6): 559-569.

Cussler, E. L. (1997). Diffusion: Mass Transfer in Fluid Systems. Cambridge, United Kingdom.

Davis, S. P. (2003). Hollow Microneedles fro Molecular Transport across Skin. Department of Chemical & Biomolecular Engineering. Atlanta, GA, Georgia Institute of Technology. **Ph.D.**

Davis, S. P., B. J. Landis, et al. (2004). "Insertion of microneedles into skin: measurement and prediction of insertion foce and needle facture force." Journal of Biomechanics **37**: 1155-63.

DrugBank. from http://redpoll.pharmacy.ualberta.ca/drugbank/index.html.

Edelhauser, H. F. and T. H. Maren (1988). "Permeability of human cornea and sclera to sulfonamide carbonic anhydrase inhibitors." Arch Ophthalmol **106**(8): 1110-5.

Edelman, E. R., J. Kost, et al. (1985). "Regulation of drug release from polymer matrices by oscillating magnetic fields." J Biomed Mater Res **19**(1): 67-83.

Edwards, A. and M. R. Prausnitz (1998). "Fiber matrix model of sclera and corneal stroma for drug delivery to the eye." AIChE Journal **44**(1): 214-225.

Ethier, C. R. (1983). Hydrodyamics of flow through gel: application to the eye. Dept. of Chemical Engineering. Cambridge, Massachussetts Institute of Technology. **SM Thesis**.

Fatt, I. and B. A. Wissman (1992). Physilogy of the Eye. An Introduction to the Vegatatve Function. Boston, MA, Buterworth-Heinemann.

Foster, C. S. and M. Sainz de la Maza (1994). The Sclera. New York, NY, Springer**:** 1-32.
Galambos, P. and F. K. Forster (1998). Micro-fluidic diffusion coefficient measurement. Micro Total Analysis Systems, Banff, Canada.

Gardnier, J. G. E., J. W. Berenschot, et al. (2002). Silicon micromachined hollow microneedles for transderal liquid transfer. IEEE International Conference.

Geroski, D. H. and H. F. Edelhauser (2000). "Drug delivery for posterior segment eye disease." Invest Ophthalmol Vis Sci **41**(5): 961-4.

Ghate, D. and H. F. Edelhauser (2006). "Ocular Drug Delivery." Expert Opinion on Drug Delivery **3**(2): 275-87.

Gilbert, J. A., A. E. Simpson, et al. (2003). "Transscleral permeability and intraocular concentrations of cisplatin from a collagen matrix." J Control Release **89**(3): 409-417.

Gill, H. S. and M. R. Prausnitz (2006). "Coated microneedles for transdermal delivery." J. Control Release **accepted**.

Girgis, D. O., J. M. Reed, et al. (2005). "Pathogenesis of Staphylococcus in the rabbit anterior chamber." Invest Ophthalmol Vis Sci **46**(4): 1371-8.

Gudauskas, G., C. Kumi, et al. (1985). "Ocular pharmacokinetics of subconjunctivally versus intravenously administered 6-mercaptopurine." Can J Ophthalmol **20**(3): 110-3.

Hale, P. N. and D. M. Maurice (1969). "Sugar transport across the corneal endothelium." Exp Eye Res **8**(2): 205-15.

Hashmi, s., P. Ling, et al. (1995). "Genetic transformation of nematodes using arrays of micromechanical piercing structures." BioTechniques **19**(5): 766-70.

Henry, S., D. V. McAllister, et al. (1998). "Microfabricated microneedles: a novel approach to transdermal drug delivery." J Pharm Sci **87**(8): 922-5.

Herrero-Vanrell, R. and M. F. Refojo (2001). "Biodegradable microspheres for vitreoretinal drug delivery." Adv Drug Deliv Rev **52**(1): 5-16.

Hoffman, A. S., A. Afrassiabi, et al. (1986). "Thermally reversible hydrogels. II: delivery and selective removal of substances from aqueous solutions." J. Control. Release **4**: 213-22.

Hogan, M. J., J. A. Alvarado, et al. (1971). Histology of the Human Eye. Philadelphia, PA, Saundrs.

Huang, X. and C. S. Brazel (2001). "On the importance and mechanisms of burst release in matrix-controlled drug delivery systems." J Control Release **73**(2-3): 121-36.

Ito, Y., J. Yoshimitsu, et al. (2006). "Self-dissolving microneedles for the percutaneous absorption of EPO in mice." J Drug Target **14**(5): 255-61.

Jimenez, M. (2006). "Medicare to cover drug's off-label use in treating sight loss." from http://www.shreveporttimes.com/apps/pbcs.dll/article?AID=/20060530/NEWS01/605300315/0/NEWS.

Jonas, J. B., I. Kreissig, et al. (2003). "Intravitreal injection of triamcinolone for diffuse diabetic macular edema." Arch Opthalmol. **121**: 57-61.

Kaushik, S., A. H. Hord, et al. (2001). "Lack of pain associated with microfabricated microneedles." Anesth Analg **92**(2): 502-4.

Keeley, F. W., J. D. Morin, et al. (1984). "Characterization of collagen from normal human sclera." Exp Eye Res **39**(5): 533-42.

Kielty, C. M. and M. E. Grant (2002). The collagen family: structure, assembly and organization in the extracellular matrix, Wiley-Liss.

Kim, J. H., J. Y. Kim, et al. (1992). "Controlled release of riboflavin and insulin through crosslinked poly(vinyl alcohol)/chitosan blend membrane." Appl. Polym. Sci. **44**: 1923-28.

Kim, J. W., J. D. Lindsey, et al. (2001). "Increased human scleral permeability with prostaglandin exposure." Invest. Ophthalmol. Vis. Sci. **42**(7): 1514-21.

Kost, J., K. Leong, et al. (1989). "Ultrasound-enhanced polymer degradation and release of incorporated substances." Proc Natl Acad Sci U S A **86**(20): 7663-6.

Kreil, G. (1999). "Hyaluronidases - a group of neglected enzymes." Protein Sci. **4**: 1666-1669.

Kwon, I. C., Y. H. Bae, et al. (1991). "Electrically erodible polymer gel for controlled release of drugs." Nature **354**(6351): 291-3.

Lam, T. T., J. Fu, et al. (1991). "A histopathologic study of retinal lesions inflicted by transscleral iontophoresis." Graefes Arch Clin Exp Ophthalmol **229**(4): 389-94.

Lang, J. (1995). "Ocular Drug Delivery Conventional Ocular Formalations." Adv. Drug Deliv. Rev. **16**: 39-43.

Lee, D. A. and E. J. Higginbotham (2005). "Glaucoma and its treatment: a review." Am J Health Syst Pharm **62**(7): 691-9.

Lee, S. B., D. H. Geroski, et al. (2004). "Drug delivery through the sclera: effects of thickness, hydration, and sustained release systems." Exp Eye Res **78**(3): 599-607.

Lee, T. W. and J. R. Robinson (2001). "Drug delivery to the posterior segment of the eye: some insights on the penetration pathways after subconjunctival injection." J Ocul Pharmacol Ther **17**(6): 565-72.

Lowman, A. M., M. Morishita, et al. (1999). "Oral delivery of insulin using pH-responsive complexation gels." J Pharm Sci **88**(9): 933-7.

Lu, L., S. J. Peter, et al. (2000). "In vitro and in vivo degradation of porous poly(DL-lactic-co-glycolic acid) foams." Biomaterials **21**(18): 1837-45.

Martanto, W. (2005). Microinjection into Skin Microneedles. Department of Chemical and Biomolecular Engineering. Atlanta, GA, Georgia Institute of Technology.

Martanto, W., S. P. Davis, et al. (2004). "Transdermal delivery of insulin using microneedles in vivo." Pharm Res **21**(6): 947-52.

Martanto, W., J. S. Moore, et al. (2006). "Microinfusion using hollow microneedles." Pharm Res **23**(1): 104-13.

Matthews, D. R., D. A. Lang, et al. (1983). "Control of pulsatile insulin secretion in man." Diabetologia **24**(4): 231-7.

Maurice, D. (2001). "Review: practical issues in intravitreal drug delivery." J Ocul Pharmacol Ther **17**(4): 393-401.

Maurice, D. M. and J. Polgar (1977). "Diffusion across the sclera." Exp Eye Res **25**(6): 577-82.

McAllister, D. V., M. G. Allen, et al. (2000). "Microfabricated microneedles for gene and drug delivery." Annu Rev Biomed Eng **2**: 289-313.

McAllister, D. V., P. M. Wang, et al. (2003). "Microfabricated needles for transdermal delivery of macromolecules and nanoparticles: fabrication methods and transport studies." Proc Natl Acad Sci U S A **100**(24): 13755-60.

McGuire, S. and F. Yuan (2001). "Quantitative analysis of intratumoral infusion of color molecules." Am J Physiol Heart Circ Physiol **281**(2): H715-21.

Mietz, H., K. Addicks, et al. (1994). "Extraocular application of mitomycin C in a rabbit model: cytotoxic effects on the ciliary body and epithelium." Ophthalmic Surg **25**(4): 240-4.

Miller, R. A., J. M. Brady, et al. (1977). "Degradation rates of oral resorbable implants (polylactates and polyglycolates): rate modification with changes in PLA/PGA copolymer ratios." J Biomed Mater Res **11**(5): 711-9.

Miyano, T., Y. Tobinaga, et al. (2005). "Sugar micro needles as transdermic drug delivery system." Biomed Microdevices **7**(3): 185-8.

Mora, P., S. Eperon, et al. (2005). "Trans-scleral diffusion of triamcinolone acetonide." Curr Eye Res **30**(5): 355-361.

Newell, F. V. (1996). Ophthalmology, Principles and Concepts. St Louis, MO, CV Mosby Co.

News, U. S. (2006). from http://www.usnews.com/usnews/health/eye_vision/glaucoma.

Okabe, K., H. Kimura, et al. (2005). "Effect of benzalkonium chloride on transscleral drug delivery " Invest. Ophthalmol. Vis. Sci. **46**(2): 703-8.

Olsen, T. W., S. Y. Aaberg, et al. (1998). "Human sclera: thickness and surface area." Am J Ophthalmol **125**(2): 237-41.

Olsen, T. W., H. F. Edelhauser, et al. (1995). "Human scleral permeability. Effects of age, cryotherapy, transscleral diode laser, and surgical thinning." Invest Ophthalmol Vis Sci **36**(9): 1893-903.

Park, J.-H., M. G. Allen, et al. (2006). "Polymer Microneedles for Controlled-Release Drug Delivery." Pharmaceutical Research **23**(5): 1008-19.

Pfizer. from http://www.pfizer.com/pfizer/download/uspi_macugen.pdf.

Prausnitz, M. R., A. Edwards, et al. (1998). "Measurement and prediction of transient transport across sclera for drug delivery to the eye." Ind. Eng. Chem. Res. **37**: 2903-7.

Prausnitz, M. R. and J. S. Noonan (1998). "Permeability of cornea, sclera and conjunctiva: a literature analysis for drug delivery to the eye." J Pharm Sci **87**(12): 1479-1488.

Raspanti, M., M. Marchini, et al. (1992). "Ultrastructure of the extracellular matrix of bovine dura mater, optic nerve sheath and sclera." J Anat **181 (Pt 2)**: 181-7.

Reed, M. L., W. Clarence, et al. (1998). "Micromechanical devices for intravascular drug delivery." J. Pharmacol. Sci. **87**(11): 1387-93.

Reiser, B. J., T. S. Ignacio, et al. (2005). "In vitro measurement of rabbit corneal epithelial thickness using ultrahigh resolution optical coherence tomography." Vet Ophthalmol **8**(2): 85-8.

Robinson, J. C. (1993). Ocular anatomy and physiology relevant to ocular drug delivery. New York, U.S., Marcel Dekker.

Robinson, J. R. and V. H. Lee (1988). Controlled Drug Delivery: Fundamentals and Applications New York, Marcel Dekker.

Rudnick, D. E., J. S. Noonan, et al. (1999). "The effect of intraocular pressure on human and rabbit scleral permeability." Invest Ophthalmol Vis Sci **40**(12): 3054-8.

Santini, J. T., Jr., A. C. Richards, et al. (2000). "Microchip technology in drug delivery." Ann Med **32**(6): 377-9.

Sarraf, D. and D. A. Lee (1994). "The role of iontophoresis in ocular drug delivery." J Ocul Pharmacol **10**(1): 69-81.

Soheilian, M., F. Karimian, et al. (1997). "Surgical management of cataract and posterior chamber intraocular lens implantation in Fuchs' heterochromic iridocyclitis." Int Ophthalmol **21**(3): 137-41.

Stjernschantz, J. and M. Astin (1993). Anatomy and Physiology of the Eye: Physiological Aspects of Ocular Drug Therapy. Biopharmaceutics of Ocular Drug Delivery. Raton, FL, P. Edman. Boca**:** 1-26.

Stoeber, B. and D. Liepmann (2000). Fluid Injection through out-of-plane microneedles. IEEE-EMBS Special Topic Conference on Microtechnologies in Medicine & Biology.

Stoeber, B. and D. Liepmann (2002). Design, fabrication, and test of a MEMS syringer. Proceedings of solid-sate sensor and acutator workshop, Hilton Head Island, SC, USA.

Tasman, W. (1995). Duane's Foundations of Clinical Ophthalmology. Philadelphia, PA, Lippincott-Raven.

Tengroth, B., M. Rehnberg, et al. (1985). "A comparative analysis of the collagen type and distribution in the trabecular meshwork, sclera, lamina cribrosa and the optic nerve in the human eye." Acta Ophthalmol Suppl **173**: 91-3.

Thale, A., B. Tillmann, et al. (1996). "Scanning electron-microscopic studies of the collagen architecture of the human sclera--normal and pathological findings." Ophthalmologica **210**(3): 137-41.

Tielsch, J. M. (2000). Vision Problems in the U.S., National Eye Institute.

Trimmer, W., P. Ling, et al. (1995). Injecion of DNA intoplant and anima tissues with micromechanical piercing structures. International Conference on Microelectromechanical Systems.

Unlu, N. and J. R. Robinson (1998). "Scleral permeability to hydrocortisone and mannitol in the albino rabbit eye." J Ocul Pharmacol Ther **14**(3): 273-81.

Uva, M. G., A. Longo, et al. (2006). "The effect of timolol-dorzolamide and timolol-pilocarpine combinations on ocular blood flow in patients with glaucoma." Am J Ophthalmol **141**(6): 1158-60.

Vingerling, J. R., C. Klaver, et al. (1995). "Epidemiology of age-related maculopathy." Epidemiology Rev. **17**: 347-360.

Vinter, J. G. (1996). "Extended electron distributions applied to the molecular mechanics of some intermolecular interactions. II. Organic complexes." J Comput Aided Mol Des **10**(5): 417-26.

Wang, P. M., M. Cornwell, et al. (2006). "Precise microinjection into skin using hollow microneedles." J Invest Dermatol **126**(5): 1080-7.

Wang, P. M., M. Cornwell, et al. (2005). "Minimally invasive extraction of dermal interstitial fluid for glucose monitoring using microneedles." Diabetes Technol Ther **7**(1): 131-41.

Weijtens, O., E. J. Feron, et al. (1999). "High concentration of dexamethasone in aqueous and vitreous after subconjunctival injection." Am J Ophthalmol **128**(2): 192-7.

Weinreb, R. N. (2001). "Enhancement of scleral macromolecular permeability with prostaglandins." Trans. Am. Ophthalmol. Soc. **99**: 319-43.

Weinreb, R. N., J. D. Lindsey, et al. (2004). "Prostaglandin FP agonists alter metalloproteinase gene expression in sclera." Invest. Ophthalmol. Vis. Sci. **45**(12): 4368-77.

Witschi, C. and E. Doelker (1998). "Influence of the microencapsulation method and peptide loading on poly(lactic acid) and poly(lactic-co-glycolic acid) degradation during in vitro testing." J Control Release **51**(2-3): 327-41.

Yasukawa, T., Y. Ogura, et al. (2006). "Drug delivery from ocular implants." Expert Opin Drug Deliv **3**(2): 261-73.

Zahn, J. D., D. Trebotich, et al. (2005). "Microdialysis microneedles for continuous medical monitoring." Biomed Microdevices **7**(1): 59-69.

VITA

Ninghao Jiang was born in Shanghai, China on December 30, 1978. At age 14, he moved to U.S.A. with his family. He graduated from Northview High school in Dothan, Alabama in 1997. He then attended the University of Alabama, Tuscaloosa, Alabama. In May 2001, he received a Bachelor of Science with Magna Cum Laude in Chemical Engineering. In August 2001, he attended Georgia Institute of Technology, Atlanta, Georgia. His dissertation title was "Ocular Drug Delivery using Microneedles". He defended his thesis on November 7, 2006 and obtained his Ph.D. in Chemical Engineering with a Minor in Bioengineering.